Highly oxygenated organic nitrates formed from NO_3 radical initiated oxidation of β-pinene

Hongru Shen,[1] Defeng Zhao,[1,2,3,4*] Iida Pullinen,[2, a] Sungah Kang,[2] Luc Vereecken,[2] Hendrik Fuchs,[2] Ismail-Hakki Acir,[2,b] Ralf Tillmann,[2] Franz Rohrer,[2] Jürgen Wildt,[2] Astrid Kiendler-Scharr,[2] Andreas Wahner,[2] Thomas F. Mentel[2*]

[1] Department of Atmospheric and Oceanic Sciences & Institute of Atmospheric Sciences, Fudan University, 200438, Shanghai, China;

[2] Institute of Energy and Climate Research, IEK-8: Troposphere, Forschungszentrum Jülich, 52425, Jülich, Germany;

[3] Big Data Institute for Carbon Emission and Environmental Pollution, Fudan University, Shanghai 200438, China.

[4] Institute of Eco-Chongming (IEC), 20 Cuiniao Road., Chenjia Zhen, Chongming, Shanghai 202162, China

[a] Now at: Department of Applied Physics, University of Eastern Finland, Kuopio, 70210, Finland.

[b] Now at: Institute of Nutrition and Food Sciences, University of Bonn, Bonn, 53115, Germany.

*Corresponding authors: dfzhao@fudan.edu.cn, t.mentel@fz-juelich.de

Table of Contents (TOC)

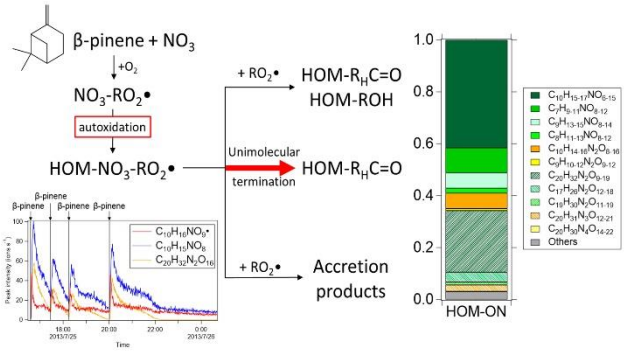

Abstract

The reactions of biogenic volatile organic compounds (BVOC) with the nitrate radical (NO_3) are major night-time sources of organic nitrates and secondary organic aerosol (SOA) in regions influenced by BVOC and anthropogenic emissions. In this study, the formation of gas-phase highly oxygenated organic molecules-organic nitrates (HOM-ON) from NO_3-initiated oxidation of a representative monoterpene, β-pinene, was investigated in the SAPHIR chamber (Simulation of Atmosphere PHotochemistry In a large Reaction chamber). Six monomer (C = 7-10, N = 1-2, O = 6-16) and five accretion product (C = 17-20, N = 2-4, O = 9-22) families were identified and further classified into first- or second-generation products based on their temporal behavior. The time lag observed in the peak concentrations between peroxy radicals containing odd and even number of oxygen atoms, as well as between radicals and their corresponding termination products, provided constraints on the HOM-ON formation mechanism. The HOM-ON formation can be explained by unimolecular or bimolecular reactions of peroxy radicals. A dominant portion of carbonylnitrates in HOM-ON was detected, highlighting the significance of unimolecular termination reactions by intramolecular H-shift for the formation of HOM-ON. A mean molar yield of HOM-ON was estimated to be 4.8% (-2.6%/+5.6%), suggesting significant HOM-ON contributions to the SOA formation.

Keywords: NO_3 radical, biogenic volatile organic compounds, organic nitrate, secondary organic aerosol, anthropogenic-biogenic interaction, night-time oxidation

Synopsis: The reactions of nighttime anthropogenic oxidants with biogenic organics form low-volatile vapors, potentially contributing a large fraction of particulate organic matter.

Introduction

Biogenic volatile organic compounds (BVOC), such as isoprene (C_5H_8) and monoterpenes ($C_{10}H_{16}$) emitted from terrestrial vegetation, constitute a large fraction of global gas-phase organic compounds.[1] In the ambient conditions, BVOC are primarily oxidized by OH in the daytime,[2, 3] NO_3 radicals at night-time,[4, 5] and O_3 during both day- and night-time.[6, 7] These reactions are believed to be the dominant contributor to the formation of secondary organic aerosols (SOA), influencing regional and global climate, air quality, and human health.[8, 9] Compared to SOA formation from OH- and O_3-initiated oxidation of BVOC, night-time NO_3 oxidation of BVOC has been less investigated, but these reactions are highly relevant in ambient conditions, particularly in regions influenced by anthropogenic NO_x ($NO + NO_2$) and natural BVOC emissions.[10-12] Reactions of BVOC + NO_3 can form organic nitrates (ON), which serve as a temporary or permanent sink for NO_x and affects regional O_3 budgets and nitrogen cycles.[13, 14] Due to their semi-/low-volatility, ON can also partition into the condensed phase participating in SOA formation. The results from the Southern Oxidant and Aerosol Study (SOAS) have shown that a large fraction of night-time SOA formation can be explained by reactions of BVOC + NO_3, about half of which is from monoterpenes + NO_3.[15] Therefore, this anthropogenic-biogenic interactions between NO_3 and BVOC, especially monoterpenes, is critical to understand night-time SOA formation.

Among the monoterpenes, β-pinene has high emission rates (being the second most abundant monoterpene, after α-pinene),[16] high reactivity with NO_3 (with a second-order rate constant of 2.5×10^{-12} cm^3 $molecule^{-1}$ s^{-1} at 298 K),[17] and high SOA yields with NO_3 (with SOA mass yields of 27-104%[18-23] compared to 0-16% for α-pinene[22-25]). The reaction of β-pinene with NO_3 contributes a significant fraction of the SOA produced by monoterpene + NO_3 and was therefore often selected as a representative monoterpene in recent laboratory studies.[15, 19-21, 26] Previous studies have investigated β-pinene + NO_3, mostly focusing on the determination of the SOA yield, chemical characterization of particle-phase products, and possible formation mechanism of products containing a low number of oxygen atoms. For example, Fry et al.[19] measured the SOA yield. Boyd et al.[20] additionally found that neither humidity nor peroxy radical fate affects SOA yields, determined ON fraction in the aerosols, and proposed a formation mechanism of the detected gas-phase ON ($C_{10}H_{15}NO_{5,6}$ and $C_{10}H_{17}NO_{4,5}$), which are formed by the bimolecular reactions of RO_2•. Claflin and Ziemann[21] observed monomers (C_{10} ON), dimers (C_{20} ON), and trimers (C_{30} ON) in the particle-phase products from reactions of β-pinene + NO_3 and highlighted oligomerization reactions in the particle-phase mechanism.

Despite previous efforts by a number of laboratory studies, the understanding of the chemistry of β-pinene with NO_3, especially regarding gas-phase reaction products containing a high number of oxygen atoms, is still incomplete. In particular, highly oxygenated organic molecules-organic nitrates (HOM-ON), a new class of gas-phase

compounds containing at least 6 oxygen atoms,[27] have been recently observed and found to play a potentially significant role in SOA formation in the NO_3 oxidation of BVOCs, including β-pinene.[28, 29] Nah et al.[30] observed a series of HOM-ON of C_{7-10} with 4-9 oxygen atoms in both particle- and gas-phase products of NO_3 oxidation of β-pinene. Takeuchi and Ng[31] additionally observed a substantial contribution of accretion products such as $C_{20}H_{32}N_2O_{8-11}$ in the particle phase. These HOM-ON are known to be formed in a short time-scale via autoxidation,[30] which involves successive intramolecular H-shifts in peroxy radicals (RO_2•) and subsequent O_2-addition,[6, 32] resulting in an oxygenated RO_2• radical reaction chain, shown in Scheme S1a. Recent studies have summarized general RO_2• reactions,[27, 33] with the most critical ones shown in Scheme S1b-j. Via bimolecular reactions with RO_2•, HO_2•, or NO_3, the RO_2• autoxidation chain will either be terminated to form a set of closed-shell products (Scheme S1b-d, g-j), including hydroxyperoxide, alcohol, carbonyl, and accretion products, or be continued via the formation of alkoxy radicals (RO•, Scheme S1e-f). Unimolecular termination pathways generally lead to the formation of carbonyls (Scheme S1h-i) or epoxides (Scheme S1j).[32] However, the specific HOM-ON formation mechanism remains elusive for the β-pinene + NO_3 system. In addition, the knowledge of the chemical composition of HOM-ON is incomplete and their contribution to SOA formation is unquantified.

In this study, experiments of NO_3-initiated oxidation of β-pinene were performed in the SAPHIR chamber in Jülich, Germany (Simulation of Atmosphere PHotochemistry In

105 a large Reaction chamber). A large number of HOM-ON were identified and quantified.
106 An example formation pathway was proposed and further constrained based on the time
107 series. An estimate of production yields of these HOM-ON formed from the β-pinene +
108 NO_3 reaction was provided to evaluate their role in the SOA formation.

109 **Experimental and Methods**

110 **Experimental Setup.** The experiments were performed in the SAPHIR chamber at
111 Forschungszentrum Jülich, Germany. It is a double-walled Teflon chamber with a volume
112 of 270 m^3. A detailed description of SAPHIR can be found elsewhere.[34, 35] Before the
113 experiment, the chamber was purged with synthetic air at ~330 $m^3\ h^{-1}$ for about 4 h to clean
114 the chamber and eliminate any interference from previous experiments. During the whole
115 experimental period, the chamber was kept under an over-pressure of 35 Pa, leading to a
116 dilution rate of $1.5\times10^{-5}\ s^{-1}$. The shutter system was closed to prevent photochemical
117 reactions, including NO_3 photodissociation. A fan was continuously operated to mix the
118 trace gases with homogenization within 2 min.

119 Experiments were designed to probe the time series of gas-phase HOM-ON formed
120 from β-pinene + NO_3, with the detailed experimental procedure shown in Figure S1. First,
121 ozone was added into the chamber, followed by NO_2 to form in-situ NO_3 radicals along
122 with the simultaneous formation of dinitrogen pentoxide (N_2O_5) as per the reactions below

123 $NO_2 + O_3 \rightarrow NO_3 + O_2$ (R1)

124 $NO_3 + NO_2 \leftrightarrow N_2O_5$ (R2)

Through the equilibrium with N_2O_5, sufficiently high concentrations of NO_3 radicals were ensured. A concentration ratio (~2:1) of NO_2 and O_3 was selected to ensure that more than 98% of β-pinene reacted with NO_3 radicals instead of O_3 during each experimental period, as shown in Figure S2. About 16 min after NO_2 addition, concentrations of NO_3 and N_2O_5 reached 90 ppt and 1.5 ppb, respectively, and β-pinene was added into the chamber, initiating the oxidation reaction. Another two β-pinene additions were deployed at respectively 50 min and 100 min after the first β-pinene addition. Later on, 12 ppb O_3 and 16 ppb NO_2 were introduced into the chamber, followed by one more addition of β-pinene. Four experimental periods were performed to probe the time series of products and distinguish first- and second-generation products. With no seed particles used in these experiments and low concentrations of β-pinene and NO_3, a negligible amount of particles were formed and observed, as shown in Figure S3. This is in contrast to previous studies,[19-22, 26, 36] which used seed aerosol and/or high concentrations of β-pinene and NO_3, leading to particle formation. Due to the low particle number and surface area concentrations in our work, particles are expected to have negligible effects on the gas-phase products' partitioning. Experiments were performed under dry conditions (relative humidity <3%) and at an average temperature of 300.0 ± 2.0 K.

Instrumentation. The chamber was equipped with a comprehensive set of instruments as described by Zhao et al.[37] In this experiment, a home-built diode laser-based, cavity ring-down spectrometer was used to measure *in-situ* concentrations of NO_3 and N_2O_5.[38] A

145 proton transfer reaction time-of-flight mass spectrometer (PTR-TOF-MS, Ionicon Analytik,
146 Austria) was used to measure the concentrations of VOC, including β-pinene and acetone.
147 From the measured concentrations, the β-pinene consumption during the experiments can
148 be derived and agrees with the expectations when considering the dilution (a loss rate
149 coefficient of 1.5×10^{-5} s^{-1}) and the reaction with NO_3 (a reaction rate constant of 2.5×10^{-12}
150 cm^3 $molecule^{-1}$ s^{-1}).[39]

151 The chemical composition of produced HOM-ON was characterized online using a
152 $^{15}NO_3^-$ chemical ionization mass spectrometer (CI-API-TOF-MS, Aerodyne Research Inc.),
153 which detects products with six or more oxygen atoms efficiently.[40] Nitrogen-15 was used
154 to distinguish the nitrogen-14 atoms in the chamber-produced ON, most of which are
155 expected to complex with the $^{15}NO_3^-$ ion.[41] The mass spectral data within the m/z 4-1400
156 range were analyzed using a Tofware analysis toolkit (Tofwerk/Aerodyne) in Igor Pro
157 (WaveMetrics, Inc.). High-resolution analysis was applied to identify ions with a resolving
158 power $m/z/\Delta m/z$ of ~3500. Isotopes were constrained during the peak assignment process.
159 The mass spectrum of the first experimental period was selected to assign peaks, as it
160 showed a mass spectrum similar to other experimental periods and the end of the
161 experiments and contained the same products as other periods (Figure S4). We observed a
162 few peaks such as m/z 289 and 334 corresponding to $C_5H_{10}N_2O_8\cdot{}^{15}NO_3^-$ and
163 $C_5H_9N_3O_{10}\cdot{}^{15}NO_3^-$,[10] which are products of isoprene + NO_3 reactions.[42] Their time series
164 are shown in Figure S5. These peaks were observed before the beginning of β-pinene +

NO_3 experiments, their concentrations increased slowly during the whole experimental period, and no obvious and regular response to each β-pinene addition was observed. This indicates that these compounds are residuals on the chamber wall from prior experiments of isoprene + NO_3 one day before and with also possible small contributions from the reaction of β-pinene + NO_3.[43] Moreover, these compounds do not contain double bonds according to their formula,[44] we expect that they do not react with NO_3 or O_3 during the β-pinene experiment, which is confirmed by the lack of response to O_3 and NO_2 addition before the experiment. Additionally, the HOM-ON formed in the reaction of β-pinene with NO_3 were absent before the first β-pinene addition. Therefore, we conclude that residual compounds do not have significant influence on the β-pinene + NO_3 reactions. We would like to note that our CIMS easily detects these HOM evaporated from the residue on the chamber wall despite their low concentrations because of its high sensitivity to HOM.

The concentrations of O_3 and NO_x were measured using an O_3 analyzer (ANSYCO, model O341M) and a NO_x analyzer (ECO PHYSICS TR480), respectively. The SOA was monitored using an SMPS (TSI DMA3081/TSI CPC3785). Measurements of physical parameters, including the temperature, relative humidity, and flow rate, were also conducted in these experiments.

Yield of products. The peak area of ions identified using the mass spectrometer was normalized to the total ion signal and then converted to concentrations using a calibration coefficient (C) of 2.5×10^{10} molecule cm^{-3} nc^{-1} (normalized count), determined using H_2SO_4

as described by Pullinen et al.[45] A mass-independent transmission efficiency equal to H_2SO_4 (with an uncertainty of -0%/+14%) was used when applying the calibration coefficient to HOM, as determined in our previous study.[45] The determination of this calibration value and its application to HOM are described in details in the Supporting Information (SI) (section S1). The concentrations of the identified ON with more than 6 O atoms were summed to the total concentrations of HOM-ON after a wall loss rate of 6×10^{-4} s^{-1}, and a dilution rate of 1.5×10^{-5} s^{-1} were accounted for.[46] Previous studies have shown that the wall loss rate of some compounds changes as the experiment continues,[47] which could affect the determined HOM yield. As the HOM yield in this study was determined over a short period after each injection (~10 min), we do not expect a large change in the wall loss rate during this period. In addition, considering the low volatility of HOM leading to their irreversible loss to the wall, a narrow distribution of the wall loss rates is expected. Sensitivity analysis shows that the HOM yield in this study is not sensitive to the wall loss rate, with a respective change of 23% and -11% in HOM yield from an increase of +100% or -50% in the wall loss rate. One uniform wall loss rate is thus used to determine HOM in this study. Such simplification may introduce additional uncertainty in HOM yield calculation. The molar yield of these HOM-ON was calculated following eq 1, where concentrations of produced HOM-ON is divided by the concentrations of β-pinene that reacted with NO_3.

$$Y = \frac{[\text{HOM ON}]}{[\beta\ \text{pinene}]_{\text{reacted}}} \quad (1)$$

Herein, [HOM-ON] represents the product concentration formed 10 min after each β-pinene addition. In other words, the molar yield *Y* refers to the primary yield, which mostly involves first-generation products and contains negligible multigeneration products. The uncertainty on the molar yield was estimated to be -55%/+117% from the combined uncertainties of HOM-ON peak intensity (~10%), β-pinene concentration (~15%), calibration factor (-52%/+101%), and transmission efficiency (-0%/+14%) using error propagation. The HOM-ON molar yield was averaged over four experiment periods, and uncertainties were estimated based on this value. Molar yields were later converted into mass yields using the molecular mass of each compound following Ehn et al.[6]

Results and Discussion

Overview of HOM-ON. Two distinct regions at m/z 280-460 (red) and m/z 510-690 (blue) in the mass spectrum of the first β-pinene + NO_3 experimental period (between the first and second β-pinene addition) were observed and segregated into monomers (C = 7-10, N = 1-2) and accretion products (C = 17-20, N = 2-4) (Figure 1a). Based on the above peak assignment methods, 153 compounds were identified, including 99 monomers, 46 accretion products, and 8 other compounds. Their detailed formula can be found in Table S1. Most of the identified products contained at least one N atom and more than six O atoms. This oxygenated feature agrees with the definition of HOM,[27] and these compounds can thus be classified as HOM-ON.

The Kendrick mass defect (O-based) plot of these identified HOM-ON is shown in Figure 1b, indicating their relative abundance and O/C ratio. Overall, the majority of the identified HOM-ON are monomers, with a fraction of 65.7%, with the rest being composed of accretion products (31.2%) and other compounds (3.1%). An average O/C ratio of 1.23 and 0.81 is observed for monomers and accretion products, respectively. Previous β-pinene + NO_3 studies generally detected O/C < 1 for monomers[20, 21, 30] and 0.45-0.55 for accretion products.[21, 31] This O/C difference can be attributed to the use of NO_3^- as a reagent ion. Specifically, NO_3^- CIMS preferentially detects compounds containing high numbers of O atoms and multiple hydrogen bond donors,[40, 48] compared with other reagent ions such as I^-.[49] The HOM-ON on each horizontal line in Figure 1b share the same number of C, N, and H-atoms, with an increasing number of O atoms from left to right, allowing further grouping into product families based on the chemical formula. We distinguished six groups of monomer families ($C_{10}H_{15\text{-}17}NO_{6\text{-}15}$, $C_7H_{9\text{-}11}NO_{8\text{-}12}$, $C_9H_{13\text{-}15}NO_{8\text{-}14}$, $C_8H_{11\text{-}13}NO_{8\text{-}12}$, $C_{10}H_{14\text{-}16}N_2O_{8\text{-}16}$, and $C_9H_{10\text{-}12}N_2O_{9\text{-}12}$) and five accretion product families ($C_{20}H_{32}N_2O_{9\text{-}19}$, $C_{17}H_{26}N_2O_{12\text{-}18}$, $C_{19}H_{30}N_2O_{11\text{-}19}$, $C_{20}H_{31}N_3O_{12\text{-}21}$, and $C_{20}H_{30}N_4O_{14\text{-}22}$). These product families can be further assigned as the first- or second-generation based on their time series.

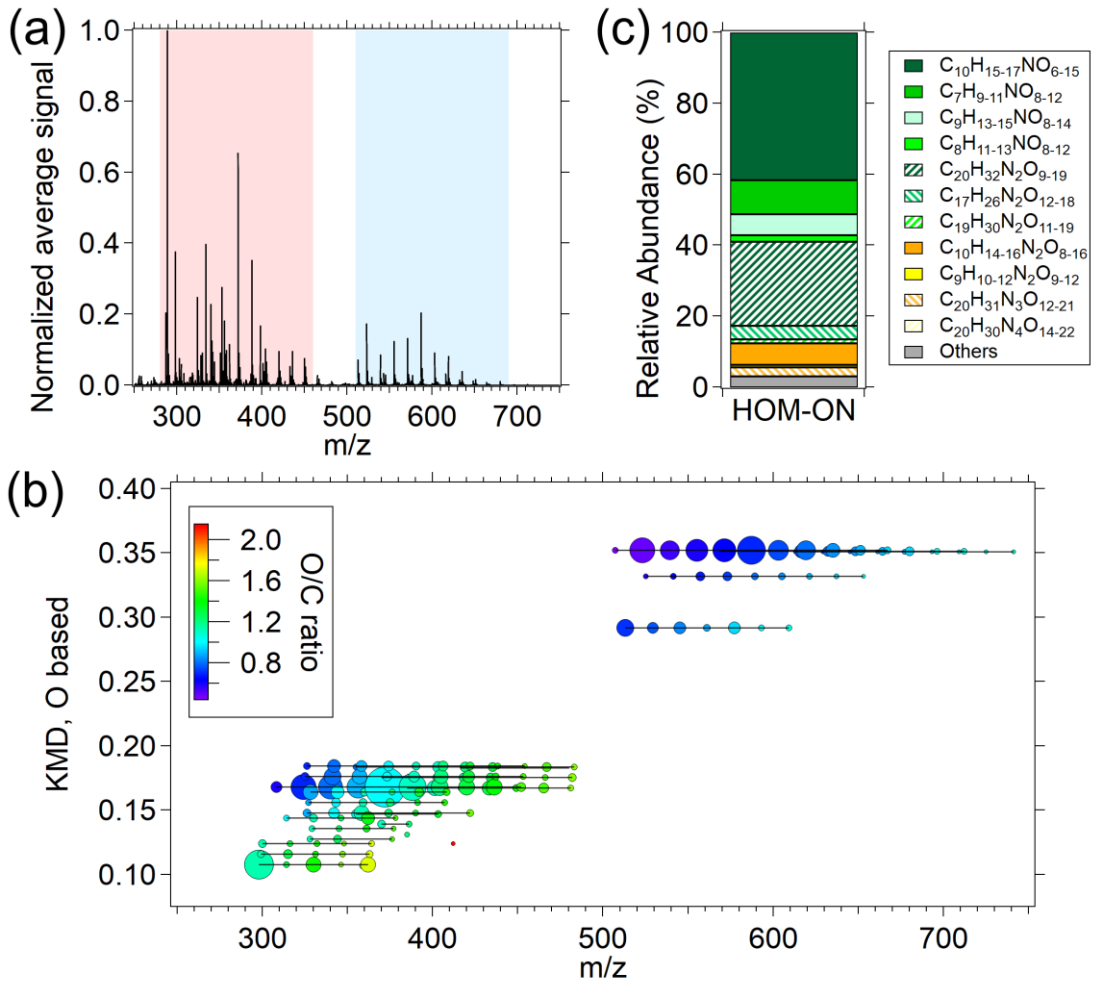

Figure 1. (a) Representative average mass spectrum of HOM-ON formed in this study, shown here for the first experimental period between the first and second β-pinene addition. (b) Kendrick mass defect (O-based) of identified products, with the area representing relative abundance and the color denoting the O/C value. (c) Stacked bar chart of identified product families, with first-generation products in green shades, second-generation products in yellow shades, and the remainder in gray.

Generally, first-generation products constituted a major fraction of total products (see figure 1c), with a value of 87.6%, including monomers of $C_{10}H_{15-17}NO_{6-15}$ (41.6%), $C_7H_{9-11}NO_{8-12}$ (9.6%), $C_9H_{13-15}NO_{8-14}$ (6.0%), and $C_8H_{11-13}NO_{8-12}$ (1.8%) and accretion products of $C_{20}H_{32}N_2O_{9-19}$ (23.7%), $C_{17}H_{26}N_2O_{12-18}$ (3.8%), and $C_{19}H_{30}N_2O_{11-19}$ (1.1%). Second-generation products, including monomers of $C_{10}H_{14-16}N_2O_{8-16}$ (6.0%) and $C_9H_{10-12}N_2O_{9-12}$

(0.74%) and accretion products of $C_{20}H_{31}N_3O_{12\text{-}21}$ (2.5%) and $C_{20}H_{30}N_4O_{14\text{-}22}$ (0.080%) were observed. Finally, the remaining 3.1% of the identified products could not be attributed to any of the above product families or could their structure be elucidated by a suitable mechanism pathway, but they are clearly products from β-pinene + NO_3 reactions based on their time series; here, they are simply grouped as "others". All of the above-identified compounds are organic nitrates, and their formation mechanism will be discussed below. We would like to note that low peaks constituting less than 0.1% of the largest product peak $C_{10}H_{15}NO_{10}$ were not assigned.

First-Generation HOM-ON and Their Formation Mechanism. A number of monomer and accretion product families were observed with a typical first-generation time series. They were quickly formed after each β-pinene addition and reached a peak concentration about 7 min later. This rapid reaction rate indicates an autoxidation formation pathway, which has a short time-scale of tens of seconds per oxidation step or less.[32] The detailed chemical composition and possible formation mechanism of these first-generation products, including C10 HOM-ON, C7-9 HOM-ON, and accretion products, are discussed in the following sections.

First-generation C10 HOM-ON. Among the first-generation product families, $C_{10}H_{15\text{-}17}NO_{6\text{-}15}$ was the most abundant. Considering how the RO_2• radical chain is terminated to form closed-shell products (see the SI),[33] they are likely to be formed via $C_{10}H_{16}NO_x$•. It has been well-established that the reaction of β-pinene + NO_3 is initiated

by the addition of NO_3 radical to the C=C double bond resulting in a nitrooxyalkyl radical $C_{10}H_{16}NO_3$• (NO_3-R•), as shown in Scheme S2. In the atmosphere, this NO_3-R• will be quickly converted to a nitrooxyperoxy radical $C_{10}H_{16}NO_5$• (NO_3-RO_2•) by reaction with O_2. Via autoxidation, $C_{10}H_{16}NO_5$• radicals rapidly undergo unimolecular H-shift and O_2 addition, resulting in a progressive series of $C_{10}H_{16}NO_{2n+1}$• radicals. Meanwhile, RO_2• such as the $C_{10}H_{16}NO_5$• radical can be involved in bimolecular reactions, including reaction with RO_2•, NO_3, HO_2•, NO_2, and NO.[50] Their reaction loss rates (Figure S6) were quantified using a zero-dimensional (0D)-model based on the Master Chemical Mechanism (MCM) v3.3.1,[39, 51] with detailed calculations in Section S2. The loss rates of RO_2• + RO_2• and RO_2• + NO_3 reactions are much higher than the reaction RO_2• with HO_2•, NO_2, and NO, especially within the short period after each β-pinene addition. Overall, bimolecular reactions within this study were then dominated by RO_2• + RO_2• and RO_2• + NO_3 reactions, where both reactions form nitrooxyalkoxy radicals (NO_3-RO•), while the RO_2• self- and cross-reactions also lead to radical chain termination (Russel mechanism, see Scheme S1b,c).

For the formation of $C_{10}H_{16}NO_{2n}$•, an "alkoxy-peroxy" pathway provides a plausible mechanism.[33, 45] For example, the nitrooxyalkoxy radical $C_{10}H_{16}NO_4$• can be competitively formed from the initially formed NO_3-RO_2• ($C_{10}H_{16}NO_5$•) and then undergo H-migration and O_2 addition forming $C_{10}H_{16}NO_6$•.[52, 53] This peroxy radical can then again undergo further autoxidation; such an autoxidation path through an alkoxy radical stage is called an

alkoxy-peroxy pathway, and yields the progressive series of $C_{10}H_{16}NO_{2n}$• products (with an even number of O atoms). In this study, both $C_{10}H_{16}NO_{2n+1}$• and $C_{10}H_{16}NO_{2n}$• radicals were observed, with time series of the most abundant radicals $C_{10}H_{16}NO_9$• and $C_{10}H_{16}NO_8$• shown in Figure 2a. Both $C_{10}H_{16}NO_9$• and $C_{10}H_{16}NO_8$• concentrations followed a typical time series as expected for a first-generation radical, quickly formed after each β-pinene addition, reaching a peak about 2-3 min later, and followed by a subsequently sharp decay. Interestingly, the peak concentration of the $C_{10}H_{16}NO_9$• showed about 30-60 s earlier than that of $C_{10}H_{16}NO_8$•. This time lag is also observed between other $C_{10}H_{16}NO_{2n+1}$• and $C_{10}H_{16}NO_{2n}$•, as shown in Figure S7. As the individual wall loss rate for each compound was not determined, we are unable to compare their formation rates precisely. However, considering that the major sink of RO_2• is via chemical reactions leading to closed-shell products rather than wall loss, this time lag can be explained by the formation mechanism of $C_{10}H_{16}NO_{2n}$•, which is expected to involve a longer-lived RO_2• intermediate that must undergo a bimolecular step forming NO_3-RO• in either NO_3-RO_2• + RO_2• or NO_3-RO_2• + NO_3 reactions, as opposed to directly produced $C_{10}H_{16}NO_{2n+1}$•. To our knowledge, no previous studies have reported such temporal lag between the formation process of radicals containing odd and even oxygen atoms.

According to previous studies, the final fate of these radicals in general is radical chain termination by RO_2• which is expected to produce an equal amount of carbonylnitrates and hydroxynitrates via the Russell mechanism, termination by HO_2• resulting in

hydroperoxynitrates,[33] or termination by unimolecular decomposition forming small radical fragments such as OH or NO_2 (see the SI). The time series of a typical NO_3-RO_2• ($C_{10}H_{16}NO_9$•) along with the corresponding termination products (carbonylnitrates of $C_{10}H_{15}NO_8$, hydroxynitrates of $C_{10}H_{17}NO_8$, and hydroperoxynitrates of $C_{10}H_{17}NO_9$) are shown in Figure 2b. Note that hydroxynitrate formed from $C_{10}H_{16}NO_x$• and hydroperoxynitrate formed from $C_{10}H_{16}NO_{x-1}$• share the same product formula and cannot be distinguished based on the mass spectra. Thus, $C_{10}H_{17}NO_8$ and $C_{10}H_{17}NO_9$ here are mixtures containing both hydroxynitrates and hydroperoxynitrates, whereas these corresponding termination products demonstrated a typical time series of first-generation products, with a quick peak appearance after each β-pinene addition and subsequent decay. Notably, the carbonylnitrates $C_{10}H_{15}NO_8$ showed a much higher signal than the other two termination products. The dominance of carbonylnitrates was commonly observed within the $C_{10}H_{15\text{-}17}NO_{6\text{-}15}$ family and will be discussed in detail below. Additionally, the termination products, especially for carbonylnitrates of $C_{10}H_{15}NO_8$, peaked about 3-6 min later than $C_{10}H_{16}NO_9$•. This time window is suggested to be due to the termination process in the autoxidation chain. To our knowledge, this is the first time such temporal formation lag between radicals and the corresponding termination products is demonstrated.

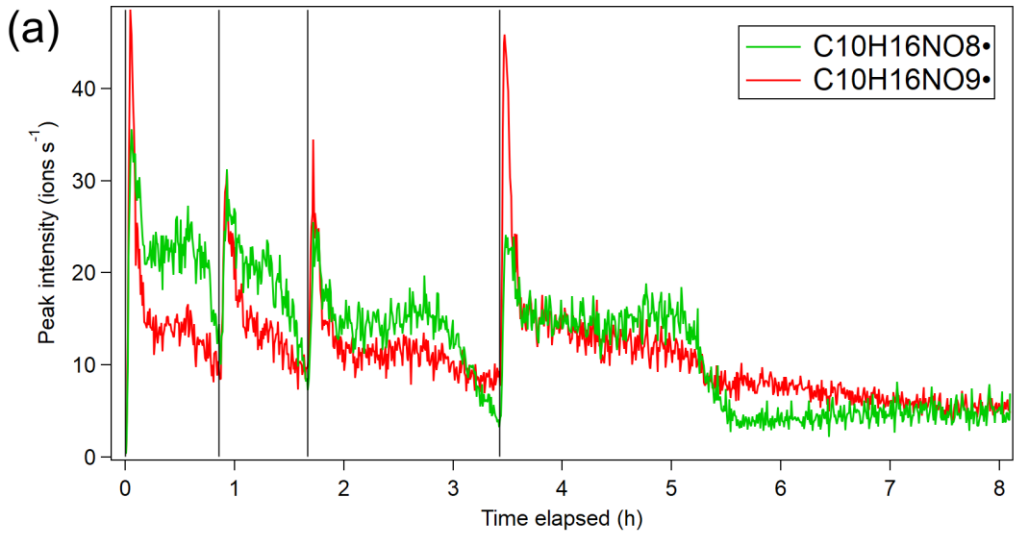
(a)
C10H16NO8•
C10H16NO9•
Peak intensity (ions s-1)
Time elapsed (h)

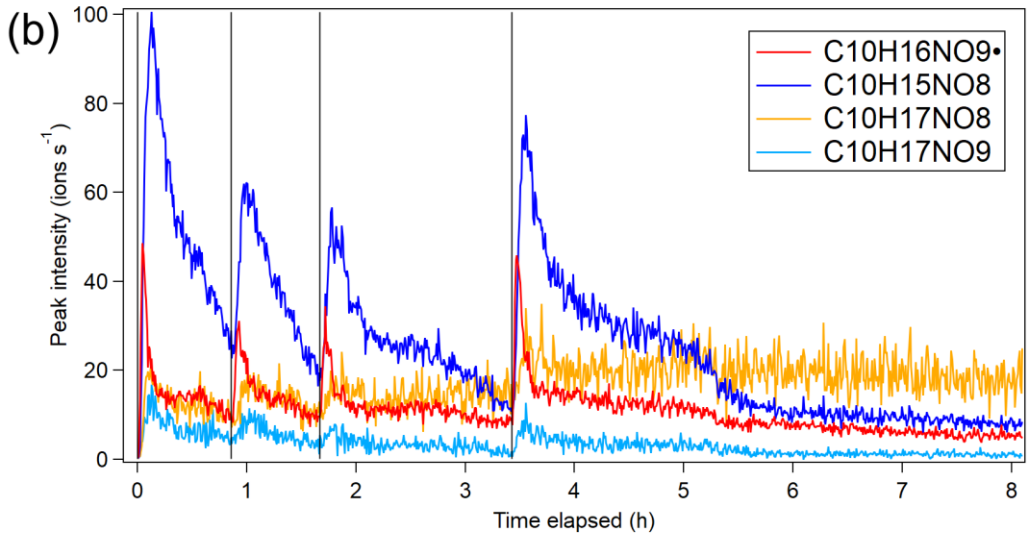
(b)
C10H16NO9•
C10H15NO8
C10H17NO8
C10H17NO9
Peak intensity (ions s-1)
Time elapsed (h)

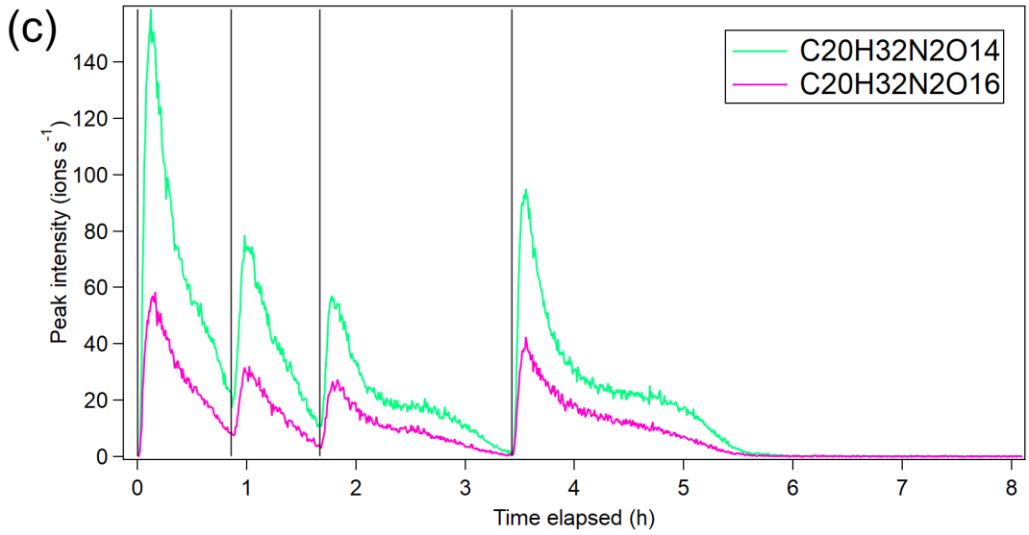
(c)
C20H32N2O14
C20H32N2O16
Peak intensity (ions s-1)
Time elapsed (h)

329

Figure 2. Time series of (a) $C_{10}H_{16}NO_8$• (green) and $C_{10}H_{16}NO_9$• (red) peroxy radicals, (b) $C_{10}H_{16}NO_9$• peroxy radical (red) and its corresponding termination products, including carbonylnitrates of $C_{10}H_{15}NO_8$ in dark blue, hydroxynitrates of $C_{10}H_{17}NO_8$ in yellow, and hydroperoxynitrates of $C_{10}H_{17}NO_9$ in light blue, and (c) accretion products of $C_{20}H_{32}N_2O_{14}$ (lime) and $C_{20}H_{32}N_2O_{16}$ (rose). The four vertical markers indicate β-pinene additions into the chamber. All signals were averaged over binned 30 s intervals.

For $C_{10}H_{16}NO_{6\text{-}15}$• peroxy radicals (corresponding to the $C_{10}H_{15\text{-}17}NO_{6\text{-}15}$ family), similar relative abundances were observed independent of odd or even numbers of O atoms (Table 1). This illustrates the importance of the alkoxy-peroxy pathway in this product family. For termination products, it should be noted that every $C_{10}H_{17}NO_x$ signal, as discussed above, comprises contributions of both hydroxynitrates and hydroperoxynitrates. Nevertheless, it is obvious that carbonylnitrates showed much higher abundances than hydroxynitrates, apparently different from the 1:1 equivalence of carbonyl/hydroxy products in the Russell mechanism, which was an important bimolecular termination channel in this study. Several mechanisms have been described in the literature that can explain this higher abundance of carbonyls. Given that these HOM-RO_2• formed via autoxidation contain multiple -OOH groups, the likely mechanism is the H-migration of an α-OOH hydrogen atom, forming an OH and a carbonyl (see Reaction S1h) and no alcohol.[32, 33, 54-56] Such a H-shift termination pathway was likewise used to explain the formation of the highest intensity peak of carbonylnitrate $C_{10}H_{15}NO_7$ from Δ-3-carene + NO_3.[41] Alternative possible pathways leading to higher abundance of carbonyls include: (1) the reaction of alkoxy RO• + O_2 forming carbonyls and HO_2•,[57] (2) decomposition of β-nitrooxyperoxynitrate,[58] (3) self-reactions of RO_2• via the Bennett and Summers

mechanism, and (4) possible unequal yield of carbonyl and hydroxyl corresponding to a given RO_2• in the cross reactions, and some other pathways. However, kinetic studies have found relatively lower rate constants (4.7×10^4 s^{-1}) for the reaction of RO• with O_2 than that of other RO• reactions, including decomposition (1.5×10^2 s^{-1} - 1.3×10^8 s^{-1}) and isomerization (2.5×10^5 s^{-1} - 3.4×10^7 s^{-1}).[53, 59-61] The decomposition of β-nitrooxyperoxynitrate formed in RO_2• + NO_2 reactions is fast in the particle phase but preferentially redissociates back to NO_3-RO_2• in the gas-phase.[62] The Bennett and Summers mechanism of RO_2• + RO_2• → $2R_HC{=}O$ + H_2O_2 was mostly reported in heterogeneous oxidation reactions and was not previously included in the gas-phase reactions.[63, 64] For cross-reactions between a small and big RO_2•, statistically an equal amount of hydroxyl and carbonyl products are expected for a large number of different RO_2•, despite potential preferences in a single case, unless an RO_2• is a tertiary or acyl RO_2•. An equal amount of hydroxyl and carbonyl is also recommended in current MCM[65, 66] and the review of Jenkin et al.[50] Furthermore, overall bimolecular loss rates of RO_2• are less than 1.5×10^{-2} s^{-1}, as shown in Figure S6. If we assume a unimolecular termination reaction rate of >0.1 s^{-1} for the HOM-RO_2• as reported both experimental measurements[32, 54, 67, 68] and theoretical studies[56, 69, 70] for RO_2• with an α-OOH hydrogen, the unimolecular termination pathway outweighs bimolecular reactions. Although the exact chemical structures of the RO_2• in this study are different from those in the literature,[32, 54, 68] they likely contain α-OOH hydrogen atoms and can be assumed to have similar unimolecular

373 reaction rates. Therefore, instead of the above discussed alternative four pathways,
374 unimolecular termination pathways are likely to be the major contributor to the high gas-
375 phase yields of carbonylnitrates observed.

376

377 **Table 1.** Family of $C_{10}H_{15\text{-}17}NO_{6\text{-}15}$ Observed, Including Nitrooxyperoxy Radicals, along
378 with Their Termination Products, Carbonylnitrates, Hydroxynitrates, and
379 Hydroperoxynitrates.[a]
380

nitrooxyperoxy radical m	carbonylnitrate m-17	hydroxynitrate m-15	hydroperoxynitrate m+1
$C_{10}H_{16}NO_7$• 1.9%	$C_{10}H_{15}NO_6$ 4.8%		$C_{10}H_{17}NO_7$ 1.1%
$C_{10}H_{16}NO_8$• 14.2%	$C_{10}H_{15}NO_7$ 34.6%	$C_{10}H_{17}NO_7$ 1.1%	$C_{10}H_{17}NO_8$ 7.8%
$C_{10}H_{16}NO_9$• 10.0%	$C_{10}H_{15}NO_8$ 32.7%	$C_{10}H_{17}NO_8$ 7.8%	$C_{10}H_{17}NO_9$ 4.4%
$C_{10}H_{16}NO_{10}$• 2.5%	$C_{10}H_{15}NO_9$ 26.6%	$C_{10}H_{17}NO_9$ 4.4%	$C_{10}H_{17}NO_{10}$ 3.0%
$C_{10}H_{16}NO_{11}$• 4.2%	$C_{10}H_{15}NO_{10}$ 100%	$C_{10}H_{17}NO_{10}$ 3.0%	$C_{10}H_{17}NO_{11}$ 2.1%
$C_{10}H_{16}NO_{12}$• 8.7%	$C_{10}H_{15}NO_{11}$ 42.0%	$C_{10}H_{17}NO_{11}$ 2.1%	$C_{10}H_{17}NO_{12}$ 3.5%
$C_{10}H_{16}NO_{13}$• 5.2%	$C_{10}H_{15}NO_{12}$ 14.3%	$C_{10}H_{17}NO_{12}$ 3.5%	$C_{10}H_{17}NO_{13}$ 1.9%
$C_{10}H_{16}NO_{14}$• 1.1%	$C_{10}H_{15}NO_{13}$ 11.7%	$C_{10}H_{17}NO_{13}$ 1.9%	$C_{10}H_{17}NO_{14}$ 0.6%
$C_{10}H_{16}NO_{15}$• 0.80%	$C_{10}H_{15}NO_{14}$ 13.2%	$C_{10}H_{17}NO_{14}$ 0.6%	$C_{10}H_{17}NO_{15}$ 0.19%
	$C_{10}H_{15}NO_{15}$ 2.8%	$C_{10}H_{17}NO_{15}$ 0.19%	

381 [a] The relative intensities for the species detected in this study during the first reaction period
382 are shown on the second line in the same cell. Their relative intensities were normalized to
383 the largest product signal of $C_{10}H_{15}NO_{10}$.

Scheme 1 shows a plausible subset of the degradation scheme, based on structure-activity relationships (SARs) and recent experimental data,[20, 71] and starting at the tertiary NO_3-R• $C_{10}H_{16}NO_3$• (R1) preferentially formed upon initial NO_3 addition to β-pinene. Similar to the OH-initiated oxidation,[72, 73] breaking of the four-membered ring has been reported as a favorable pathway, forming R2,[20, 21] which after O_2 addition forms an unsaturated tertiary $C_{10}H_{16}NO_5$• (R3) radical. A structure similar to R3 was reported in the β-pinene + OH system and was suggested to undergo quick unimolecular reactions.[72, 74-76] Moreover, recent studies have shown that a C=C double bond in an RO_2• radical is a key functionality, leading to fast unimolecular reactions.[56, 77] Thus, we suggest that R3 opens a gateway to fast unimolecular reactions, including autoxidation. The expected rate coefficient of the following unimolecular H-shift has been derived using the SAR by Vereecken and Nozière.[56] Nitrooxyperoxy radical R5 can undergo a rapid scrambling reaction to produce R6, which can either undergo a 1,5 H-shift to form R7, or be terminated via 1,6 H-shift to form carbonylnitrate $C_{10}H_{15}NO_6$ (P1) + OH. Similar unimolecular H-shift termination reactions are suggested for R8, R10, and R12, producing carbonylnitrates. All of these $C_{10}H_{16}NO_{2n+1}$• radicals (R5, R8, R10, R12) could also undergo bimolecular reactions with RO_2•/NO_3 to form $C_{10}H_{16}NO_{2n}$•. Taking R5 as an example, the resulting R13 followed by an H-shift leads to the formation of R14. Both the -OH group and the C=C double bond within R14 further favor fast unimolecular reactions,[56] leading to more oxidized $C_{10}H_{16}NO_{2n}$• radicals via autoxidation or to the formation of P1. Note that Scheme

1 is just one of many possible unimolecular reaction chains, and some radicals observed in this study are not included in Scheme 1, such as the formation of $C_{10}H_{16}NO_{15}$•. Further rigorous studies are needed to constrain its unimolecular pathway. Additionally, the C=C double bond in some of these products can be attacked by the NO_3 radical and lead to second-generation products, which was also observed in this study and will be discussed below. Note that this is not the only pathway leading to HOM. Nah et al.[30] proposed a ring-retaining pathway, with a simplified mechanism shown in Scheme S3a. However, this pathway cannot explain the formation of the second-generation products (e.g., $C_{10}H_{14-16}N_2O_{8-16}$) and C7 compounds in this study. Moreover, according to previous studies,[74, 77] the ring-opening pathway is more likely to lead to autoxidation and to HOM in many monoterpene oxidation reactions, such as α-pinene + NO_3[78] and β-pinene + OH[72-74, 77] due to the steric hindrance for H-shift in the ring-retaining RO_2•. Particularly, for β-pinene, the yield of ring-opening RO_2• is expected to be high, as shown in the work of Vereecken and Peeters[72] and Kaminski et al.[73] for the reaction of β-pinene + OH. Overall, combining our observation and the literature above, HOM formation is more likely to be formed via the ring-opening pathway in β-pinene + NO_3 reactions, although the autoxidation pathway is complex and still not fully clear in this reaction system and multiple pathways might be present simultaneously. Claflin and Ziemann[21] proposed another ring-opening pathway (Scheme S3b). For the two ring-opening pathways, their relative importance is currently unclear. Compared to Nah et al.[30] and Claflin and Ziemann,[21] Scheme 1 provides a

formation pathway for RO_2• containing the C=C double bond, which leads to fast HOM-ON formation and provides a plausible explanation for the second-generation products observed in this study.

Scheme 1. Example Unimolecular Pathway Chain of β-pinene + NO_3 Reactions Leading to the Formation of HOM-ON, specifically Carbonylnitrates.[a]

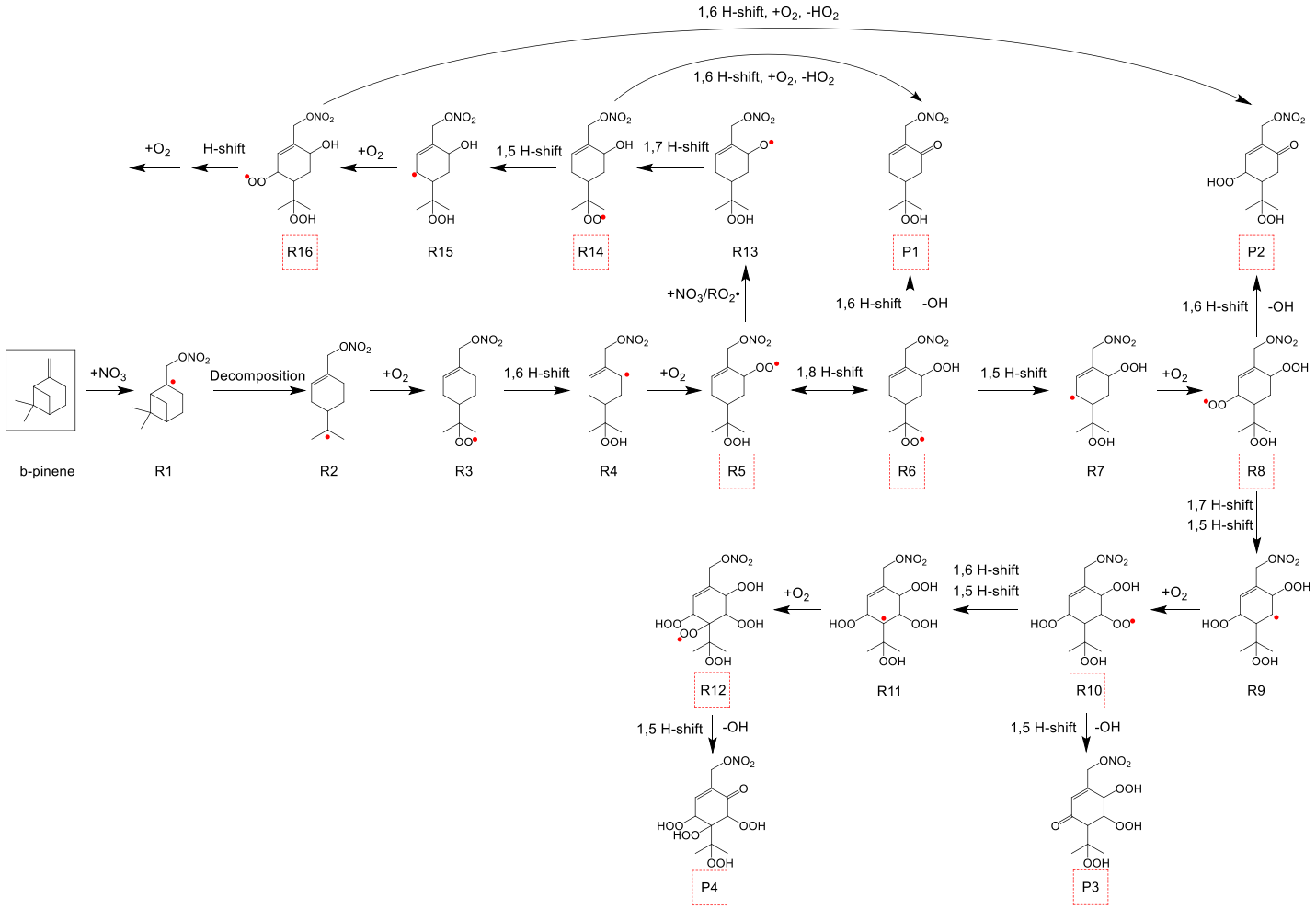

[a] The formula of radicals and products observed in the experiments were highlighted in red-dashed boxes. This is only a small subset of the full oxidation mechanism omitting many competing channels and is not intended to be complete.

First-Generation C7-9 HOM-ON. Besides C10 products, C7-9 compounds were also observed in this study, including product families of $C_7H_{9-11}NO_{8-12}$, $C_9H_{13-15}NO_{8-14}$, and $C_8H_{11-13}NO_{8-12}$, consistent with the study by Nah et al.[30] These first-generation products were suggested to be formed from the decomposition of NO_3-RO• radicals followed by an autoxidation pathway. This decomposition process was already recognized as another important unimolecular reaction, forming ring-opened products.[72, 75, 78, 79] Taking $C_7H_{9-11}NO_{8-12}$ as an example for R3, besides the fast H-shift as shown in Scheme 1, it can undergo bimolecular reactions with RO_2• or NO_3 reactions forming a NO_3-RO•, which will further decompose into acetone and an unsaturated NO_3-R•, such as $C_7H_{10}NO_3$•,[75, 76] as shown in Scheme S4. Radicals like $C_7H_{10}NO_3$• can react with O_2, forming $C_7H_{10}NO_5$•, which can then further undergo autoxidation.

Similar to the $C_{10}H_{15-17}NO_{6-15}$ family, the $C_7H_{9-11}NO_{8-12}$ family followed a typical first-generation time series, with a representative radical $C_7H_{10}NO_9$• and its corresponding termination products shown in Figure S8. When β-pinene was added, $C_7H_{10}NO_9$• peaked instantaneously, followed by the formation of $C_7H_9NO_8$, $C_7H_{11}NO_8$, and $C_7H_{11}NO_9$. A time window of 3-4 min between the peaks of radicals and termination products was observed, indicating the typical period of the termination processes. Carbonylnitrates were again observed as the dominant termination products, suggesting termination by unimolecular H-shift and OH formation to be a major reaction pathway in the $C_7H_{9-11}NO_{8-12}$ family as well. Moreover, higher concentrations, as well as higher carbonylnitrate abundance, were

observed in $C_7H_{10}NO_{2n+1}$• compared to $C_7H_{10}NO_{2n}$•. This indicates that the alkoxy-peroxy channel is a minor, less competitive pathway in the $C_7H_{9\text{-}11}NO_{8\text{-}12}$ family. Additionally, a distinct increase of acetone from 0.04 ppb to 0.44 ppb was observed throughout the experiments, as shown in Figure S1. This confirms the presence of fragmentation process in β-pinene + NO_3, such as the above discussed C_{10} decomposition to form C_7 compounds and acetone. The two remaining product families, $C_9H_{13\text{-}15}NO_{8\text{-}14}$ and $C_8H_{11\text{-}13}NO_{8\text{-}12}$, were hypothesized to be formed in a similar pathway, but the exact bond scission position is not yet known.

First-Generation Accretion Products. Three accretion product families were found to follow a typical first-generation product time series, including $C_{20}H_{32}N_2O_{9\text{-}19}$, $C_{17}H_{26}N_2O_{12\text{-}18}$, and $C_{19}H_{30}N_2O_{11\text{-}19}$. Recent studies have identified the importance of rapid reaction of RO_2• + RO_2• → ROOR + O_2 in the formation of gas-phase accretion products.[80-82] Figure S10 lists the expected accretion products produced from the above-identified NO_3-RO_2• monomers. These three accretion product families can all be explained via RO_2• self- or cross-reaction channels. Notably, $C_{20}H_{32}N_2O_{9\text{-}19}$ were the most abundant accretion products, consistent with the dominance of its corresponding parent NO_3-RO_2•. Figure 2c shows the time series of $C_{20}H_{32}N_2O_{14,16}$, formed from self-reaction of $C_{10}H_{16}NO_{8,9}$• discussed above. Both of them peaked about 6-8 min after each β-pinene addition and decayed afterward. This is consistent with a quick formation process from RO_2• reactions. Moreover, $C_{20}H_{32}N_2O_{14}$ was the most abundant product among the $C_{20}H_{32}N_2O_{9\text{-}19}$ family.

Its corresponding precursor $C_{10}H_{16}NO_8$• also dominated among $C_{10}H_{16}NO_x$• as shown in Figure S11. However, it should be noted that accretion products with the same formula could arise from cross-reactions of several combinations of RO_2•; for example, $C_{10}H_{16}NO_7$• + $C_{10}H_{16}NO_9$• or $C_{10}H_{16}NO_6$• + $C_{10}H_{16}NO_{10}$• could both contribute to $C_{20}H_{32}N_2O_{14}$. Currently, we cannot quantify the relative contribution of different RO_2• recombinations to the accretion products, as the reaction rate coefficients of RO_2• self- or cross-reactions depend on specific RO_2•, and many of them are unknown.[81] The two remaining product families, $C_{17}H_{26}N_2O_{12\text{-}18}$ and $C_{19}H_{30}N_2O_{11\text{-}19}$, showed a similar first-generation time series and likewise followed RO_2• self- and cross-reaction channels.

Second-Generation HOM-ON and Their Tormation Mechanism. Two monomer families ($C_{10}H_{14\text{-}16}N_2O_{8\text{-}16}$ and $C_9H_{10\text{-}12}N_2O_{9\text{-}12}$) and two accretion product families ($C_{20}H_{31}N_3O_{12\text{-}21}$ and $C_{20}H_{30}N_4O_{14\text{-}22}$), which contain two N atoms (monomers) and three or more N atoms (accretion products), showed a time series differing from first-generation products. They mostly showed a concentration peak after β-pinene addition at a much later phase than typical first-generation products, shown in Figure S9. These compounds were assigned as second-generation reaction products. Among those, $C_{10}H_{14\text{-}16}N_2O_{8\text{-}16}$ dominated and were suggested to be formed via NO_3 addition to the first-generation carbonylnitrates products ($C_{10}H_{15}NO_{6\text{-}15}$). As discussed above, the carbonylnitrates formed via unimolecular H-shift termination reactions contain one C=C double bond, which can be attacked by NO_3 radicals to form $C_{10}H_{15}N_2O_x$•. For example, P2 in Scheme 1 could form

493 a tertiary dinitrooxyalkyl radical [$(NO_3)_2$-R•] $C_{10}H_{15}N_2O_{11}$•, which will be quickly
494 converted to a dinitrooxyperoxy radical [$(NO_3)_2$-RO_2•] $C_{10}H_{15}N_2O_{13}$• via O_2 addition, as
495 shown in Scheme S5. This radical can undergo a unimolecular H-shift to either propagate
496 the radical chain or terminate it by the formation of carbonyldinitrates + OH. Via
497 bimolecular reactions of RO_2• + RO_2•, carbonyldinitrates ($C_{10}H_{14}N_2O_x$) and
498 hydroxydinitrates ($C_{10}H_{16}N_2O_x$) can be formed, and hydroperoxydinitrates ($C_{10}H_{16}N_2O_x$)
499 can be formed via RO_2• + HO_2•. These second-generation HOM-ON have not been
500 reported in previous β-pinene + NO_3 studies because these studies mainly focused on the
501 first-generation products and/or used different analysis methods.[20, 21, 30] The observation of
502 these dinitrates in this study highlighted the importance of the C=C double bond formed in
503 R2 in Scheme 1.

504 Accretion products, such as $C_{20}H_{31}N_3O_{12\text{-}21}$ and $C_{20}H_{30}N_4O_{14\text{-}22}$, were also observed
505 and are generated from self- or cross-reactions of later generation RO_2•, likely formed via
506 reactions of $C_{10}H_{15}N_2O_x$• + $C_{10}H_{16}NO_x$• and $C_{10}H_{15}N_2O_x$• + $C_{10}H_{15}N_2O_x$•, respectively.
507 Figure 3a shows the time series of a typical $(NO_3)_2$-RO_2• $C_{10}H_{15}N_2O_9$•, compared against
508 that of $C_{20}H_{30}N_4O_{16}$, the accretion products resulting from its self-reaction. Both of them
509 gradually increased after each β-pinene addition. Moreover, when $C_{10}H_{15}N_2O_9$• reached
510 peak concentration, the signal of $C_{20}H_{30}N_4O_{16}$ showed the largest rate of change. This is
511 consistent with the kinetics shown in eq 2.

512 $$\frac{d[C_{20}H_{30}N_4O_{16}]}{dt} = k_r[C_{10}H_{15}N_2O_9\ \bullet]^2 - k_w[C_{20}H_{30}N_4O_{16}] \quad (2)$$

513 where k_r and k_w are rate constant of $C_{10}H_{15}N_2O_9$• self-reaction and the wall loss rate of
514 $C_{20}H_{30}N_4O_{16}$, respectively. A linear relationship between the rate of accretion products
515 produced and the squared concentrations of RO_2• has also been reported in previous HOM
516 studies.[6, 82] Accretion products of $C_{20}H_{31}N_3O_x$ formed from $C_{10}H_{15}N_2O_x$• + $C_{10}H_{16}NO_x$•
517 were also observed in this study, with the representative time series of $C_{20}H_{31}N_3O_{16}$ and its
518 corresponding precursors RO_2•, $C_{10}H_{15}N_2O_9$• and $C_{10}H_{16}NO_9$•, as shown in Figure 3b. The
519 radical $C_{10}H_{15}N_2O_9$• and its accretion product $C_{20}H_{31}N_3O_{16}$ likewise followed a time series
520 typical of second-generation products, as well as a similar kinetic dependence. The
521 concentrations of $C_{20}H_{31}N_3O_{16}$ peaked earlier than its precursor RO_2• corresponding
522 second-generation $C_{10}H_{15}N_2O_9$• while $C_{20}H_{30}N_4O_{22}$ showed up later than $C_{10}H_{15}N_2O_9$•.
523 This can be because another precursor RO_2• of $C_{20}H_{31}N_3O_{16}$, $C_{10}H_{16}NO_9$•, is a first-
524 generation feature that accelerates the formation of $C_{20}H_{31}N_3O_{16}$. Additionally,
525 $C_{20}H_{31}N_3O_{16}$ showed a small peak after β-pinene addition, especially those in third and
526 fourth β-pinene additions. This shows that $C_{20}H_{31}N_3O_{16}$ followed the trend of its first-
527 generation radical $C_{10}H_{16}NO_9$• more and indicated a role in the cross-reaction formation of
528 $C_{20}H_{31}N_3O_{16}$. Overall, the above discussion on kinetics further confirms the contribution
529 of RO_2• self- and cross-reactions to the accretion product formation in this study.

530 Finally, we observed a family of C_9 products with second generation behavior. We
531 suggest that the second-generation $C_9H_{10\text{-}12}N_2O_{9\text{-}12}$ was likely to be formed by a secondary
532 NO_3 addition pathway, similarly to $C_{10}H_{14\text{-}16}N_2O_{8\text{-}16}$. However, the first generation of

unsaturated C_9 compounds from β-pinene + NO_3 was not detected with our technique, such that the detailed formation mechanism of $C_9H_{10\text{-}12}N_2O_{9\text{-}12}$ cannot be elucidated at this time.

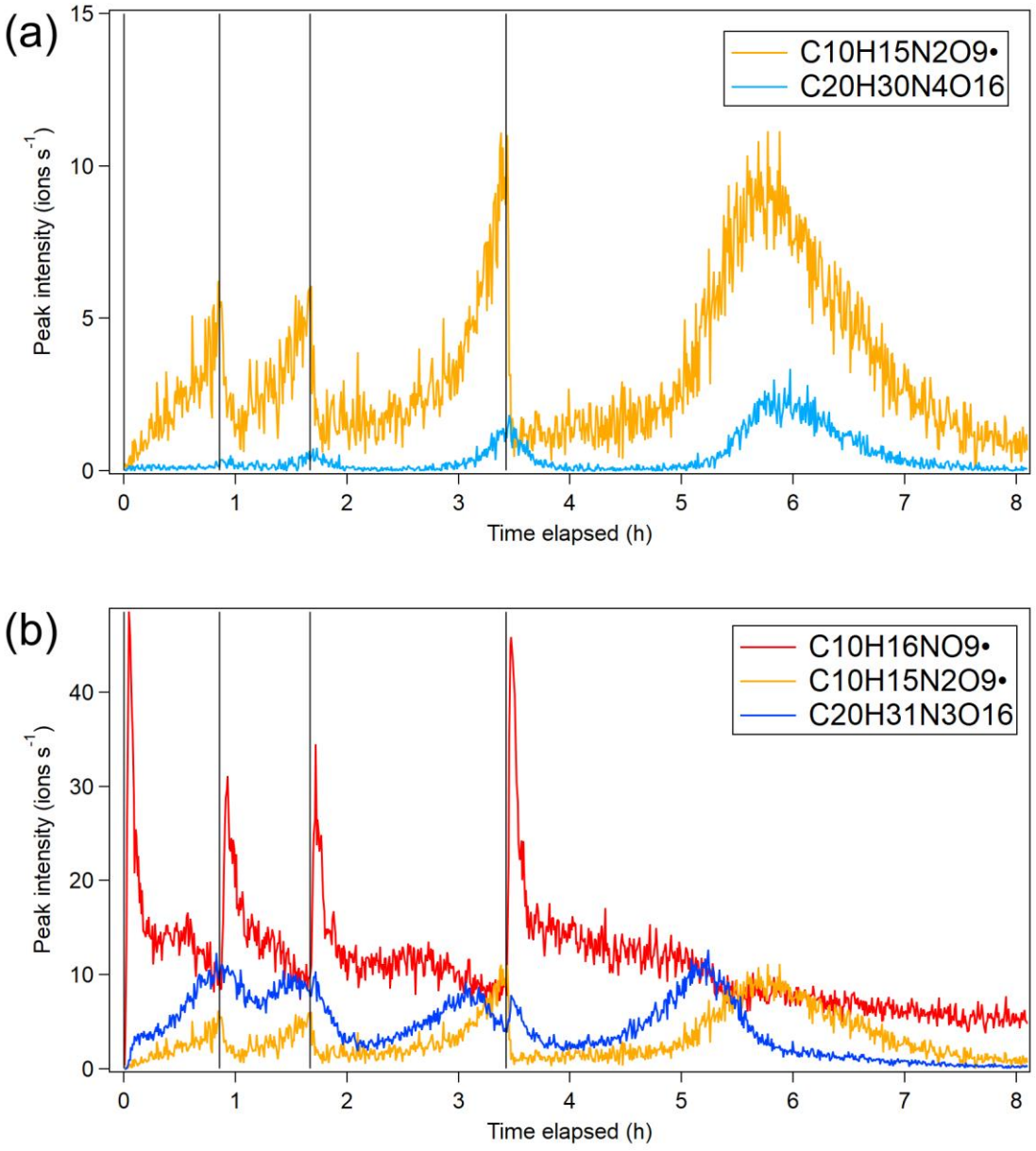

Figure 3. Time series of (a) a representative second-generation peroxy radical ($C_{10}H_{15}N_2O_{12}$•, orange) and its self-reaction accretion product ($C_{20}H_{30}N_4O_{16}$, cyan), and (b) $C_{20}H_{31}N_3O_{16}$ (navy) resulting from the cross-reaction of $C_{10}H_{15}N_2O_{12}$• (orange) and $C_{10}H_{16}NO_9$• (red). The four vertical markers indicate β-pinene additions into the chamber. All signals were averaged over binned 30 s intervals for plotting.

Production Yield Determination. The molar yield of HOM-ON (O≥6) in the NO_3 oxidation of β-pinene was estimated to be 4.8% (-2.6%/+5.6%). The large uncertainty in HOM yield is attributed to a number of factors, including the HOM-ON peak intensity, β-pinene concentration, calibration factor, and transmission efficiency, as described in the Experimental and Methods section and the SI. Note that the HOM produced during this short reaction time (10 min) consists of 93.4% first-generation products and 4.4% second-generation products. This reported value refers to a primary HOM yield. Compared to molar yields of HOM from β-pinene oxidation by O_3 or OH radicals (<0.1%),[6, 83] the NO_3 radical is exceptionally efficient in oxidizing β-pinene to produce HOM. Moreover, the average value of all currently determined HOM yields is around 5%, including OH, O_3, and Cl systems.[27, 84] This means the reaction of β-pinene + NO_3 is competitive enough to produce a sizable fraction of the HOM products. Using the signal-weighted average of the mass of the produced HOM-ON (353.7 g mol^{-1}), we estimate the mass yields to be roughly 2.6 (=353.7 g mol^{-1} / 136.1 g mol^{-1}) times the molar yield. The value in this study is slightly larger than the factor 2.4 calculated for the α-pinene ozonolysis system.[6] This indicates that reactions with NO_3 radicals lead to higher mass oxidation products, as expected, and contribute more to SOA than ozonolysis reactions. The converted mass yields of HOM-ON from β-pinene + NO_3 were averaged to 12.5% (-6.8%/+14.6%), assuming that the volatility of HOM-ON was low enough to condense irreversibly onto the particle phase.[6, 45] Considering the SOA yields of β-pinene + NO_3,[18-20, 22, 23, 26] these HOM-ON should

561 contribute a significant fraction, especially at low organic aerosol loadings in ambient
562 atmosphere. Note that the volatility of HOM-ON was not determined in this study. Yet
563 Pullinen et al.[45] determined a range of 0.5-1 for effective uptake coefficients of HOM-ON
564 from β-pinene + OH. Therefore, it is reasonable to approximate the uptake of most of the
565 HOM-ON as being irreversible when estimating their contribution to SOA. Even an uptake
566 coefficient of 0.5 would cause HOM to condense efficiently on particles. Assuming that
567 all HOM condensing on particles provides an upper limit of the contribution of HOM-ON
568 to SOA, and most of HOM will thus reside in the particle phase. Although HOM-ON in
569 this study are not identical to those in Pullinen et al.,[45] they are expected to have generally
570 similar structures, and HOM-ON contribution to SOA formation is considered to be
571 significant in β-pinene + NO_3 reactions.

572 **Atmospheric Implications**

573 We observed a large number of HOM-ON formed from NO_3 oxidation of β-pinene in
574 the SAPHIR chamber, including six monomer (C=7-10, N=1-2, O=6-16) and five accretion
575 product (C=17-20, N=2-4, O=9-22) families. An example formation mechanism was
576 proposed and constrained based on the time series of the closed-shell HOM, which were
577 different for first- and second-generation products and depended on the precursor RO_2•.
578 Such HOM-ON are expected to be formed under the conditions of the nocturnal planetary
579 boundary layer (PBL), especially when both biogenic VOC and anthropogenic NO_x sources
580 are present. Recent field studies have shown that these HOM-ON are prevalent at night-

time in the Southeastern US and contribute to a large fraction of SOA.[13, 15] The precursor peroxy radicals, especially $C_{10}H_{16}NO_9$•, formed from monoterpene + NO_3 are observed at night-time in SORPES station in eastern China, where the BVOC oxidation is strongly influenced by NO_x.[85]

Direct experimental evidence was provided in our study to highlight the importance of the unimolecular H-shift termination pathway in the NO_3 system, producing unsaturated carbonylnitrates as first-generation products, similar to OH systems.[32, 55, 74] We expect that a large portion of HOM-ON formed at night-time in the ambient atmosphere over a forest environment affected by anthropogenic emissions contains a carbonyl group and one or more -OOH groups, in addition to the initiating -NO_3 group. These unsaturated first-generation carbonylnitrates are anticipated to react further with additional NO_3 and lead to the formation of second-generation products. Although some studies found that second-generation ON containing two or more nitrogens were much less abundant than mononitrates,[86] second-generation products might be important when NO_3 is abundant or during the next day when unsaturated carbonylnitrate can react with OH.

The production yields of HOM-ON from β-pinene + NO_3 were estimated with a mean molar yield of 4.8% (-2.6%/+5.6%). This yield is much higher than the HOM yield in β-pinene oxidation by OH (0.58%) and O_3 (0.12%) reported by Jokinen et al.[83] and HOM yield in the isoprene oxidation by NO_3 (1.2%).[87] This higher HOM yield of β-pinene + NO_3 indicated the potential significance of HOM-ON to the formation of SOA in the

nocturnal PBL in areas influenced by biogenic VOC and anthropogenic NO_x emissions as observed by a number of field studies.[88] Incorporating the HOM-ON yield determined in this study into future models can lead to a better interpretation of ambient data and a more accurate prediction of atmospheric and climate effects of β-pinene + NO_3 reactions. Furthermore, negligible second-generation products are included in the production yield. It is unclear that whether their contribution to HOM yields will outweigh the first-generation products and further influence the SOA formation in the ambient atmosphere. Further laboratory studies and field observations are needed.

SUPPORTING INFORMATION

Additional information deriving the calibration coefficient of CIMS and HOM yields (Section S1) and calculations of RO_2• bimolecular loss rates (Section S2); figures showing the experimental procedure (Figure S1); relative contributions of reactions of β-pinene with NO_3 and O_3 to total β-pinene loss (Figure S2); SMPS data (Figure S3); the average mass spectrum of each experimental period (Figure S4); time series of residuals (Figure S5); RO_2• bimolecular loss rates (Figure S6); peroxy radicals of $C_{10}H_{16}NO_x$• (Figure S7); C7 compounds (Figure S8); second-generation products (Figure S9); and permutation reactions of identified first-generation NO_3-RO_2• radicals (Figure S10) and $C_{10}H_{16}NO_x$• (Figure S11). Schemes demonstrating HOM formation mechanism involving RO_2• (Scheme S1); general autoxidation of NO_3 oxidation of β-pinene (Scheme S2); the simplified HOM formation pathway proposed in prior studies (Scheme S3); the possible

formation pathway of C7 compounds (Scheme S4); and example formation pathway of second-generation products (Scheme S5); tables listing HR peak list (Table S1); reaction rates used to calculate RO_2• bimolecular loss rates (Table S2); and relative intensities of the $C_7H_{9\text{-}11}NO_{8\text{-}12}$ product family (Table S3).

ACKNOWLEDGMENTS

The authors thank the SAPHIR team for supporting our measurements and providing helpful data. H.S and D.Z would like to thank the funding support of the National Natural Science Foundation of China (41875145) and Science and Technology Commission of Shanghai Municipality (20230711400).

REFERENCES

(1) Sindelarova, K.; Granier, C.; Bouarar, I.; Guenther, A.; Tilmes, S.; Stavrakou, T.; Müller, J. F.; Kuhn, U.; Stefani, P.; Knorr, W., Global data set of biogenic VOC emissions calculated by the MEGAN model over the last 30 years. *Atmos. Chem. Phys.* **2014**, *14* (17), 9317-9341.

(2) Berndt, T.; Richters, S.; Jokinen, T.; Hyttinen, N.; Kurtén, T.; Otkjær, R. V.; Kjaergaard, H. G.; Stratmann, F.; Herrmann, H.; Sipilä, M.; Kulmala, M.; Ehn, M., Hydroxyl radical-induced formation of highly oxidized organic compounds. *Nat. Commun.* **2016**, *7*, 13677.

(3) Surratt, J. D.; Chan, A. W. H.; Eddingsaas, N. C.; Chan, M. N.; Loza, C. L.; Kwan, A. J.; Hersey, S. P.; Flagan, R. C.; Wennberg, P. O.; Seinfeld, J. H., Reactive intermediates revealed in secondary organic aerosol formation from isoprene. *Proc. Natl. Acad. Sci. U.S.A.* **2010**, *107* (15), 6640-6645.

(4) Brown, S. S.; Stutz, J., Nighttime radical observations and chemistry. *Chem. Soc. Rev.* **2012**, *41* (19), 6405-6447.

(5) Ng, N. L.; Brown, S. S.; Archibald, A. T.; Atlas, E.; Cohen, R. C.; Crowley, J. N.; Day, D. A.; Donahue, N. M.; Fry, J. L.; Fuchs, H.; Griffin, R. J.; Guzman, M. I.; Herrmann, H.; Hodzic, A.; Iinuma, Y.; Jimenez, J. L.; Kiendler-Scharr, A.; Lee, B. H.; Luecken, D. J.; Mao, J. Q.; McLaren, R.; Mutzel, A.; Osthoff, H. D.; Ouyang, B.; Picquet-Varrault, B.; Platt, U.; Pye, H. O. T.; Rudich, Y.; Schwantes, R. H.; Shiraiwa, M.; Stutz, J.; Thornton, J. A.; Tilgner, A.; Williams, B. J.; Zaveri, R. A., Nitrate radicals and biogenic volatile organic

650 compounds: oxidation, mechanisms, and organic aerosol. *Atmos. Chem. Phys.* **2017**, *17*
651 (3), 2103-2162.
652 (6) Ehn, M.; Thornton, J. A.; Kleist, E.; Sipilä, M.; Junninen, H.; Pullinen, I.; Springer, M.;
653 Rubach, F.; Tillmann, R.; Lee, B.; Lopez-Hilfiker, F.; Andres, S.; Acir, I. H.; Rissanen, M.;
654 Jokinen, T.; Schobesberger, S.; Kangasluoma, J.; Kontkanen, J.; Nieminen, T.; Kurtén, T.;
655 Nielsen, L. B.; Jørgensen, S.; Kjaergaard, H. G.; Canagaratna, M.; Dal Maso, M.; Berndt,
656 T.; Petäjä, T.; Wahner, A.; Kerminen, V. M.; Kulmala, M.; Worsnop, D. R.; Wildt, J.;
657 Mentel, T. F., A large source of low-volatility secondary organic aerosol. *Nature* **2014**, *506*
658 (7489), 476-479.
659 (7) Tröstl, J.; Chuang, W. K.; Gordon, H.; Heinritzi, M.; Yan, C.; Molteni, U.; Ahlm, L.;
660 Frege, C.; Bianchi, F.; Wagner, R.; Simon, M.; Lehtipalo, K.; Williamson, C.; Craven, J.
661 S.; Duplissy, J.; Adamov, A.; Almeida, J.; Bernhammer, A. K.; Breitenlechner, M.; Brilke,
662 S.; Dias, A.; Ehrhart, S.; Flagan, R. C.; Franchin, A.; Fuchs, C.; Guida, R.; Gysel, M.;
663 Hansel, A.; Hoyle, C. R.; Jokinen, T.; Junninen, H.; Kangasluoma, J.; Keskinen, H.; Kim,
664 J.; Krapf, M.; Kürten, A.; Laaksonen, A.; Lawler, M.; Leiminger, M.; Mathot, S.; Möhler,
665 O.; Nieminen, T.; Onnela, A.; Petäjä, T.; Piel, F. M.; Miettinen, P.; Rissanen, M. P.; Rondo,
666 L.; Sarnela, N.; Schobesberger, S.; Sengupta, K.; Sipilä, M.; Smith, J. N.; Steiner, G.; Tomè,
667 A.; Virtanen, A.; Wagner, A. C.; Weingartner, E.; Wimmer, D.; Winkler, P. M.; Ye, P. L.;
668 Carslaw, K. S.; Curtius, J.; Dommen, J.; Kirkby, J.; Kulmala, M.; Riipinen, I.; Worsnop, D.
669 R.; Donahue, N. M.; Baltensperger, U., The role of low-volatility organic compounds in
670 initial particle growth in the atmosphere. *Nature* **2016**, *533* (7604), 527-531.
671 (8) Hallquist, M.; Wenger, J. C.; Baltensperger, U.; Rudich, Y.; Simpson, D.; Claeys, M.;
672 Dommen, J.; Donahue, N. M.; George, C.; Goldstein, A. H.; Hamilton, J. F.; Herrmann,
673 H.; Hoffmann, T.; Iinuma, Y.; Jang, M.; Jenkin, M. E.; Jimenez, J. L.; Kiendler-Scharr, A.;
674 Maenhaut, W.; McFiggans, G.; Mentel, T. F.; Monod, A.; Prévôt, A. S. H.; Seinfeld, J. H.;
675 Surratt, J. D.; Szmigielski, R.; Wildt, J., The formation, properties and impact of secondary
676 organic aerosol: current and emerging issues. *Atmos. Chem. Phys.* **2009**, *9* (14), 5155-5236.
677 (9) Shrivastava, M.; Cappa, C. D.; Fan, J. W.; Goldstein, A. H.; Guenther, A. B.; Jimenez,
678 J. L.; Kuang, C.; Laskin, A.; Martin, S. T.; Ng, N. L.; Petaja, T.; Pierce, J. R.; Rasch, P. J.;
679 Roldin, P.; Seinfeld, J. H.; Shilling, J.; Smith, J. N.; Thornton, J. A.; Volkamer, R.; Wang,
680 J.; Worsnop, D. R.; Zaveri, R. A.; Zelenyuk, A.; Zhang, Q., Recent advances in
681 understanding secondary organic aerosol: implications for global climate forcing. *Rev.*
682 *Geophys.* **2017**, *55* (2), 509-559.
683 (10) Ng, N. L.; Kwan, A. J.; Surratt, J. D.; Chan, A. W. H.; Chhabra, P. S.; Sorooshian, A.;
684 Pye, H. O. T.; Crounse, J. D.; Wennberg, P. O.; Flagan, R. C.; Seinfeld, J. H., Secondary
685 organic aerosol (SOA) formation from reaction of isoprene with nitrate radicals (NO_3).
686 *Atmos. Chem. Phys.* **2008**, *8* (14), 4117-4140.
687 (11) Rollins, A. W.; Kiendler-Scharr, A.; Fry, J. L.; Brauers, T.; Brown, S. S.; Dorn, H. P.;
688 Dubé, W. P.; Fuchs, H.; Mensah, A.; Mentel, T. F.; Rohrer, F.; Tillmann, R.; Wegener, R.;

Wooldridge, P. J.; Cohen, R. C., Isoprene oxidation by nitrate radical: alkyl nitrate and secondary organic aerosol yields. *Atmos. Chem. Phys.* **2009**, *9* (18), 6685-6703.
(12) Pye, H. O. T.; Chan, A. W. H.; Barkley, M. P.; Seinfeld, J. H., Global modeling of organic aerosol: the importance of reactive nitrogen (NO_x and NO_3). *Atmos. Chem. Phys.* **2010**, *10* (22), 11261-11276.
(13) Ayres, B. R.; Allen, H. M.; Draper, D. C.; Brown, S. S.; Wild, R. J.; Jimenez, J. L.; Day, D. A.; Campuzano-Jost, P.; Hu, W.; de Gouw, J.; Koss, A.; Cohen, R. C.; Duffey, K. C.; Romer, P.; Baumann, K.; Edgerton, E.; Takahama, S.; Thornton, J. A.; Lee, B. H.; Lopez-Hilfiker, F. D.; Mohr, C.; Wennberg, P. O.; Nguyen, T. B.; Teng, A.; Goldstein, A. H.; Olson, K.; Fry, J. L., Organic nitrate aerosol formation via NO_3 + biogenic volatile organic compounds in the southeastern United States. *Atmos. Chem. Phys.* **2015**, *15* (23), 13377-13392.
(14) Fisher, J. A.; Jacob, D. J.; Travis, K. R.; Kim, P. S.; Marais, E. A.; Miller, C. C.; Yu, K. R.; Zhu, L.; Yantosca, R. M.; Sulprizio, M. P.; Mao, J. Q.; Wennberg, P. O.; Crounse, J. D.; Teng, A. P.; Nguyen, T. B.; St Clair, J. M.; Cohen, R. C.; Romer, P.; Nault, B. A.; Wooldridge, P. J.; Jimenez, J. L.; Campuzano-Jost, P.; Day, D. A.; Hu, W. W.; Shepson, P. B.; Xiong, F. L. Z.; Blake, D. R.; Goldstein, A. H.; Misztal, P. K.; Hanisco, T. F.; Wolfe, G. M.; Ryerson, T. B.; Wisthaler, A.; Mikoviny, T., Organic nitrate chemistry and its implications for nitrogen budgets in an isoprene- and monoterpene-rich atmosphere: constraints from aircraft (SEAC(4)RS) and ground-based (SOAS) observations in the Southeast US. *Atmos. Chem. Phys.* **2016**, *16* (9), 5969-5991.
(15) Xu, L.; Guo, H. Y.; Boyd, C. M.; Klein, M.; Bougiatioti, A.; Cerully, K. M.; Hite, J. R.; Isaacman-VanWertz, G.; Kreisberg, N. M.; Knote, C.; Olson, K.; Koss, A.; Goldstein, A. H.; Hering, S. V.; de Gouw, J.; Baumann, K.; Lee, S. H.; Nenes, A.; Weber, R. J.; Ng, N. L., Effects of anthropogenic emissions on aerosol formation from isoprene and monoterpenes in the southeastern United States. *Proc. Natl. Acad. Sci. U.S.A.* **2015**, *112* (1), 37-42.
(16) Guenther, A. B.; Jiang, X.; Heald, C. L.; Sakulyanontvittaya, T.; Duhl, T.; Emmons, L. K.; Wang, X., The model of emissions of gases and aerosols from nature version 2.1 (MEGAN2.1): an extended and updated framework for modeling biogenic emissions. *Geosci. Model. Dev.* **2012**, *5* (6), 1471-1492.
(17) Atkinson, R.; Arey, J., Atmospheric degradation of volatile organic compounds. *Chem. Rev.* **2003**, *103* (12), 4605-4638.
(18) Griffin, R. J.; Cocker, D. R.; Flagan, R. C.; Seinfeld, J. H., Organic aerosol formation from the oxidation of biogenic hydrocarbons. *J. Geophys. Res.: Atmos.* **1999**, *104* (D3), 3555-3567.
(19) Fry, J. L.; Kiendler-Scharr, A.; Rollins, A. W.; Wooldridge, P. J.; Brown, S. S.; Fuchs, H.; Dubé, W.; Mensah, A.; dal Maso, M.; Tillmann, R.; Dorn, H. P.; Brauers, T.; Cohen, R. C., Organic nitrate and secondary organic aerosol yield from NO_3 oxidation of beta-pinene

evaluated using a gas-phase kinetics/aerosol partitioning model. *Atmos. Chem. Phys.* **2009**, *9* (4), 1431-1449.
(20) Boyd, C. M.; Sanchez, J.; Xu, L.; Eugene, A. J.; Nah, T.; Tuet, W. Y.; Guzman, M. I.; Ng, N. L., Secondary organic aerosol formation from the beta-pinene+NO_3 system: effect of humidity and peroxy radical fate. *Atmos. Chem. Phys.* **2015**, *15* (13), 7497-7522.
(21) Claflin, M. S.; Ziemann, P. J., Identification and quantitation of aerosol products of the reaction of beta-pinene with NO_3 radicals and implications for gas- and particle-phase reaction mechanisms. *J. Phys. Chem. A* **2018**, *122* (14), 3640-3652.
(22) Fry, J. L.; Draper, D. C.; Barsanti, K. C.; Smith, J. N.; Ortega, J.; Winkle, P. M.; Lawler, M. J.; Brown, S. S.; Edwards, P. M.; Cohen, R. C.; Lee, L., Secondary organic aerosol formation and organic nitrate yield from NO_3 oxidation of biogenic hydrocarbons. *Environ. Sci. Technol.* **2014**, *48* (20), 11944-11953.
(23) Hallquist, M.; Wängberg, I.; Ljungström, E.; Barnes, I.; Becker, K. H., Aerosol and product yields from NO_3 radical-initiated oxidation of selected monoterpenes. *Environ. Sci. Technol.* **1999**, *33* (4), 553-559.
(24) Perraud, V.; Bruns, E. A.; Ezell, M. J.; Johnson, S. N.; Greaves, J.; Finlayson-Pitts, B. J., Identification of organic nitrates in the NO_3 radical initiated oxidation of alpha-pinene by atmospheric pressure chemical ionization mass spectrometry. *Environ. Sci. Technol.* **2010**, *44* (15), 5887-5893.
(25) Spittler, M.; Barnes, I.; Bejan, I.; Brockmann, K. J.; Benter, T.; Wirtz, K., Reactions of NO_3 radicals with limonene and alpha-pinene: product and SOA formation. *Atmos. Environ.* **2006**, *40* S116-S127.
(26) Lambe, A. T.; Wood, E. C.; Krechmer, J. E.; Majluf, F.; Williams, L. R.; Croteau, P. L.; Cirtog, M.; Féron, A.; Petit, J. E.; Albinet, A.; Jimenez, J. L.; Peng, Z., Nitrate radical generation via continuous generation of dinitrogen pentoxide in a laminar flow reactor coupled to an oxidation flow reactor. *Atmos. Meas. Tech.* **2020**, *13* (5), 2397-2411.
(27) Bianchi, F.; Kurtén, T.; Riva, M.; Mohr, C.; Rissanen, M. P.; Roldin, P.; Berndt, T.; Crounse, J. D.; Wennberg, P. O.; Mentel, T. F.; Wildt, J.; Junninen, H.; Jokinen, T.; Kulmala, M.; Worsnop, D. R.; Thornton, J. A.; Donahue, N.; Kjaergaard, H. G.; Ehn, M., Highly oxygenated organic molecules (HOM) from gas-phase autoxidation involving peroxy radicals: a key contributor to atmospheric aerosol. *Chem. Rev.* **2019**, *119* (6), 3472-3509.
(28) Huang, W.; Saathoff, H.; Shen, X. L.; Ramisetty, R.; Leisner, T.; Mohr, C., Chemical characterization of highly functionalized organonitrates contributing to night-time organic aerosol mass loadings and particle growth. *Environ. Sci. Technol.* **2019**, *53* (3), 1165-1174.
(29) Kirkby, J.; Duplissy, J.; Sengupta, K.; Frege, C.; Gordon, H.; Williamson, C.; Heinritzi, M.; Simon, M.; Yan, C.; Almeida, J.; Tröstl, J.; Nieminen, T.; Ortega, I. K.; Wagner, R.; Adamov, A.; Amorim, A.; Bernhammer, A. K.; Bianchi, F.; Breitenlechner, M.; Brilke, S.; Chen, X. M.; Craven, J.; Dias, A.; Ehrhart, S.; Flagan, R. C.; Franchin, A.; Fuchs, C.; Guida, R.; Hakala, J.; Hoyle, C. R.; Jokinen, T.; Junninen, H.; Kangasluoma, J.; Kim,

767 J.; Krapf, M.; Kürten, A.; Laaksonen, A.; Lehtipalo, K.; Makhmutov, V.; Mathot, S.;
768 Molteni, U.; Onnela, A.; Peräkylä, O.; Piel, F.; Petäjä, T.; Praplan, A. P.; Pringle, K.; Rap,
769 A.; Richards, N. A. D.; Riipinen, I.; Rissanen, M. P.; Rondo, L.; Sarnela, N.; Schobesberger,
770 S.; Scott, C. E.; Seinfeld, J. H.; Sipilä, M.; Steiner, G.; Stozhkov, Y.; Stratmann, F.; Tomé,
771 A.; Virtanen, A.; Vogel, A. L.; Wagner, A. C.; Wagner, P. E.; Weingartner, E.; Wimmer, D.;
772 Winkler, P. M.; Ye, P. L.; Zhang, X.; Hansel, A.; Dommen, J.; Donahue, N. M.; Worsnop,
773 D. R.; Baltensperger, U.; Kulmala, M.; Carslaw, K. S.; Curtius, J., Ion-induced nucleation
774 of pure biogenic particles. *Nature* **2016**, *533* (7604), 521-525.
775 (30) Nah, T.; Sanchez, J.; Boyd, C. M.; Ng, N. L., Photochemical aging of alpha-pinene
776 and beta-pinene secondary organic aerosol formed from nitrate radical oxidation. *Environ.*
777 *Sci. Technol.* **2016**, *50* (1), 222-231.
778 (31) Takeuchi, M.; Ng, N. L., Chemical composition and hydrolysis of organic nitrate
779 aerosol formed from hydroxyl and nitrate radical oxidation of alpha-pinene and beta-
780 pinene. *Atmos. Chem. Phys.* **2019**, *19* (19), 12749-12766.
781 (32) Crounse, J. D.; Nielsen, L. B.; Jørgensen, S.; Kjaergaard, H. G.; Wennberg, P. O.,
782 Autoxidation of organic compounds in the atmosphere. *J. Phys. Chem. Lett.* **2013**, *4* (20),
783 3513-3520.
784 (33) Mentel, T. F.; Springer, M.; Ehn, M.; Kleist, E.; Pullinen, I.; Kurtén, T.; Rissanen, M.;
785 Wahner, A.; Wildt, J., Formation of highly oxidized multifunctional compounds:
786 autoxidation of peroxy radicals formed in the ozonolysis of alkenes - deduced from
787 structure-product relationships. *Atmos. Chem. Phys.* **2015**, *15* (12), 6745-6765.
788 (34) Bohn, B.; Rohrer, F.; Brauers, T.; Wahner, A., Actinometric measurements of NO_2
789 photolysis frequencies in the atmosphere simulation chamber SAPHIR. *Atmos. Chem.*
790 *Phys.* **2005**, *5* 493-503.
791 (35) Rohrer, F.; Bohn, B.; Brauers, T.; Brüning, D.; Johnen, F. J.; Wahner, A.; Kleffmann,
792 J., Characterisation of the photolytic HONO-source in the atmosphere simulation chamber
793 SAPHIR. *Atmos. Chem. Phys.* **2005**, *5* 2189-2201.
794 (36) Sarrafzadeh, M.; Wildt, J.; Pullinen, I.; Springer, M.; Kleist, E.; Tillmann, R.; Schmitt,
795 S. H.; Wu, C.; Mentel, T. F.; Zhao, D. F.; Hastie, D. R.; Kiendler-Scharr, A., Impact of NO_x
796 and OH on secondary organic aerosol formation from beta-pinene photooxidation. *Atmos.*
797 *Chem. Phys.* **2016**, *16* (17), 11237-11248.
798 (37) Zhao, D. F.; Schmitt, S. H.; Wang, M. J.; Acir, I. H.; Tillmann, R.; Tan, Z. F.; Novelli,
799 A.; Fuchs, H.; Pullinen, I.; Wegener, R.; Rohrer, F.; Wildt, J.; Kiendler-Scharr, A.; Wahner,
800 A.; Mentel, T. F., Effects of NO_x and SO_2 on the secondary organic aerosol formation from
801 photooxidation of alpha-pinene and limonene. *Atmos. Chem. Phys.* **2018**, *18* (3), 1611-
802 1628.
803 (38) Wagner, N. L.; Dubé, W. P.; Washenfelder, R. A.; Young, C. J.; Pollack, I. B.; Ryerson,
804 T. B.; Brown, S. S., Diode laser-based cavity ring-down instrument for NO_3, N_2O_5, NO,
805 NO_2 and O_3 from aircraft. *Atmos. Meas. Tech.* **2011**, *4* (6), 1227-1240.

(39) Saunders, S. M.; Jenkin, M. E.; Derwent, R. G.; Pilling, M. J., Protocol for the development of the Master Chemical Mechanism, MCM v3 (Part A): tropospheric degradation of non-aromatic volatile organic compounds. *Atmos. Chem. Phys.* **2003**, *3* 161-180.
(40) Hyttinen, N.; Rissanen, M. P.; Kurtén, T., Computational comparison of acetate and nitrate chemical ionization of highly oxidized cyclohexene ozonolysis intermediates and products. *J. Phys. Chem. A.* **2017**, *121* (10), 2172-2179.
(41) Draper, D. C.; Myllys, N.; Hyttinen, N.; Møller, K. H.; Kjaergaard, H. G.; Fry, J. L.; Smith, J. N.; Kurtén, T., Formation of highly oxidized molecules from NO_3 radical initiated oxidation of delta-3-carene: a mechanistic study. *ACS Earth Space Chem.* **2019**, *3* (8), 1460-1470.
(42) Massoli, P.; Stark, H.; Canagaratna, M. R.; Krechmer, J. E.; Xu, L.; Ng, N. L.; Mauldin, R. L.; Yan, C.; Kimmel, J.; Misztal, P. K.; Jimenez, J. L.; Jayne, J. T.; Worsnop, D. R., Ambient measurements of highly oxidized gas-phase molecules during the Southern Oxidant and Aerosol Study (SOAS) 2013. *ACS Earth Space Chem.* **2018**, *2* (7), 653-672.
(43) Wennberg, P. O.; Bates, K. H.; Crounse, J. D.; Dodson, L. G.; McVay, R. C.; Mertens, L. A.; Nguyen, T. B.; Praske, E.; Schwantes, R. H.; Smarte, M. D.; St Clair, J. M.; Teng, A. P.; Zhang, X.; Seinfeld, J. H., Gas-phase reactions of isoprene and its major oxidation products. *Chem. Rev.* **2018**, *118* (7), 3337-3390.
(44) Zhao, D. F.; Pullinen, I.; Fuchs, H.; Schrade, S.; Wu, R. R.; Acir, I. H.; Tillmann, R.; Rohrer, F.; Wildt, J.; Guo, Y. D.; Kiendler-Scharr, A.; Wahner, A.; Kang, S.; Vereecken, L.; Mentel, T. F., Highly oxygenated organic molecule (HOM) formation in the isoprene oxidation by NO_3 radical. *Atmos. Chem. Phys.* **2021**, *21* (12), 9681-9704.
(45) Pullinen, I.; Schmitt, S.; Kang, S.; Sarrafzadeh, M.; Schlag, P.; Andres, S.; Kleist, E.; Mentel, T. F.; Rohrer, F.; Springer, M.; Tillmann, R.; Wildt, J.; Wu, C.; Zhao, D. F.; Wahner, A.; Kiendler-Scharr, A., Impact of NO_x on secondary organic aerosol (SOA) formation from alpha-pinene and beta-pinene photooxidation: the role of highly oxygenated organic nitrates. *Atmos. Chem. Phys.* **2020**, *20* (17), 10125-10147.
(46) Zhao, D. F.; Kaminski, M.; Schlag, P.; Fuchs, H.; Acir, I. H.; Bohn, B.; Häseler, R.; Kiendler-Scharr, A.; Rohrer, F.; Tillmann, R.; Wang, M. J.; Wegener, R.; Wildt, J.; Wahner, A.; Mentel, T. F., Secondary organic aerosol formation from hydroxyl radical oxidation and ozonolysis of monoterpenes. *Atmos. Chem. Phys.* **2015**, *15* (2), 991-1012.
(47) Huang, Y. L.; Zhao, R.; Charan, S. M.; Kenseth, C. M.; Zhang, X.; Seinfeld, J. H., Unified theory of vapor-wall mass transport in teflon-walled environmental chambers. *Environ. Sci. Technol.* **2018**, *52* (4), 2134-2142.
(48) Riva, M.; Rantala, P.; Krechmer, J. E.; Peräkylä, O.; Zhang, Y. J.; Heikkinen, L.; Garmash, O.; Yan, C.; Kulmala, M.; Worsnop, D.; Ehn, M., Evaluating the performance of five different chemical ionization techniques for detecting gaseous oxygenated organic species. *Atmos. Meas. Tech.* **2019**, *12* (4), 2403-2421.

(49) Lee, B. H.; Lopez-Hilfiker, F. D.; Mohr, C.; Kurtén, T.; Worsnop, D. R.; Thornton, J. A., An iodide-adduct high-resolution time-of-flight chemical-ionization mass spectrometer: application to atmospheric inorganic and organic compounds. *Environ. Sci. Technol.* **2014**, *48* (11), 6309-6317.
(50) Jenkin, M. E.; Valorso, R.; Aumont, B.; Rickard, A. R., Estimation of rate coefficients and branching ratios for reactions of organic peroxy radicals for use in automated mechanism construction. *Atmos. Chem. Phys.* **2019**, *19* (11), 7691-7717.
(51) Wang, S. Y.; Pratt, K. A., Molecular halogens above the arctic snowpack: emissions, diurnal variations, and recycling mechanisms. *J. Geophys. Res.: Atmos.* **2017**, *122* (21), 11991-12007.
(52) Vereecken, L.; Francisco, J. S., Theoretical studies of atmospheric reaction mechanisms in the troposphere. *Chem. Soc. Rev.* **2012**, *41* (19), 6259-6293.
(53) Vereecken, L.; Peeters, J., A structure-activity relationship for the rate coefficient of H-migration in substituted alkoxy radicals. *Phys. Chem. Chem. Phys.* **2010**, *12* (39), 12608-12620.
(54) Praske, E.; Otkjær, R. V.; Crounse, J. D.; Hethcox, J. C.; Stoltz, B. M.; Kjaergaard, H. G.; Wennberg, P. O., Atmospheric autoxidation is increasingly important in urban and suburban North America. *Proc. Natl. Acad. Sci. U.S.A.* **2018**, *115* (1), 64-69.
(55) Rissanen, M. P.; Kurtén, T.; Sipilä, M.; Thornton, J. A.; Kangasluoma, J.; Sarnela, N.; Junninen, H.; Jørgensen, S.; Schallhart, S.; Kajos, M. K.; Taipale, R.; Springer, M.; Mentel, T. F.; Ruuskanen, T.; Petäjä, T.; Worsnop, D. R.; Kjaergaard, H. G.; Ehn, M., The formation of highly oxidized multifunctional products in the ozonolysis of cyclohexene. *J. Am. Chem. Soc.* **2014**, *136* (44), 15596-15606.
(56) Vereecken, L.; Nozière, B., H migration in peroxy radicals under atmospheric conditions. *Atmos. Chem. Phys.* **2020**, *20* (12), 7429-7458.
(57) Atkinson, R.; Arey, J.; Aschmann, S. M., Atmospheric chemistry of alkanes: review and recent developments. *Atmos. Environ.* **2008**, *42* (23), 5859-5871.
(58) Yeh, G. K.; Claflin, M. S.; Ziemann, P. J., Products and mechanism of the reaction of 1-pentadecene with NO_3 radicals and the effect of a -ONO_2 group on alkoxy radical decomposition. *J. Phys. Chem. A* **2015**, *119* (43), 10684-10696.
(59) Kroll, J. H.; Seinfeld, J. H., Chemistry of secondary organic aerosol: formation and evolution of low-volatility organics in the atmosphere. *Atmos. Environ.* **2008**, *42* (16), 3593-3624.
(60) Novelli, A.; Cho, C.; Fuchs, H.; Hofzumahaus, A.; Rohrer, F.; Tillmann, R.; Kiendler-Scharr, A.; Wahner, A.; Vereecken, L., Experimental and theoretical study on the impact of a nitrate group on the chemistry of alkoxy radicals. *Phys. Chem. Chem. Phys.* **2021**, *23* (9), 5474-5495.

(61) Vereecken, L.; Peeters, J., Decomposition of substituted alkoxy radicals-part I: a generalized structure-activity relationship for reaction barrier heights. *Phys. Chem. Chem. Phys.* **2009**, *11* (40), 9062-9074.
(62) Lachowicz, D. R.; Kreuz, K. L., Peroxy nitrates. Unstable products of olefin nitration with dinitrogen tetroxide in the presence of oxygen. New route to .alpha.-nitroketones. *J. Org. Chem.* **1967**, *32* (12), 3885-3888.
(63) Bennett, J. E.; Summers, R., Product studies of the mutual termination reactions of sec-alkylperoxy radicals: evidence for non-cyclic termination. *Can. J. Chem.* **1974**, *52* (8), 1377-1379.
(64) Chim, M. M.; Cheng, C. T.; Davies, J. F.; Berkemeier, T.; Shiraiwa, M.; Zuend, A.; Chan, M. N., Compositional evolution of particle-phase reaction products and water in the heterogeneous OH oxidation of model aqueous organic aerosols. *Atmos. Chem. Phys.* **2017**, *17* (23), 14415-14431.
(65) Jenkin, M. E.; Saunders, S. M.; Pilling, M. J., The tropospheric degradation of volatile organic compounds: a protocol for mechanism development. *Atmos. Environ.* **1997**, *31* (1), 81-104.
(66) Junninen, H.; Ehn, M.; Petäjä, T.; Luosujarvi, L.; Kotiaho, T.; Kostiainen, R.; Rohner, U.; Gonin, M.; Fuhrer, K.; Kulmala, M.; Worsnop, D. R., A high-resolution mass spectrometer to measure atmospheric ion composition. *Atmos. Meas. Tech.* **2010**, *3* (4), 1039-1053.
(67) Paulot, F.; Crounse, J. D.; Kjaergaard, H. G.; Kürten, A.; St Clair, J. M.; Seinfeld, J. H.; Wennberg, P. O., Unexpected epoxide formation in the gas-phase photooxidation of isoprene. *Science* **2009**, *325* (5941), 730-733.
(68) Praske, E.; Otkjær, R. V.; Crounse, J. D.; Hethcox, J. C.; Stoltz, B. M.; Kjaergaard, H. G.; Wennberg, P. O., Intramolecular hydrogen shift chemistry of hydroperoxy-substituted peroxy radicals. *J. Phys. Chem. A* **2019**, *123* (2), 590-600.
(69) Miyoshi, A., Systematic computational study on the unimolecular reactions of alkylperoxy (RO_2), hydroperoxyalkyl (QOOH), and hydroperoxyalkylperoxy (O_2QOOH) radicals. *J. Phys. Chem. A* **2011**, *115* (15), 3301-3325.
(70) Peeters, J.; Müller, J. F.; Stavrakou, T.; Nguyen, V. S., Hydroxyl radical recycling in isoprene oxidation driven by hydrogen bonding and hydrogen tunneling: the upgraded LIM1 mechanism. *J. Phys. Chem. A* **2014**, *118* (38), 8625-8643.
(71) Kerdouci, J.; Picquet-Varrault, B.; Doussin, J. F., Prediction of rate constants for gas-phase reactions of nitrate radical with organic compounds: a new structure-activity relationship. *Chem. Phys. Chem.* **2010**, *11* (18), 3909-3920.
(72) Vereecken, L.; Peeters, J., A theoretical study of the OH-initiated gas-phase oxidation mechanism of β-pinene ($C_{10}H_{16}$): first generation products. *Phys. Chem. Chem. Phys.* **2012**, *14* (11), 3802-3815.

(73) Kaminski, M.; Fuchs, H.; Acir, I. H.; Bohn, B.; Brauers, T.; Dorn, H. P.; Häseler, R.; Hofzumahaus, A.; Li, X.; Lutz, A.; Nehr, S.; Rohrer, F.; Tillmann, R.; Vereecken, L.; Wegener, R.; Wahner, A., Investigation of the beta-pinene photooxidation by OH in the atmosphere simulation chamber SAPHIR. *Atmos. Chem. Phys.* **2017**, *17* (11), 6631-6650.
(74) Xu, L.; Møller, K. H.; Crounse, J. D.; Otkjær, R. V.; Kjaergaard, H. G.; Wennberg, P. O., Unimolecular reactions of peroxy radicals formed in the oxidation of alpha-pinene and beta-pinene by hydroxyl radicals. *J. Phys. Chem. A* **2019**, *123* (8), 1661-1674.
(75) Vereecken, L.; Peeters, J., Theoretical study of the formation of acetone in the OH-initiated atmospheric oxidation of alpha-pinene. *J. Phys. Chem. A.* **2000**, *104* (47), 11140-11146.
(76) Peeters, J.; Vereecken, L.; Fantechi, G., The detailed mechanism of the OH-initiated atmospheric oxidation of alpha-pinene: a theoretical study. *Phys. Chem. Chem. Phys.* **2001**, *3* (24), 5489-5504.
(77) Møller, K. H.; Otkjær, R. V.; Chen, J.; Kjaergaard, H. G., Double bonds are key to fast unimolecular reactivity in first-generation monoterpene hydroxy peroxy radicals. *J. Phys. Chem. A* **2020**, *124* (14), 2885-2896.
(78) Kurtén, T.; Møller, K. H.; Nguyen, T. B.; Schwantes, R. H.; Misztal, P. K.; Su, L. P.; Wennberg, P. O.; Fry, J. L.; Kjaergaard, H. G., Alkoxy radical bond scissions explain the anomalously low secondary organic aerosol and organonitrate yields from alpha-pinene + NO_3. *J. Phys. Chem. Lett.* **2017**, *8* (13), 2826-2834.
(79) Fouqueau, A.; Cirtog, M.; Cazaunau, M.; Pangui, E.; Doussin, J. F.; Picquet-Varrault, B., A comparative and experimental study of the reactivity with nitrate radical of two terpenes: alpha-terpinene and gamma-terpinene. *Atmos. Chem. Phys.* **2020**, *20* (23), 15167-15189.
(80) Berndt, T.; Mender, B.; Scholz, W.; Fischer, L.; Herrmann, H.; Kulmala, M.; Hansel, A., Accretion product formation from ozonolysis and OH radical reaction of alpha-pinene: mechanistic insight and the influence of isoprene and ethylene. *Environ. Sci. Technol.* **2018**, *52* (19), 11069-11077.
(81) Berndt, T.; Scholz, W.; Mentler, B.; Fischer, L.; Herrmann, H.; Kulmala, M.; Hansel, A., Accretion product formation from self- and cross-reactions of RO_2 radicals in the atmosphere. *Angew. Chem., Int. Ed.* **2018**, *57* (14), 3820-3824.
(82) Zhao, Y.; Thornton, J. A.; Pye, H. O. T., Quantitative constraints on autoxidation and dimer formation from direct probing of monoterpene-derived peroxy radical chemistry. *Proc. Natl. Acad. Sci. U.S.A.* **2018**, *115* (48), 12142-12147.
(83) Jokinen, T.; Berndt, T.; Makkonen, R.; Kerminen, V. M.; Junninen, H.; Paasonen, P.; Stratmann, F.; Herrmann, H.; Guenther, A. B.; Worsnop, D. R.; Kulmala, M.; Ehn, M.; Sipilä, M., Production of extremely low volatile organic compounds from biogenic emissions: measured yields and atmospheric implications. *Proc. Natl. Acad. Sci. U.S.A.* **2015**, *112* (23), 7123-7128.

(84) Wang, Y. H.; Riva, M.; Xie, H. B.; Heikkinen, L.; Schallhart, S.; Zha, Q. Z.; Yan, C.; He, X. C.; Peräkylä, O.; Ehn, M., Formation of highly oxygenated organic molecules from chlorine-atom-initiated oxidation of alpha-pinene. *Atmos. Chem. Phys.* **2020**, *20* (8), 5145-5155.
(85) Liu, Y.; Nie, W.; Li, Y.; Ge, D.; Liu, C.; Xu, Z.; Chen, L.; Wang, T.; Wang, L.; Sun, P.; Qi, X.; Wang, J.; Xu, Z.; Yuan, J.; Yan, C.; Zhang, Y.; Huang, D.; Wang, Z.; Donahue, N. M.; Worsnop, D.; Chi, X.; Ehn, M.; Ding, A., Formation of condensable organic vapors from anthropogenic and biogenic VOCs is strongly perturbed by NO_x in eastern China. *Atmos. Chem. Phys.* **2021**, *21*, 14789-14814.
(86) Roldin, P.; Ehn, M.; Kurtén, T.; Olenius, T.; Rissanen, M. P.; Sarnela, N.; Elm, J.; Rantala, P.; Hao, L. Q.; Hyttinen, N.; Heikkinen, L.; Worsnop, D. R.; Pichelstorfer, L.; Xavier, C.; Clusius, P.; Öström, E.; Petäjä, T.; Kulmala, M.; Vehkamäki, H.; Virtanen, A.; Riipinen, I.; Boy, M., The role of highly oxygenated organic molecules in the boreal aerosol-cloud-climate system. *Nat. Commun.* **2019**, *10*, 4370.
(87) Pye, H. O. T.; D'Ambro, E. L.; Lee, B.; Schobesberger, S.; Takeuchi, M.; Zhao, Y.; Lopez-Hilfiker, F.; Liu, J. M.; Shilling, J. E.; Xing, J.; Mathur, R.; Middlebrook, A. M.; Liao, J.; Welti, A.; Graus, M.; Warneke, C.; de Gouw, J. A.; Holloway, J. S.; Ryerson, T. B.; Pollack, I. B.; Thornton, J. A., Anthropogenic enhancements to production of highly oxygenated molecules from autoxidation. *Proc. Natl. Acad. Sci. U.S.A.* **2019**, *116* (14), 6641-6646.
(88) Weber, J.; Archer-Nicholls, S.; Griffiths, P.; Berndt, T.; Jenkin, M.; Gordon, H.; Knote, C.; Archibald, A. T., CRI-HOM: A novel chemical mechanism for simulating highly oxygenated organic molecules (HOMs) in global chemistry-aerosol-climate models. *Atmos. Chem. Phys.* **2020**, *20* (18), 10889-10910.

Highly oxygenated organic nitrates formed from NO_3 radical initiated oxidation of β-pinene

Hongru Shen,[1] Defeng Zhao,[1,2,3,4*] Iida Pullinen,[2, a] Sungah Kang,[2] Luc Vereecken,[2] Hendrik Fuchs,[2] Ismail-Hakki Acir,[2,b] Ralf Tillmann,[2] Franz Rohrer,[2] Jürgen Wildt,[2] Astrid Kiendler-Scharr,[2] Andreas Wahner,[2] Thomas F. Mentel[2*]

[1] Department of Atmospheric and Oceanic Sciences & Institute of Atmospheric Sciences, Fudan University, 200438, Shanghai, China;

[2] Institute of Energy and Climate Research, IEK-8: Troposphere, Forschungszentrum Jülich, 52425, Jülich, Germany;

[3] Big Data Institute for Carbon Emission and Environmental Pollution, Fudan University, Shanghai 200438, China.

[4] Institute of Eco-Chongming (IEC), 20 Cuiniao Road., Chenjia Zhen, Chongming, Shanghai 202162, China

[a] Now at: Department of Applied Physics, University of Eastern Finland, Kuopio, 70210, Finland.

[b] Now at: Institute of Nutrition and Food Sciences, University of Bonn, Bonn, 53115, Germany.

*Corresponding authors: dfzhao@fudan.edu.cn, t.mentel@fz-juelich.de

Table of Contents (TOC)

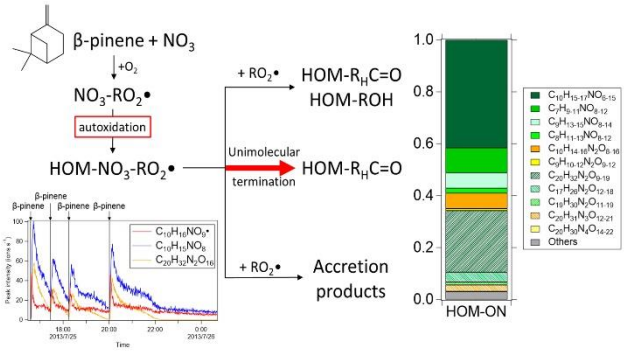

Abstract

The reactions of biogenic volatile organic compounds (BVOC) with the nitrate radical (NO_3) are major night-time sources of organic nitrates and secondary organic aerosol (SOA) in regions influenced by BVOC and anthropogenic emissions. In this study, the formation of gas-phase highly oxygenated organic molecules-organic nitrates (HOM-ON) from NO_3-initiated oxidation of a representative monoterpene, β-pinene, was investigated in the SAPHIR chamber (Simulation of Atmosphere PHotochemistry In a large Reaction chamber). Six monomer (C = 7-10, N = 1-2, O = 6-16) and five accretion product (C = 17-20, N = 2-4, O = 9-22) families were identified and further classified into first- or second-generation products based on their temporal behavior. The time lag observed in the peak concentrations between peroxy radicals containing odd and even number of oxygen atoms, as well as between radicals and their corresponding termination products, provided constraints on the HOM-ON formation mechanism. The HOM-ON formation can be explained by unimolecular or bimolecular reactions of peroxy radicals. A dominant portion of carbonylnitrates in HOM-ON was detected, highlighting the significance of unimolecular termination reactions by intramolecular H-shift for the formation of HOM-ON. A mean molar yield of HOM-ON was estimated to be 4.8% (-2.6%/+5.6%), suggesting significant HOM-ON contributions to the SOA formation.

Keywords: NO_3 radical, biogenic volatile organic compounds, organic nitrate, secondary organic aerosol, anthropogenic-biogenic interaction, night-time oxidation

Synopsis: The reactions of nighttime anthropogenic oxidants with biogenic organics form low-volatile vapors, potentially contributing a large fraction of particulate organic matter.

Introduction

Biogenic volatile organic compounds (BVOC), such as isoprene (C_5H_8) and monoterpenes ($C_{10}H_{16}$) emitted from terrestrial vegetation, constitute a large fraction of global gas-phase organic compounds.[1] In the ambient conditions, BVOC are primarily oxidized by OH in the daytime,[2, 3] NO_3 radicals at night-time,[4, 5] and O_3 during both day- and night-time.[6, 7] These reactions are believed to be the dominant contributor to the formation of secondary organic aerosols (SOA), influencing regional and global climate, air quality, and human health.[8, 9] Compared to SOA formation from OH- and O_3-initiated oxidation of BVOC, night-time NO_3 oxidation of BVOC has been less investigated, but these reactions are highly relevant in ambient conditions, particularly in regions influenced by anthropogenic NO_x ($NO + NO_2$) and natural BVOC emissions.[10-12] Reactions of BVOC + NO_3 can form organic nitrates (ON), which serve as a temporary or permanent sink for NO_x and affects regional O_3 budgets and nitrogen cycles.[13, 14] Due to their semi-/low-volatility, ON can also partition into the condensed phase participating in SOA formation. The results from the Southern Oxidant and Aerosol Study (SOAS) have shown that a large fraction of night-time SOA formation can be explained by reactions of BVOC + NO_3, about half of which is from monoterpenes + NO_3.[15] Therefore, this anthropogenic-biogenic interactions between NO_3 and BVOC, especially monoterpenes, is critical to understand night-time SOA formation.

Among the monoterpenes, β-pinene has high emission rates (being the second most abundant monoterpene, after α-pinene),[16] high reactivity with NO_3 (with a second-order rate constant of 2.5×10^{-12} cm^3 $molecule^{-1}$ s^{-1} at 298 K),[17] and high SOA yields with NO_3 (with SOA mass yields of 27-104%[18-23] compared to 0-16% for α-pinene[22-25]). The reaction of β-pinene with NO_3 contributes a significant fraction of the SOA produced by monoterpene + NO_3 and was therefore often selected as a representative monoterpene in recent laboratory studies.[15, 19-21, 26] Previous studies have investigated β-pinene + NO_3, mostly focusing on the determination of the SOA yield, chemical characterization of particle-phase products, and possible formation mechanism of products containing a low number of oxygen atoms. For example, Fry et al.[19] measured the SOA yield. Boyd et al.[20] additionally found that neither humidity nor peroxy radical fate affects SOA yields, determined ON fraction in the aerosols, and proposed a formation mechanism of the detected gas-phase ON ($C_{10}H_{15}NO_{5,6}$ and $C_{10}H_{17}NO_{4,5}$), which are formed by the bimolecular reactions of RO_2•. Claflin and Ziemann[21] observed monomers (C_{10} ON), dimers (C_{20} ON), and trimers (C_{30} ON) in the particle-phase products from reactions of β-pinene + NO_3 and highlighted oligomerization reactions in the particle-phase mechanism.

Despite previous efforts by a number of laboratory studies, the understanding of the chemistry of β-pinene with NO_3, especially regarding gas-phase reaction products containing a high number of oxygen atoms, is still incomplete. In particular, highly oxygenated organic molecules-organic nitrates (HOM-ON), a new class of gas-phase

compounds containing at least 6 oxygen atoms,[27] have been recently observed and found to play a potentially significant role in SOA formation in the NO_3 oxidation of BVOCs, including β-pinene.[28, 29] Nah et al.[30] observed a series of HOM-ON of C_{7-10} with 4-9 oxygen atoms in both particle- and gas-phase products of NO_3 oxidation of β-pinene. Takeuchi and Ng[31] additionally observed a substantial contribution of accretion products such as $C_{20}H_{32}N_2O_{8-11}$ in the particle phase. These HOM-ON are known to be formed in a short time-scale via autoxidation,[30] which involves successive intramolecular H-shifts in peroxy radicals (RO_2•) and subsequent O_2-addition,[6, 32] resulting in an oxygenated RO_2• radical reaction chain, shown in Scheme S1a. Recent studies have summarized general RO_2• reactions,[27, 33] with the most critical ones shown in Scheme S1b-j. Via bimolecular reactions with RO_2•, HO_2•, or NO_3, the RO_2• autoxidation chain will either be terminated to form a set of closed-shell products (Scheme S1b-d, g-j), including hydroxyperoxide, alcohol, carbonyl, and accretion products, or be continued via the formation of alkoxy radicals (RO•, Scheme S1e-f). Unimolecular termination pathways generally lead to the formation of carbonyls (Scheme S1h-i) or epoxides (Scheme S1j).[32] However, the specific HOM-ON formation mechanism remains elusive for the β-pinene + NO_3 system. In addition, the knowledge of the chemical composition of HOM-ON is incomplete and their contribution to SOA formation is unquantified.

In this study, experiments of NO_3-initiated oxidation of β-pinene were performed in the SAPHIR chamber in Jülich, Germany (Simulation of Atmosphere PHotochemistry In

105 a large Reaction chamber). A large number of HOM-ON were identified and quantified.
106 An example formation pathway was proposed and further constrained based on the time
107 series. An estimate of production yields of these HOM-ON formed from the β-pinene +
108 NO_3 reaction was provided to evaluate their role in the SOA formation.

109 **Experimental and Methods**

110 **Experimental Setup.** The experiments were performed in the SAPHIR chamber at
111 Forschungszentrum Jülich, Germany. It is a double-walled Teflon chamber with a volume
112 of 270 m^3. A detailed description of SAPHIR can be found elsewhere.[34, 35] Before the
113 experiment, the chamber was purged with synthetic air at ~330 $m^3\ h^{-1}$ for about 4 h to clean
114 the chamber and eliminate any interference from previous experiments. During the whole
115 experimental period, the chamber was kept under an over-pressure of 35 Pa, leading to a
116 dilution rate of $1.5\times10^{-5}\ s^{-1}$. The shutter system was closed to prevent photochemical
117 reactions, including NO_3 photodissociation. A fan was continuously operated to mix the
118 trace gases with homogenization within 2 min.

119 Experiments were designed to probe the time series of gas-phase HOM-ON formed
120 from β-pinene + NO_3, with the detailed experimental procedure shown in Figure S1. First,
121 ozone was added into the chamber, followed by NO_2 to form in-situ NO_3 radicals along
122 with the simultaneous formation of dinitrogen pentoxide (N_2O_5) as per the reactions below

123 $NO_2 + O_3 \rightarrow NO_3 + O_2$ (R1)

124 $NO_3 + NO_2 \leftrightarrow N_2O_5$ (R2)

Through the equilibrium with N_2O_5, sufficiently high concentrations of NO_3 radicals were ensured. A concentration ratio (~2:1) of NO_2 and O_3 was selected to ensure that more than 98% of β-pinene reacted with NO_3 radicals instead of O_3 during each experimental period, as shown in Figure S2. About 16 min after NO_2 addition, concentrations of NO_3 and N_2O_5 reached 90 ppt and 1.5 ppb, respectively, and β-pinene was added into the chamber, initiating the oxidation reaction. Another two β-pinene additions were deployed at respectively 50 min and 100 min after the first β-pinene addition. Later on, 12 ppb O_3 and 16 ppb NO_2 were introduced into the chamber, followed by one more addition of β-pinene. Four experimental periods were performed to probe the time series of products and distinguish first- and second-generation products. With no seed particles used in these experiments and low concentrations of β-pinene and NO_3, a negligible amount of particles were formed and observed, as shown in Figure S3. This is in contrast to previous studies,[19-22, 26, 36] which used seed aerosol and/or high concentrations of β-pinene and NO_3, leading to particle formation. Due to the low particle number and surface area concentrations in our work, particles are expected to have negligible effects on the gas-phase products' partitioning. Experiments were performed under dry conditions (relative humidity <3%) and at an average temperature of 300.0 ± 2.0 K.

Instrumentation. The chamber was equipped with a comprehensive set of instruments as described by Zhao et al.[37] In this experiment, a home-built diode laser-based, cavity ring-down spectrometer was used to measure *in-situ* concentrations of NO_3 and N_2O_5.[38] A

145 proton transfer reaction time-of-flight mass spectrometer (PTR-TOF-MS, Ionicon Analytik,
146 Austria) was used to measure the concentrations of VOC, including β-pinene and acetone.
147 From the measured concentrations, the β-pinene consumption during the experiments can
148 be derived and agrees with the expectations when considering the dilution (a loss rate
149 coefficient of 1.5×10^{-5} s^{-1}) and the reaction with NO_3 (a reaction rate constant of 2.5×10^{-12}
150 cm^3 $molecule^{-1}$ s^{-1}).[39]

151 The chemical composition of produced HOM-ON was characterized online using a
152 $^{15}NO_3^-$ chemical ionization mass spectrometer (CI-API-TOF-MS, Aerodyne Research Inc.),
153 which detects products with six or more oxygen atoms efficiently.[40] Nitrogen-15 was used
154 to distinguish the nitrogen-14 atoms in the chamber-produced ON, most of which are
155 expected to complex with the $^{15}NO_3^-$ ion.[41] The mass spectral data within the m/z 4-1400
156 range were analyzed using a Tofware analysis toolkit (Tofwerk/Aerodyne) in Igor Pro
157 (WaveMetrics, Inc.). High-resolution analysis was applied to identify ions with a resolving
158 power $m/z/\Delta m/z$ of ~3500. Isotopes were constrained during the peak assignment process.
159 The mass spectrum of the first experimental period was selected to assign peaks, as it
160 showed a mass spectrum similar to other experimental periods and the end of the
161 experiments and contained the same products as other periods (Figure S4). We observed a
162 few peaks such as m/z 289 and 334 corresponding to $C_5H_{10}N_2O_8\cdot{}^{15}NO_3^-$ and
163 $C_5H_9N_3O_{10}\cdot{}^{15}NO_3^-$,[10] which are products of isoprene + NO_3 reactions.[42] Their time series
164 are shown in Figure S5. These peaks were observed before the beginning of β-pinene +

NO_3 experiments, their concentrations increased slowly during the whole experimental period, and no obvious and regular response to each β-pinene addition was observed. This indicates that these compounds are residuals on the chamber wall from prior experiments of isoprene + NO_3 one day before and with also possible small contributions from the reaction of β-pinene + NO_3.[43] Moreover, these compounds do not contain double bonds according to their formula,[44] we expect that they do not react with NO_3 or O_3 during the β-pinene experiment, which is confirmed by the lack of response to O_3 and NO_2 addition before the experiment. Additionally, the HOM-ON formed in the reaction of β-pinene with NO_3 were absent before the first β-pinene addition. Therefore, we conclude that residual compounds do not have significant influence on the β-pinene + NO_3 reactions. We would like to note that our CIMS easily detects these HOM evaporated from the residue on the chamber wall despite their low concentrations because of its high sensitivity to HOM.

The concentrations of O_3 and NO_x were measured using an O_3 analyzer (ANSYCO, model O341M) and a NO_x analyzer (ECO PHYSICS TR480), respectively. The SOA was monitored using an SMPS (TSI DMA3081/TSI CPC3785). Measurements of physical parameters, including the temperature, relative humidity, and flow rate, were also conducted in these experiments.

Yield of products. The peak area of ions identified using the mass spectrometer was normalized to the total ion signal and then converted to concentrations using a calibration coefficient (C) of 2.5×10^{10} molecule cm^{-3} nc^{-1} (normalized count), determined using H_2SO_4

as described by Pullinen et al.[45] A mass-independent transmission efficiency equal to H_2SO_4 (with an uncertainty of -0%/+14%) was used when applying the calibration coefficient to HOM, as determined in our previous study.[45] The determination of this calibration value and its application to HOM are described in details in the Supporting Information (SI) (section S1). The concentrations of the identified ON with more than 6 O atoms were summed to the total concentrations of HOM-ON after a wall loss rate of 6×10^{-4} s^{-1}, and a dilution rate of 1.5×10^{-5} s^{-1} were accounted for.[46] Previous studies have shown that the wall loss rate of some compounds changes as the experiment continues,[47] which could affect the determined HOM yield. As the HOM yield in this study was determined over a short period after each injection (~10 min), we do not expect a large change in the wall loss rate during this period. In addition, considering the low volatility of HOM leading to their irreversible loss to the wall, a narrow distribution of the wall loss rates is expected. Sensitivity analysis shows that the HOM yield in this study is not sensitive to the wall loss rate, with a respective change of 23% and -11% in HOM yield from an increase of +100% or -50% in the wall loss rate. One uniform wall loss rate is thus used to determine HOM in this study. Such simplification may introduce additional uncertainty in HOM yield calculation. The molar yield of these HOM-ON was calculated following eq 1, where concentrations of produced HOM-ON is divided by the concentrations of β-pinene that reacted with NO_3.

$$Y = \frac{[\text{HOM ON}]}{[\beta\ \text{pinene}]_{\text{reacted}}} \quad (1)$$

Herein, [HOM-ON] represents the product concentration formed 10 min after each β-pinene addition. In other words, the molar yield *Y* refers to the primary yield, which mostly involves first-generation products and contains negligible multigeneration products. The uncertainty on the molar yield was estimated to be -55%/+117% from the combined uncertainties of HOM-ON peak intensity (~10%), β-pinene concentration (~15%), calibration factor (-52%/+101%), and transmission efficiency (-0%/+14%) using error propagation. The HOM-ON molar yield was averaged over four experiment periods, and uncertainties were estimated based on this value. Molar yields were later converted into mass yields using the molecular mass of each compound following Ehn et al.[6]

Results and Discussion

Overview of HOM-ON. Two distinct regions at m/z 280-460 (red) and m/z 510-690 (blue) in the mass spectrum of the first β-pinene + NO_3 experimental period (between the first and second β-pinene addition) were observed and segregated into monomers (C = 7-10, N = 1-2) and accretion products (C = 17-20, N = 2-4) (Figure 1a). Based on the above peak assignment methods, 153 compounds were identified, including 99 monomers, 46 accretion products, and 8 other compounds. Their detailed formula can be found in Table S1. Most of the identified products contained at least one N atom and more than six O atoms. This oxygenated feature agrees with the definition of HOM,[27] and these compounds can thus be classified as HOM-ON.

The Kendrick mass defect (O-based) plot of these identified HOM-ON is shown in Figure 1b, indicating their relative abundance and O/C ratio. Overall, the majority of the identified HOM-ON are monomers, with a fraction of 65.7%, with the rest being composed of accretion products (31.2%) and other compounds (3.1%). An average O/C ratio of 1.23 and 0.81 is observed for monomers and accretion products, respectively. Previous β-pinene + NO_3 studies generally detected O/C < 1 for monomers[20, 21, 30] and 0.45-0.55 for accretion products.[21, 31] This O/C difference can be attributed to the use of NO_3^- as a reagent ion. Specifically, NO_3^- CIMS preferentially detects compounds containing high numbers of O atoms and multiple hydrogen bond donors,[40, 48] compared with other reagent ions such as I^-.[49] The HOM-ON on each horizontal line in Figure 1b share the same number of C, N, and H-atoms, with an increasing number of O atoms from left to right, allowing further grouping into product families based on the chemical formula. We distinguished six groups of monomer families ($C_{10}H_{15\text{-}17}NO_{6\text{-}15}$, $C_7H_{9\text{-}11}NO_{8\text{-}12}$, $C_9H_{13\text{-}15}NO_{8\text{-}14}$, $C_8H_{11\text{-}13}NO_{8\text{-}12}$, $C_{10}H_{14\text{-}16}N_2O_{8\text{-}16}$, and $C_9H_{10\text{-}12}N_2O_{9\text{-}12}$) and five accretion product families ($C_{20}H_{32}N_2O_{9\text{-}19}$, $C_{17}H_{26}N_2O_{12\text{-}18}$, $C_{19}H_{30}N_2O_{11\text{-}19}$, $C_{20}H_{31}N_3O_{12\text{-}21}$, and $C_{20}H_{30}N_4O_{14\text{-}22}$). These product families can be further assigned as the first- or second-generation based on their time series.

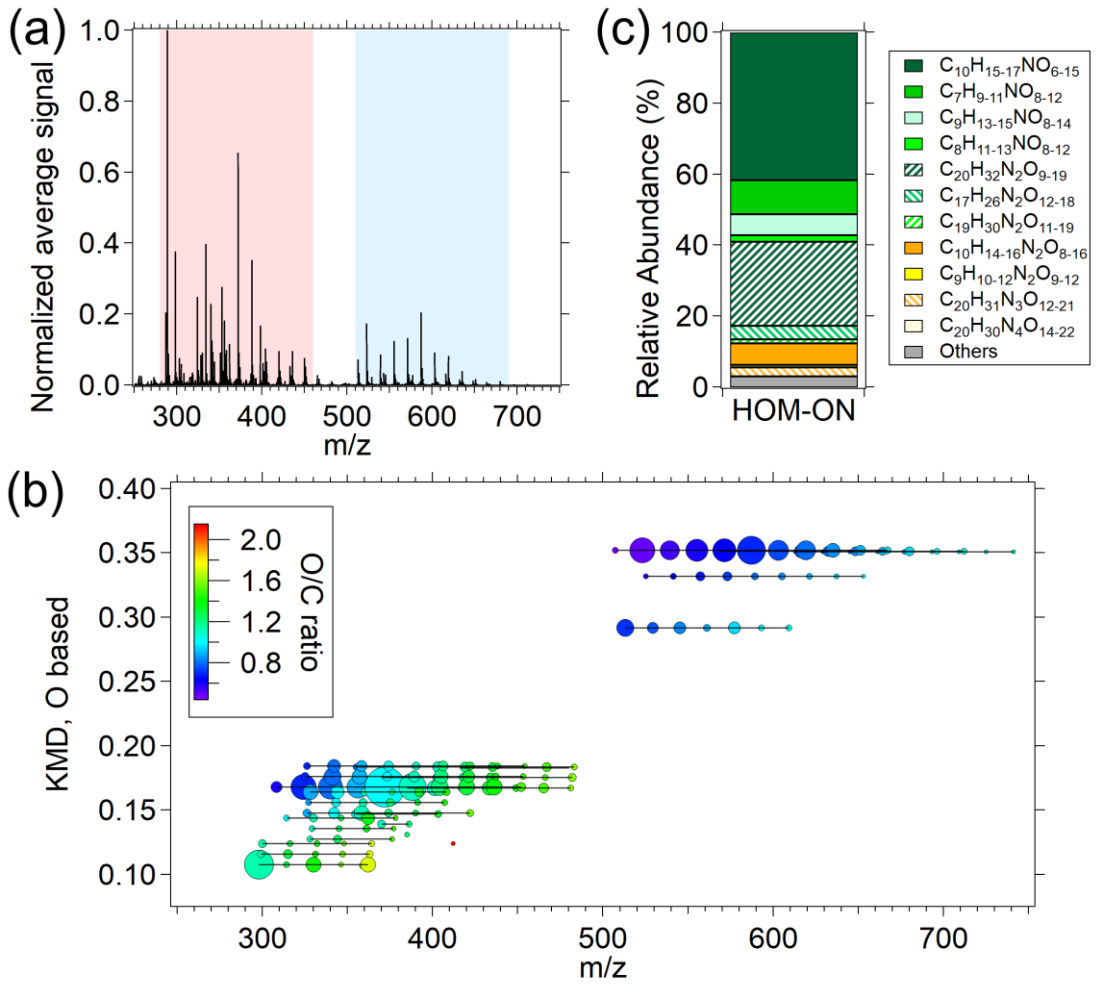

Figure 1. (a) Representative average mass spectrum of HOM-ON formed in this study, shown here for the first experimental period between the first and second β-pinene addition. (b) Kendrick mass defect (O-based) of identified products, with the area representing relative abundance and the color denoting the O/C value. (c) Stacked bar chart of identified product families, with first-generation products in green shades, second-generation products in yellow shades, and the remainder in gray.

Generally, first-generation products constituted a major fraction of total products (see figure 1c), with a value of 87.6%, including monomers of $C_{10}H_{15-17}NO_{6-15}$ (41.6%), $C_7H_{9-11}NO_{8-12}$ (9.6%), $C_9H_{13-15}NO_{8-14}$ (6.0%), and $C_8H_{11-13}NO_{8-12}$ (1.8%) and accretion products of $C_{20}H_{32}N_2O_{9-19}$ (23.7%), $C_{17}H_{26}N_2O_{12-18}$ (3.8%), and $C_{19}H_{30}N_2O_{11-19}$ (1.1%). Second-generation products, including monomers of $C_{10}H_{14-16}N_2O_{8-16}$ (6.0%) and $C_9H_{10-12}N_2O_{9-12}$

(0.74%) and accretion products of $C_{20}H_{31}N_3O_{12\text{-}21}$ (2.5%) and $C_{20}H_{30}N_4O_{14\text{-}22}$ (0.080%) were observed. Finally, the remaining 3.1% of the identified products could not be attributed to any of the above product families or could their structure be elucidated by a suitable mechanism pathway, but they are clearly products from β-pinene + NO_3 reactions based on their time series; here, they are simply grouped as "others". All of the above-identified compounds are organic nitrates, and their formation mechanism will be discussed below. We would like to note that low peaks constituting less than 0.1% of the largest product peak $C_{10}H_{15}NO_{10}$ were not assigned.

First-Generation HOM-ON and Their Formation Mechanism. A number of monomer and accretion product families were observed with a typical first-generation time series. They were quickly formed after each β-pinene addition and reached a peak concentration about 7 min later. This rapid reaction rate indicates an autoxidation formation pathway, which has a short time-scale of tens of seconds per oxidation step or less.[32] The detailed chemical composition and possible formation mechanism of these first-generation products, including C10 HOM-ON, C7-9 HOM-ON, and accretion products, are discussed in the following sections.

First-generation C10 HOM-ON. Among the first-generation product families, $C_{10}H_{15\text{-}17}NO_{6\text{-}15}$ was the most abundant. Considering how the RO_2• radical chain is terminated to form closed-shell products (see the SI),[33] they are likely to be formed via $C_{10}H_{16}NO_x$•. It has been well-established that the reaction of β-pinene + NO_3 is initiated

by the addition of NO_3 radical to the C=C double bond resulting in a nitrooxyalkyl radical $C_{10}H_{16}NO_3$• (NO_3-R•), as shown in Scheme S2. In the atmosphere, this NO_3-R• will be quickly converted to a nitrooxyperoxy radical $C_{10}H_{16}NO_5$• (NO_3-RO_2•) by reaction with O_2. Via autoxidation, $C_{10}H_{16}NO_5$• radicals rapidly undergo unimolecular H-shift and O_2 addition, resulting in a progressive series of $C_{10}H_{16}NO_{2n+1}$• radicals. Meanwhile, RO_2• such as the $C_{10}H_{16}NO_5$• radical can be involved in bimolecular reactions, including reaction with RO_2•, NO_3, HO_2•, NO_2, and NO.[50] Their reaction loss rates (Figure S6) were quantified using a zero-dimensional (0D)-model based on the Master Chemical Mechanism (MCM) v3.3.1,[39, 51] with detailed calculations in Section S2. The loss rates of RO_2• + RO_2• and RO_2• + NO_3 reactions are much higher than the reaction RO_2• with HO_2•, NO_2, and NO, especially within the short period after each β-pinene addition. Overall, bimolecular reactions within this study were then dominated by RO_2• + RO_2• and RO_2• + NO_3 reactions, where both reactions form nitrooxyalkoxy radicals (NO_3-RO•), while the RO_2• self- and cross-reactions also lead to radical chain termination (Russel mechanism, see Scheme S1b,c).

For the formation of $C_{10}H_{16}NO_{2n}$•, an "alkoxy-peroxy" pathway provides a plausible mechanism.[33, 45] For example, the nitrooxyalkoxy radical $C_{10}H_{16}NO_4$• can be competitively formed from the initially formed NO_3-RO_2• ($C_{10}H_{16}NO_5$•) and then undergo H-migration and O_2 addition forming $C_{10}H_{16}NO_6$•.[52, 53] This peroxy radical can then again undergo further autoxidation; such an autoxidation path through an alkoxy radical stage is called an

alkoxy-peroxy pathway, and yields the progressive series of $C_{10}H_{16}NO_{2n}$• products (with an even number of O atoms). In this study, both $C_{10}H_{16}NO_{2n+1}$• and $C_{10}H_{16}NO_{2n}$• radicals were observed, with time series of the most abundant radicals $C_{10}H_{16}NO_9$• and $C_{10}H_{16}NO_8$• shown in Figure 2a. Both $C_{10}H_{16}NO_9$• and $C_{10}H_{16}NO_8$• concentrations followed a typical time series as expected for a first-generation radical, quickly formed after each β-pinene addition, reaching a peak about 2-3 min later, and followed by a subsequently sharp decay. Interestingly, the peak concentration of the $C_{10}H_{16}NO_9$• showed about 30-60 s earlier than that of $C_{10}H_{16}NO_8$•. This time lag is also observed between other $C_{10}H_{16}NO_{2n+1}$• and $C_{10}H_{16}NO_{2n}$•, as shown in Figure S7. As the individual wall loss rate for each compound was not determined, we are unable to compare their formation rates precisely. However, considering that the major sink of RO_2• is via chemical reactions leading to closed-shell products rather than wall loss, this time lag can be explained by the formation mechanism of $C_{10}H_{16}NO_{2n}$•, which is expected to involve a longer-lived RO_2• intermediate that must undergo a bimolecular step forming NO_3-RO• in either NO_3-RO_2• + RO_2• or NO_3-RO_2• + NO_3 reactions, as opposed to directly produced $C_{10}H_{16}NO_{2n+1}$•. To our knowledge, no previous studies have reported such temporal lag between the formation process of radicals containing odd and even oxygen atoms.

According to previous studies, the final fate of these radicals in general is radical chain termination by RO_2• which is expected to produce an equal amount of carbonylnitrates and hydroxynitrates via the Russell mechanism, termination by HO_2• resulting in

hydroperoxynitrates,[33] or termination by unimolecular decomposition forming small radical fragments such as OH or NO_2 (see the SI). The time series of a typical NO_3-RO_2• ($C_{10}H_{16}NO_9$•) along with the corresponding termination products (carbonylnitrates of $C_{10}H_{15}NO_8$, hydroxynitrates of $C_{10}H_{17}NO_8$, and hydroperoxynitrates of $C_{10}H_{17}NO_9$) are shown in Figure 2b. Note that hydroxynitrate formed from $C_{10}H_{16}NO_x$• and hydroperoxynitrate formed from $C_{10}H_{16}NO_{x-1}$• share the same product formula and cannot be distinguished based on the mass spectra. Thus, $C_{10}H_{17}NO_8$ and $C_{10}H_{17}NO_9$ here are mixtures containing both hydroxynitrates and hydroperoxynitrates, whereas these corresponding termination products demonstrated a typical time series of first-generation products, with a quick peak appearance after each β-pinene addition and subsequent decay. Notably, the carbonylnitrates $C_{10}H_{15}NO_8$ showed a much higher signal than the other two termination products. The dominance of carbonylnitrates was commonly observed within the $C_{10}H_{15\text{-}17}NO_{6\text{-}15}$ family and will be discussed in detail below. Additionally, the termination products, especially for carbonylnitrates of $C_{10}H_{15}NO_8$, peaked about 3-6 min later than $C_{10}H_{16}NO_9$•. This time window is suggested to be due to the termination process in the autoxidation chain. To our knowledge, this is the first time such temporal formation lag between radicals and the corresponding termination products is demonstrated.

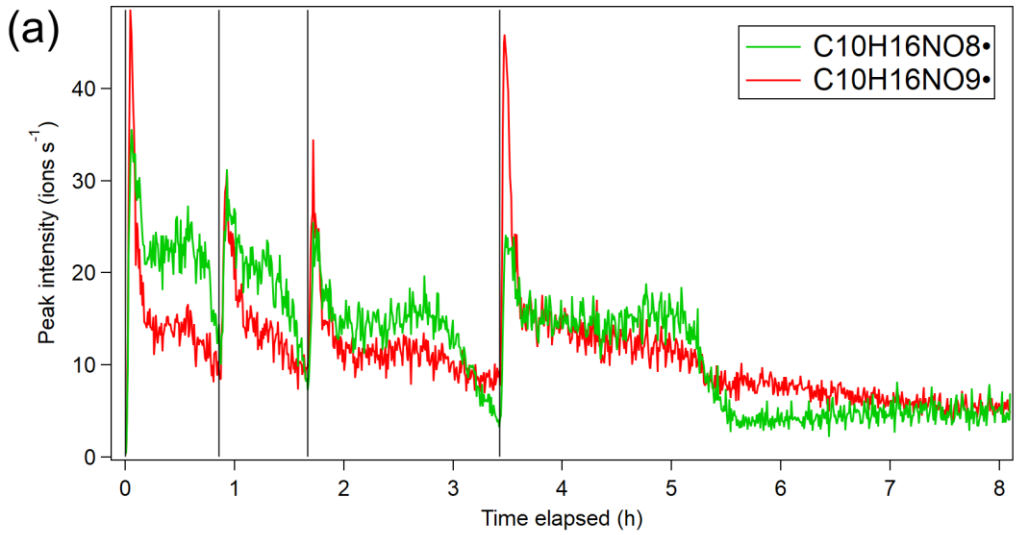
(a)
C10H16NO8•
C10H16NO9•
Peak intensity (ions s-1)
Time elapsed (h)

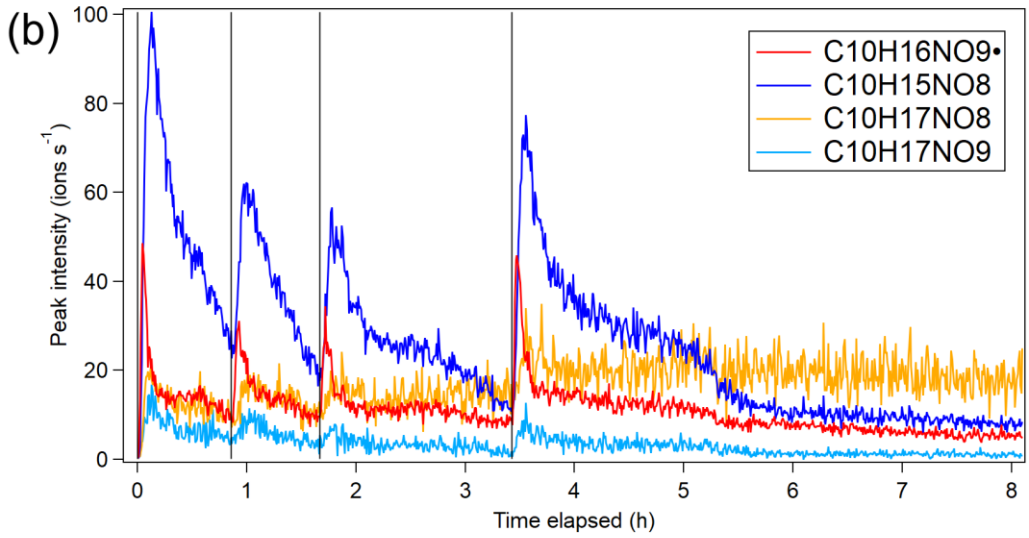
(b)
C10H16NO9•
C10H15NO8
C10H17NO8
C10H17NO9
Peak intensity (ions s-1)
Time elapsed (h)

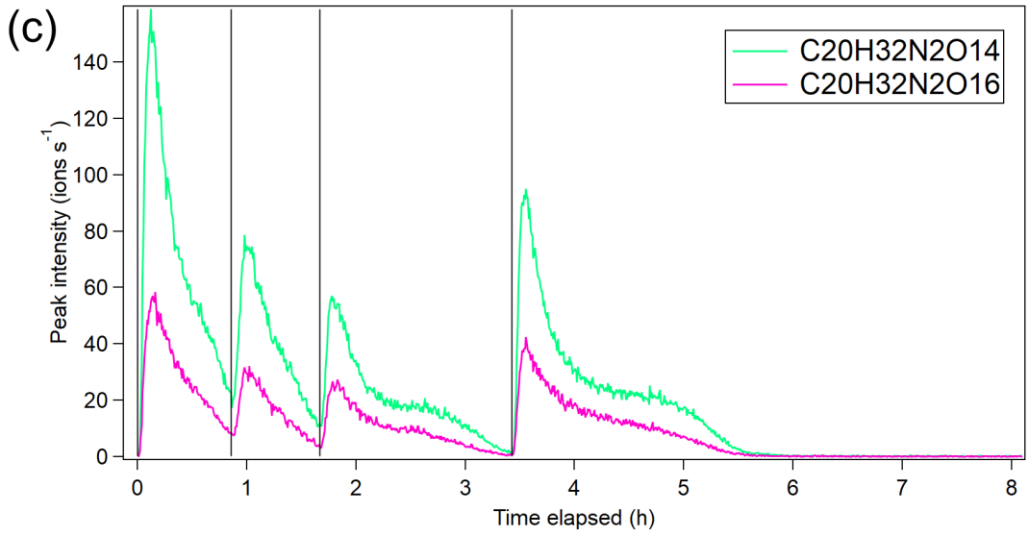
(c)
C20H32N2O14
C20H32N2O16
Peak intensity (ions s-1)
Time elapsed (h)

329

Figure 2. Time series of (a) $C_{10}H_{16}NO_8$• (green) and $C_{10}H_{16}NO_9$• (red) peroxy radicals, (b) $C_{10}H_{16}NO_9$• peroxy radical (red) and its corresponding termination products, including carbonylnitrates of $C_{10}H_{15}NO_8$ in dark blue, hydroxynitrates of $C_{10}H_{17}NO_8$ in yellow, and hydroperoxynitrates of $C_{10}H_{17}NO_9$ in light blue, and (c) accretion products of $C_{20}H_{32}N_2O_{14}$ (lime) and $C_{20}H_{32}N_2O_{16}$ (rose). The four vertical markers indicate β-pinene additions into the chamber. All signals were averaged over binned 30 s intervals.

For $C_{10}H_{16}NO_{6\text{-}15}$• peroxy radicals (corresponding to the $C_{10}H_{15\text{-}17}NO_{6\text{-}15}$ family), similar relative abundances were observed independent of odd or even numbers of O atoms (Table 1). This illustrates the importance of the alkoxy-peroxy pathway in this product family. For termination products, it should be noted that every $C_{10}H_{17}NO_x$ signal, as discussed above, comprises contributions of both hydroxynitrates and hydroperoxynitrates. Nevertheless, it is obvious that carbonylnitrates showed much higher abundances than hydroxynitrates, apparently different from the 1:1 equivalence of carbonyl/hydroxy products in the Russell mechanism, which was an important bimolecular termination channel in this study. Several mechanisms have been described in the literature that can explain this higher abundance of carbonyls. Given that these HOM-RO_2• formed via autoxidation contain multiple -OOH groups, the likely mechanism is the H-migration of an α-OOH hydrogen atom, forming an OH and a carbonyl (see Reaction S1h) and no alcohol.[32, 33, 54-56] Such a H-shift termination pathway was likewise used to explain the formation of the highest intensity peak of carbonylnitrate $C_{10}H_{15}NO_7$ from Δ-3-carene + NO_3.[41] Alternative possible pathways leading to higher abundance of carbonyls include: (1) the reaction of alkoxy RO• + O_2 forming carbonyls and HO_2•,[57] (2) decomposition of β-nitrooxyperoxynitrate,[58] (3) self-reactions of RO_2• via the Bennett and Summers

mechanism, and (4) possible unequal yield of carbonyl and hydroxyl corresponding to a given RO_2• in the cross reactions, and some other pathways. However, kinetic studies have found relatively lower rate constants (4.7×10^4 s^{-1}) for the reaction of RO• with O_2 than that of other RO• reactions, including decomposition (1.5×10^2 s^{-1} - 1.3×10^8 s^{-1}) and isomerization (2.5×10^5 s^{-1} - 3.4×10^7 s^{-1}).[53, 59-61] The decomposition of β-nitrooxyperoxynitrate formed in RO_2• + NO_2 reactions is fast in the particle phase but preferentially redissociates back to NO_3-RO_2• in the gas-phase.[62] The Bennett and Summers mechanism of RO_2• + RO_2• → $2R_HC{=}O$ + H_2O_2 was mostly reported in heterogeneous oxidation reactions and was not previously included in the gas-phase reactions.[63, 64] For cross-reactions between a small and big RO_2•, statistically an equal amount of hydroxyl and carbonyl products are expected for a large number of different RO_2•, despite potential preferences in a single case, unless an RO_2• is a tertiary or acyl RO_2•. An equal amount of hydroxyl and carbonyl is also recommended in current MCM[65, 66] and the review of Jenkin et al.[50] Furthermore, overall bimolecular loss rates of RO_2• are less than 1.5×10^{-2} s^{-1}, as shown in Figure S6. If we assume a unimolecular termination reaction rate of >0.1 s^{-1} for the HOM-RO_2• as reported both experimental measurements[32, 54, 67, 68] and theoretical studies[56, 69, 70] for RO_2• with an α-OOH hydrogen, the unimolecular termination pathway outweighs bimolecular reactions. Although the exact chemical structures of the RO_2• in this study are different from those in the literature,[32, 54, 68] they likely contain α-OOH hydrogen atoms and can be assumed to have similar unimolecular

373 reaction rates. Therefore, instead of the above discussed alternative four pathways,
374 unimolecular termination pathways are likely to be the major contributor to the high gas-
375 phase yields of carbonylnitrates observed.

376

377 **Table 1.** Family of $C_{10}H_{15\text{-}17}NO_{6\text{-}15}$ Observed, Including Nitrooxyperoxy Radicals, along
378 with Their Termination Products, Carbonylnitrates, Hydroxynitrates, and
379 Hydroperoxynitrates.[a]
380

nitrooxyperoxy radical m	carbonylnitrate m-17	hydroxynitrate m-15	hydroperoxynitrate m+1
$C_{10}H_{16}NO_7$• 1.9%	$C_{10}H_{15}NO_6$ 4.8%		$C_{10}H_{17}NO_7$ 1.1%
$C_{10}H_{16}NO_8$• 14.2%	$C_{10}H_{15}NO_7$ 34.6%	$C_{10}H_{17}NO_7$ 1.1%	$C_{10}H_{17}NO_8$ 7.8%
$C_{10}H_{16}NO_9$• 10.0%	$C_{10}H_{15}NO_8$ 32.7%	$C_{10}H_{17}NO_8$ 7.8%	$C_{10}H_{17}NO_9$ 4.4%
$C_{10}H_{16}NO_{10}$• 2.5%	$C_{10}H_{15}NO_9$ 26.6%	$C_{10}H_{17}NO_9$ 4.4%	$C_{10}H_{17}NO_{10}$ 3.0%
$C_{10}H_{16}NO_{11}$• 4.2%	$C_{10}H_{15}NO_{10}$ 100%	$C_{10}H_{17}NO_{10}$ 3.0%	$C_{10}H_{17}NO_{11}$ 2.1%
$C_{10}H_{16}NO_{12}$• 8.7%	$C_{10}H_{15}NO_{11}$ 42.0%	$C_{10}H_{17}NO_{11}$ 2.1%	$C_{10}H_{17}NO_{12}$ 3.5%
$C_{10}H_{16}NO_{13}$• 5.2%	$C_{10}H_{15}NO_{12}$ 14.3%	$C_{10}H_{17}NO_{12}$ 3.5%	$C_{10}H_{17}NO_{13}$ 1.9%
$C_{10}H_{16}NO_{14}$• 1.1%	$C_{10}H_{15}NO_{13}$ 11.7%	$C_{10}H_{17}NO_{13}$ 1.9%	$C_{10}H_{17}NO_{14}$ 0.6%
$C_{10}H_{16}NO_{15}$• 0.80%	$C_{10}H_{15}NO_{14}$ 13.2%	$C_{10}H_{17}NO_{14}$ 0.6%	$C_{10}H_{17}NO_{15}$ 0.19%
	$C_{10}H_{15}NO_{15}$ 2.8%	$C_{10}H_{17}NO_{15}$ 0.19%	

381 [a] The relative intensities for the species detected in this study during the first reaction period
382 are shown on the second line in the same cell. Their relative intensities were normalized to
383 the largest product signal of $C_{10}H_{15}NO_{10}$.

Scheme 1 shows a plausible subset of the degradation scheme, based on structure-activity relationships (SARs) and recent experimental data,[20, 71] and starting at the tertiary NO_3-R• $C_{10}H_{16}NO_3$• (R1) preferentially formed upon initial NO_3 addition to β-pinene. Similar to the OH-initiated oxidation,[72, 73] breaking of the four-membered ring has been reported as a favorable pathway, forming R2,[20, 21] which after O_2 addition forms an unsaturated tertiary $C_{10}H_{16}NO_5$• (R3) radical. A structure similar to R3 was reported in the β-pinene + OH system and was suggested to undergo quick unimolecular reactions.[72, 74-76] Moreover, recent studies have shown that a C=C double bond in an RO_2• radical is a key functionality, leading to fast unimolecular reactions.[56, 77] Thus, we suggest that R3 opens a gateway to fast unimolecular reactions, including autoxidation. The expected rate coefficient of the following unimolecular H-shift has been derived using the SAR by Vereecken and Nozière.[56] Nitrooxyperoxy radical R5 can undergo a rapid scrambling reaction to produce R6, which can either undergo a 1,5 H-shift to form R7, or be terminated via 1,6 H-shift to form carbonylnitrate $C_{10}H_{15}NO_6$ (P1) + OH. Similar unimolecular H-shift termination reactions are suggested for R8, R10, and R12, producing carbonylnitrates. All of these $C_{10}H_{16}NO_{2n+1}$• radicals (R5, R8, R10, R12) could also undergo bimolecular reactions with RO_2•/NO_3 to form $C_{10}H_{16}NO_{2n}$•. Taking R5 as an example, the resulting R13 followed by an H-shift leads to the formation of R14. Both the -OH group and the C=C double bond within R14 further favor fast unimolecular reactions,[56] leading to more oxidized $C_{10}H_{16}NO_{2n}$• radicals via autoxidation or to the formation of P1. Note that Scheme

1 is just one of many possible unimolecular reaction chains, and some radicals observed in this study are not included in Scheme 1, such as the formation of $C_{10}H_{16}NO_{15}$•. Further rigorous studies are needed to constrain its unimolecular pathway. Additionally, the C=C double bond in some of these products can be attacked by the NO_3 radical and lead to second-generation products, which was also observed in this study and will be discussed below. Note that this is not the only pathway leading to HOM. Nah et al.[30] proposed a ring-retaining pathway, with a simplified mechanism shown in Scheme S3a. However, this pathway cannot explain the formation of the second-generation products (e.g., $C_{10}H_{14-16}N_2O_{8-16}$) and C7 compounds in this study. Moreover, according to previous studies,[74, 77] the ring-opening pathway is more likely to lead to autoxidation and to HOM in many monoterpene oxidation reactions, such as α-pinene + NO_3[78] and β-pinene + OH[72-74, 77] due to the steric hindrance for H-shift in the ring-retaining RO_2•. Particularly, for β-pinene, the yield of ring-opening RO_2• is expected to be high, as shown in the work of Vereecken and Peeters[72] and Kaminski et al.[73] for the reaction of β-pinene + OH. Overall, combining our observation and the literature above, HOM formation is more likely to be formed via the ring-opening pathway in β-pinene + NO_3 reactions, although the autoxidation pathway is complex and still not fully clear in this reaction system and multiple pathways might be present simultaneously. Claflin and Ziemann[21] proposed another ring-opening pathway (Scheme S3b). For the two ring-opening pathways, their relative importance is currently unclear. Compared to Nah et al.[30] and Claflin and Ziemann,[21] Scheme 1 provides a

formation pathway for RO_2• containing the C=C double bond, which leads to fast HOM-ON formation and provides a plausible explanation for the second-generation products observed in this study.

Scheme 1. Example Unimolecular Pathway Chain of β-pinene + NO_3 Reactions Leading to the Formation of HOM-ON, specifically Carbonylnitrates.[a]

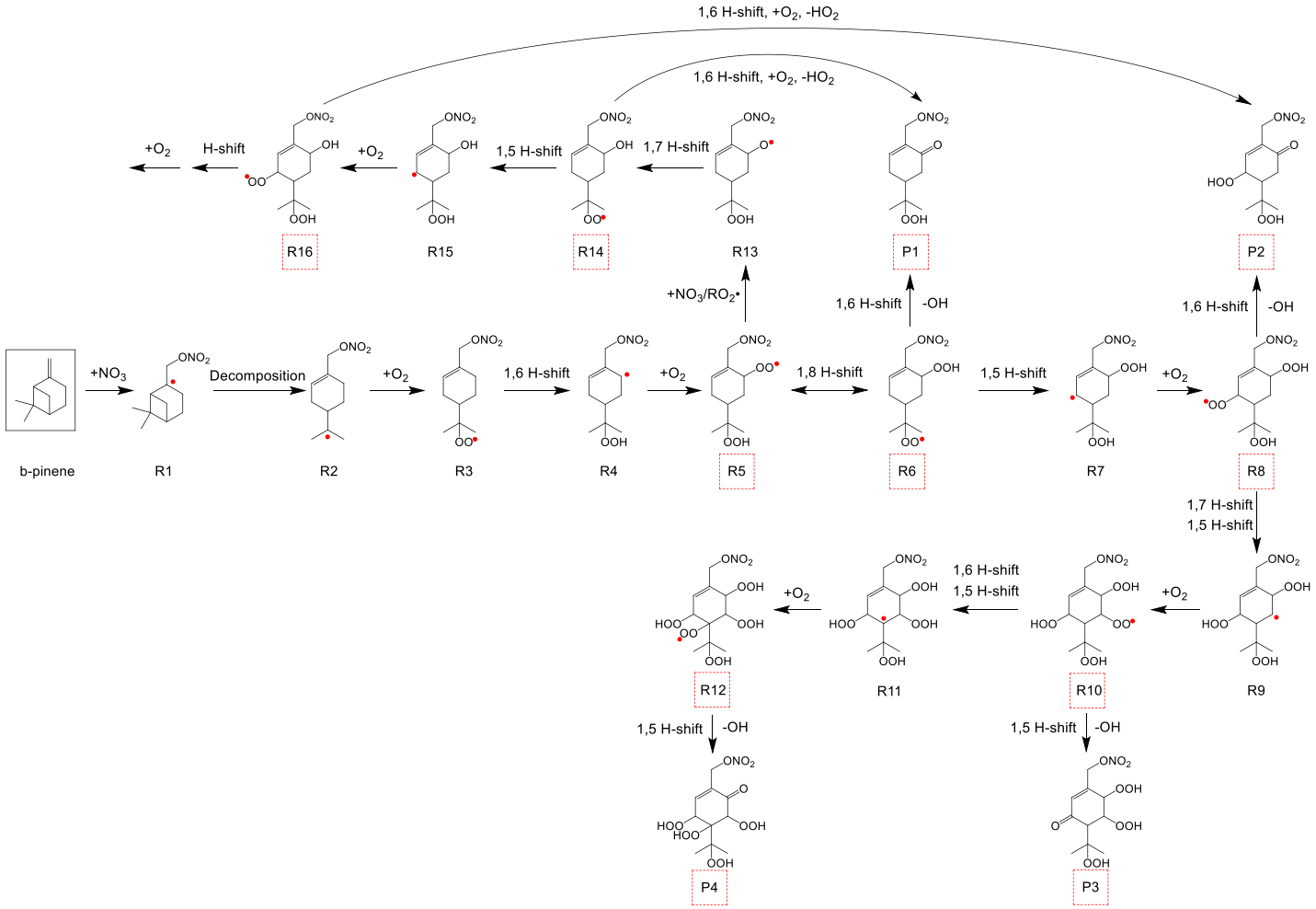

[a] The formula of radicals and products observed in the experiments were highlighted in red-dashed boxes. This is only a small subset of the full oxidation mechanism omitting many competing channels and is not intended to be complete.

First-Generation C7-9 HOM-ON. Besides C10 products, C7-9 compounds were also observed in this study, including product families of $C_7H_{9-11}NO_{8-12}$, $C_9H_{13-15}NO_{8-14}$, and $C_8H_{11-13}NO_{8-12}$, consistent with the study by Nah et al.[30] These first-generation products were suggested to be formed from the decomposition of NO_3-RO• radicals followed by an autoxidation pathway. This decomposition process was already recognized as another important unimolecular reaction, forming ring-opened products.[72, 75, 78, 79] Taking $C_7H_{9-11}NO_{8-12}$ as an example for R3, besides the fast H-shift as shown in Scheme 1, it can undergo bimolecular reactions with RO_2• or NO_3 reactions forming a NO_3-RO•, which will further decompose into acetone and an unsaturated NO_3-R•, such as $C_7H_{10}NO_3$•,[75, 76] as shown in Scheme S4. Radicals like $C_7H_{10}NO_3$• can react with O_2, forming $C_7H_{10}NO_5$•, which can then further undergo autoxidation.

Similar to the $C_{10}H_{15-17}NO_{6-15}$ family, the $C_7H_{9-11}NO_{8-12}$ family followed a typical first-generation time series, with a representative radical $C_7H_{10}NO_9$• and its corresponding termination products shown in Figure S8. When β-pinene was added, $C_7H_{10}NO_9$• peaked instantaneously, followed by the formation of $C_7H_9NO_8$, $C_7H_{11}NO_8$, and $C_7H_{11}NO_9$. A time window of 3-4 min between the peaks of radicals and termination products was observed, indicating the typical period of the termination processes. Carbonylnitrates were again observed as the dominant termination products, suggesting termination by unimolecular H-shift and OH formation to be a major reaction pathway in the $C_7H_{9-11}NO_{8-12}$ family as well. Moreover, higher concentrations, as well as higher carbonylnitrate abundance, were

observed in $C_7H_{10}NO_{2n+1}$• compared to $C_7H_{10}NO_{2n}$•. This indicates that the alkoxy-peroxy channel is a minor, less competitive pathway in the $C_7H_{9\text{-}11}NO_{8\text{-}12}$ family. Additionally, a distinct increase of acetone from 0.04 ppb to 0.44 ppb was observed throughout the experiments, as shown in Figure S1. This confirms the presence of fragmentation process in β-pinene + NO_3, such as the above discussed C_{10} decomposition to form C_7 compounds and acetone. The two remaining product families, $C_9H_{13\text{-}15}NO_{8\text{-}14}$ and $C_8H_{11\text{-}13}NO_{8\text{-}12}$, were hypothesized to be formed in a similar pathway, but the exact bond scission position is not yet known.

First-Generation Accretion Products. Three accretion product families were found to follow a typical first-generation product time series, including $C_{20}H_{32}N_2O_{9\text{-}19}$, $C_{17}H_{26}N_2O_{12\text{-}18}$, and $C_{19}H_{30}N_2O_{11\text{-}19}$. Recent studies have identified the importance of rapid reaction of RO_2• + RO_2• → ROOR + O_2 in the formation of gas-phase accretion products.[80-82] Figure S10 lists the expected accretion products produced from the above-identified NO_3-RO_2• monomers. These three accretion product families can all be explained via RO_2• self- or cross-reaction channels. Notably, $C_{20}H_{32}N_2O_{9\text{-}19}$ were the most abundant accretion products, consistent with the dominance of its corresponding parent NO_3-RO_2•. Figure 2c shows the time series of $C_{20}H_{32}N_2O_{14,16}$, formed from self-reaction of $C_{10}H_{16}NO_{8,9}$• discussed above. Both of them peaked about 6-8 min after each β-pinene addition and decayed afterward. This is consistent with a quick formation process from RO_2• reactions. Moreover, $C_{20}H_{32}N_2O_{14}$ was the most abundant product among the $C_{20}H_{32}N_2O_{9\text{-}19}$ family.

Its corresponding precursor $C_{10}H_{16}NO_8$• also dominated among $C_{10}H_{16}NO_x$• as shown in Figure S11. However, it should be noted that accretion products with the same formula could arise from cross-reactions of several combinations of RO_2•; for example, $C_{10}H_{16}NO_7$• + $C_{10}H_{16}NO_9$• or $C_{10}H_{16}NO_6$• + $C_{10}H_{16}NO_{10}$• could both contribute to $C_{20}H_{32}N_2O_{14}$. Currently, we cannot quantify the relative contribution of different RO_2• recombinations to the accretion products, as the reaction rate coefficients of RO_2• self- or cross-reactions depend on specific RO_2•, and many of them are unknown.[81] The two remaining product families, $C_{17}H_{26}N_2O_{12\text{-}18}$ and $C_{19}H_{30}N_2O_{11\text{-}19}$, showed a similar first-generation time series and likewise followed RO_2• self- and cross-reaction channels.

Second-Generation HOM-ON and Their Tormation Mechanism. Two monomer families ($C_{10}H_{14\text{-}16}N_2O_{8\text{-}16}$ and $C_9H_{10\text{-}12}N_2O_{9\text{-}12}$) and two accretion product families ($C_{20}H_{31}N_3O_{12\text{-}21}$ and $C_{20}H_{30}N_4O_{14\text{-}22}$), which contain two N atoms (monomers) and three or more N atoms (accretion products), showed a time series differing from first-generation products. They mostly showed a concentration peak after β-pinene addition at a much later phase than typical first-generation products, shown in Figure S9. These compounds were assigned as second-generation reaction products. Among those, $C_{10}H_{14\text{-}16}N_2O_{8\text{-}16}$ dominated and were suggested to be formed via NO_3 addition to the first-generation carbonylnitrates products ($C_{10}H_{15}NO_{6\text{-}15}$). As discussed above, the carbonylnitrates formed via unimolecular H-shift termination reactions contain one C=C double bond, which can be attacked by NO_3 radicals to form $C_{10}H_{15}N_2O_x$•. For example, P2 in Scheme 1 could form

493 a tertiary dinitrooxyalkyl radical [$(NO_3)_2$-R•] $C_{10}H_{15}N_2O_{11}$•, which will be quickly
494 converted to a dinitrooxyperoxy radical [$(NO_3)_2$-RO_2•] $C_{10}H_{15}N_2O_{13}$• via O_2 addition, as
495 shown in Scheme S5. This radical can undergo a unimolecular H-shift to either propagate
496 the radical chain or terminate it by the formation of carbonyldinitrates + OH. Via
497 bimolecular reactions of RO_2• + RO_2•, carbonyldinitrates ($C_{10}H_{14}N_2O_x$) and
498 hydroxydinitrates ($C_{10}H_{16}N_2O_x$) can be formed, and hydroperoxydinitrates ($C_{10}H_{16}N_2O_x$)
499 can be formed via RO_2• + HO_2•. These second-generation HOM-ON have not been
500 reported in previous β-pinene + NO_3 studies because these studies mainly focused on the
501 first-generation products and/or used different analysis methods.[20, 21, 30] The observation of
502 these dinitrates in this study highlighted the importance of the C=C double bond formed in
503 R2 in Scheme 1.

504 Accretion products, such as $C_{20}H_{31}N_3O_{12\text{-}21}$ and $C_{20}H_{30}N_4O_{14\text{-}22}$, were also observed
505 and are generated from self- or cross-reactions of later generation RO_2•, likely formed via
506 reactions of $C_{10}H_{15}N_2O_x$• + $C_{10}H_{16}NO_x$• and $C_{10}H_{15}N_2O_x$• + $C_{10}H_{15}N_2O_x$•, respectively.
507 Figure 3a shows the time series of a typical $(NO_3)_2$-RO_2• $C_{10}H_{15}N_2O_9$•, compared against
508 that of $C_{20}H_{30}N_4O_{16}$, the accretion products resulting from its self-reaction. Both of them
509 gradually increased after each β-pinene addition. Moreover, when $C_{10}H_{15}N_2O_9$• reached
510 peak concentration, the signal of $C_{20}H_{30}N_4O_{16}$ showed the largest rate of change. This is
511 consistent with the kinetics shown in eq 2.

512 $$\frac{d[C_{20}H_{30}N_4O_{16}]}{dt} = k_r[C_{10}H_{15}N_2O_9\ \bullet]^2 - k_w[C_{20}H_{30}N_4O_{16}] \quad (2)$$

513 where k_r and k_w are rate constant of $C_{10}H_{15}N_2O_9$• self-reaction and the wall loss rate of
514 $C_{20}H_{30}N_4O_{16}$, respectively. A linear relationship between the rate of accretion products
515 produced and the squared concentrations of RO_2• has also been reported in previous HOM
516 studies.[6, 82] Accretion products of $C_{20}H_{31}N_3O_x$ formed from $C_{10}H_{15}N_2O_x$• + $C_{10}H_{16}NO_x$•
517 were also observed in this study, with the representative time series of $C_{20}H_{31}N_3O_{16}$ and its
518 corresponding precursors RO_2•, $C_{10}H_{15}N_2O_9$• and $C_{10}H_{16}NO_9$•, as shown in Figure 3b. The
519 radical $C_{10}H_{15}N_2O_9$• and its accretion product $C_{20}H_{31}N_3O_{16}$ likewise followed a time series
520 typical of second-generation products, as well as a similar kinetic dependence. The
521 concentrations of $C_{20}H_{31}N_3O_{16}$ peaked earlier than its precursor RO_2• corresponding
522 second-generation $C_{10}H_{15}N_2O_9$• while $C_{20}H_{30}N_4O_{22}$ showed up later than $C_{10}H_{15}N_2O_9$•.
523 This can be because another precursor RO_2• of $C_{20}H_{31}N_3O_{16}$, $C_{10}H_{16}NO_9$•, is a first-
524 generation feature that accelerates the formation of $C_{20}H_{31}N_3O_{16}$. Additionally,
525 $C_{20}H_{31}N_3O_{16}$ showed a small peak after β-pinene addition, especially those in third and
526 fourth β-pinene additions. This shows that $C_{20}H_{31}N_3O_{16}$ followed the trend of its first-
527 generation radical $C_{10}H_{16}NO_9$• more and indicated a role in the cross-reaction formation of
528 $C_{20}H_{31}N_3O_{16}$. Overall, the above discussion on kinetics further confirms the contribution
529 of RO_2• self- and cross-reactions to the accretion product formation in this study.

530 Finally, we observed a family of C_9 products with second generation behavior. We
531 suggest that the second-generation $C_9H_{10\text{-}12}N_2O_{9\text{-}12}$ was likely to be formed by a secondary
532 NO_3 addition pathway, similarly to $C_{10}H_{14\text{-}16}N_2O_{8\text{-}16}$. However, the first generation of

unsaturated C_9 compounds from β-pinene + NO_3 was not detected with our technique, such that the detailed formation mechanism of $C_9H_{10\text{-}12}N_2O_{9\text{-}12}$ cannot be elucidated at this time.

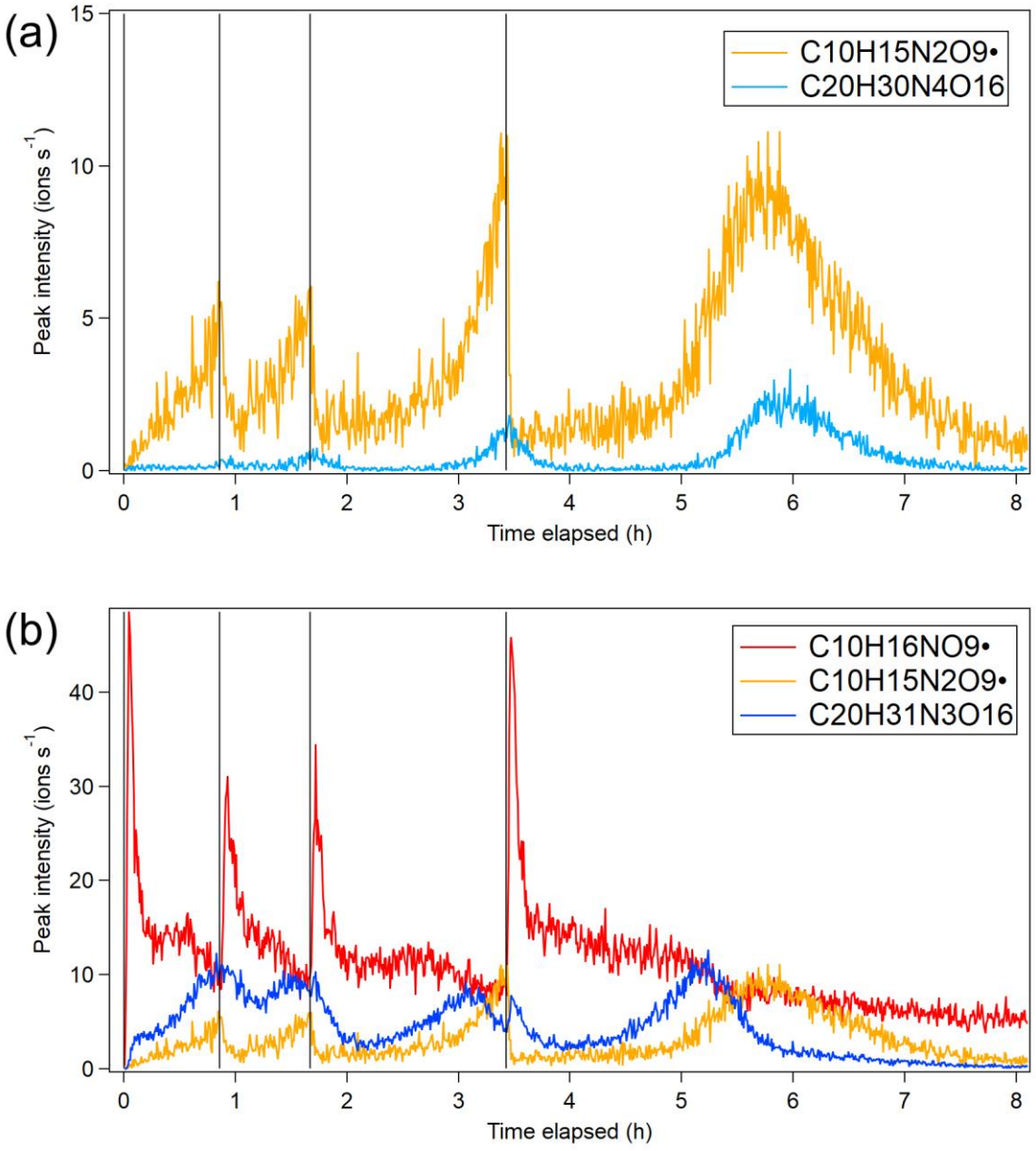

Figure 3. Time series of (a) a representative second-generation peroxy radical ($C_{10}H_{15}N_2O_{12}$•, orange) and its self-reaction accretion product ($C_{20}H_{30}N_4O_{16}$, cyan), and (b) $C_{20}H_{31}N_3O_{16}$ (navy) resulting from the cross-reaction of $C_{10}H_{15}N_2O_{12}$• (orange) and $C_{10}H_{16}NO_9$• (red). The four vertical markers indicate β-pinene additions into the chamber. All signals were averaged over binned 30 s intervals for plotting.

Production Yield Determination. The molar yield of HOM-ON (O≥6) in the NO_3 oxidation of β-pinene was estimated to be 4.8% (-2.6%/+5.6%). The large uncertainty in HOM yield is attributed to a number of factors, including the HOM-ON peak intensity, β-pinene concentration, calibration factor, and transmission efficiency, as described in the Experimental and Methods section and the SI. Note that the HOM produced during this short reaction time (10 min) consists of 93.4% first-generation products and 4.4% second-generation products. This reported value refers to a primary HOM yield. Compared to molar yields of HOM from β-pinene oxidation by O_3 or OH radicals (<0.1%),[6, 83] the NO_3 radical is exceptionally efficient in oxidizing β-pinene to produce HOM. Moreover, the average value of all currently determined HOM yields is around 5%, including OH, O_3, and Cl systems.[27, 84] This means the reaction of β-pinene + NO_3 is competitive enough to produce a sizable fraction of the HOM products. Using the signal-weighted average of the mass of the produced HOM-ON (353.7 g mol^{-1}), we estimate the mass yields to be roughly 2.6 (=353.7 g mol^{-1} / 136.1 g mol^{-1}) times the molar yield. The value in this study is slightly larger than the factor 2.4 calculated for the α-pinene ozonolysis system.[6] This indicates that reactions with NO_3 radicals lead to higher mass oxidation products, as expected, and contribute more to SOA than ozonolysis reactions. The converted mass yields of HOM-ON from β-pinene + NO_3 were averaged to 12.5% (-6.8%/+14.6%), assuming that the volatility of HOM-ON was low enough to condense irreversibly onto the particle phase.[6, 45] Considering the SOA yields of β-pinene + NO_3,[18-20, 22, 23, 26] these HOM-ON should

561 contribute a significant fraction, especially at low organic aerosol loadings in ambient
562 atmosphere. Note that the volatility of HOM-ON was not determined in this study. Yet
563 Pullinen et al.[45] determined a range of 0.5-1 for effective uptake coefficients of HOM-ON
564 from β-pinene + OH. Therefore, it is reasonable to approximate the uptake of most of the
565 HOM-ON as being irreversible when estimating their contribution to SOA. Even an uptake
566 coefficient of 0.5 would cause HOM to condense efficiently on particles. Assuming that
567 all HOM condensing on particles provides an upper limit of the contribution of HOM-ON
568 to SOA, and most of HOM will thus reside in the particle phase. Although HOM-ON in
569 this study are not identical to those in Pullinen et al.,[45] they are expected to have generally
570 similar structures, and HOM-ON contribution to SOA formation is considered to be
571 significant in β-pinene + NO_3 reactions.

572 **Atmospheric Implications**

573 We observed a large number of HOM-ON formed from NO_3 oxidation of β-pinene in
574 the SAPHIR chamber, including six monomer (C=7-10, N=1-2, O=6-16) and five accretion
575 product (C=17-20, N=2-4, O=9-22) families. An example formation mechanism was
576 proposed and constrained based on the time series of the closed-shell HOM, which were
577 different for first- and second-generation products and depended on the precursor RO_2•.
578 Such HOM-ON are expected to be formed under the conditions of the nocturnal planetary
579 boundary layer (PBL), especially when both biogenic VOC and anthropogenic NO_x sources
580 are present. Recent field studies have shown that these HOM-ON are prevalent at night-

time in the Southeastern US and contribute to a large fraction of SOA.[13, 15] The precursor peroxy radicals, especially $C_{10}H_{16}NO_9$•, formed from monoterpene + NO_3 are observed at night-time in SORPES station in eastern China, where the BVOC oxidation is strongly influenced by NO_x.[85]

Direct experimental evidence was provided in our study to highlight the importance of the unimolecular H-shift termination pathway in the NO_3 system, producing unsaturated carbonylnitrates as first-generation products, similar to OH systems.[32, 55, 74] We expect that a large portion of HOM-ON formed at night-time in the ambient atmosphere over a forest environment affected by anthropogenic emissions contains a carbonyl group and one or more -OOH groups, in addition to the initiating -NO_3 group. These unsaturated first-generation carbonylnitrates are anticipated to react further with additional NO_3 and lead to the formation of second-generation products. Although some studies found that second-generation ON containing two or more nitrogens were much less abundant than mononitrates,[86] second-generation products might be important when NO_3 is abundant or during the next day when unsaturated carbonylnitrate can react with OH.

The production yields of HOM-ON from β-pinene + NO_3 were estimated with a mean molar yield of 4.8% (-2.6%/+5.6%). This yield is much higher than the HOM yield in β-pinene oxidation by OH (0.58%) and O_3 (0.12%) reported by Jokinen et al.[83] and HOM yield in the isoprene oxidation by NO_3 (1.2%).[87] This higher HOM yield of β-pinene + NO_3 indicated the potential significance of HOM-ON to the formation of SOA in the

nocturnal PBL in areas influenced by biogenic VOC and anthropogenic NO_x emissions as observed by a number of field studies.[88] Incorporating the HOM-ON yield determined in this study into future models can lead to a better interpretation of ambient data and a more accurate prediction of atmospheric and climate effects of β-pinene + NO_3 reactions. Furthermore, negligible second-generation products are included in the production yield. It is unclear that whether their contribution to HOM yields will outweigh the first-generation products and further influence the SOA formation in the ambient atmosphere. Further laboratory studies and field observations are needed.

SUPPORTING INFORMATION

Additional information deriving the calibration coefficient of CIMS and HOM yields (Section S1) and calculations of RO_2• bimolecular loss rates (Section S2); figures showing the experimental procedure (Figure S1); relative contributions of reactions of β-pinene with NO_3 and O_3 to total β-pinene loss (Figure S2); SMPS data (Figure S3); the average mass spectrum of each experimental period (Figure S4); time series of residuals (Figure S5); RO_2• bimolecular loss rates (Figure S6); peroxy radicals of $C_{10}H_{16}NO_x$• (Figure S7); C7 compounds (Figure S8); second-generation products (Figure S9); and permutation reactions of identified first-generation NO_3-RO_2• radicals (Figure S10) and $C_{10}H_{16}NO_x$• (Figure S11). Schemes demonstrating HOM formation mechanism involving RO_2• (Scheme S1); general autoxidation of NO_3 oxidation of β-pinene (Scheme S2); the simplified HOM formation pathway proposed in prior studies (Scheme S3); the possible

formation pathway of C7 compounds (Scheme S4); and example formation pathway of second-generation products (Scheme S5); tables listing HR peak list (Table S1); reaction rates used to calculate RO_2• bimolecular loss rates (Table S2); and relative intensities of the $C_7H_{9\text{-}11}NO_{8\text{-}12}$ product family (Table S3).

ACKNOWLEDGMENTS

The authors thank the SAPHIR team for supporting our measurements and providing helpful data. H.S and D.Z would like to thank the funding support of the National Natural Science Foundation of China (41875145) and Science and Technology Commission of Shanghai Municipality (20230711400).

REFERENCES

(1) Sindelarova, K.; Granier, C.; Bouarar, I.; Guenther, A.; Tilmes, S.; Stavrakou, T.; Müller, J. F.; Kuhn, U.; Stefani, P.; Knorr, W., Global data set of biogenic VOC emissions calculated by the MEGAN model over the last 30 years. *Atmos. Chem. Phys.* **2014**, *14* (17), 9317-9341.

(2) Berndt, T.; Richters, S.; Jokinen, T.; Hyttinen, N.; Kurtén, T.; Otkjær, R. V.; Kjaergaard, H. G.; Stratmann, F.; Herrmann, H.; Sipilä, M.; Kulmala, M.; Ehn, M., Hydroxyl radical-induced formation of highly oxidized organic compounds. *Nat. Commun.* **2016**, *7*, 13677.

(3) Surratt, J. D.; Chan, A. W. H.; Eddingsaas, N. C.; Chan, M. N.; Loza, C. L.; Kwan, A. J.; Hersey, S. P.; Flagan, R. C.; Wennberg, P. O.; Seinfeld, J. H., Reactive intermediates revealed in secondary organic aerosol formation from isoprene. *Proc. Natl. Acad. Sci. U.S.A.* **2010**, *107* (15), 6640-6645.

(4) Brown, S. S.; Stutz, J., Nighttime radical observations and chemistry. *Chem. Soc. Rev.* **2012**, *41* (19), 6405-6447.

(5) Ng, N. L.; Brown, S. S.; Archibald, A. T.; Atlas, E.; Cohen, R. C.; Crowley, J. N.; Day, D. A.; Donahue, N. M.; Fry, J. L.; Fuchs, H.; Griffin, R. J.; Guzman, M. I.; Herrmann, H.; Hodzic, A.; Iinuma, Y.; Jimenez, J. L.; Kiendler-Scharr, A.; Lee, B. H.; Luecken, D. J.; Mao, J. Q.; McLaren, R.; Mutzel, A.; Osthoff, H. D.; Ouyang, B.; Picquet-Varrault, B.; Platt, U.; Pye, H. O. T.; Rudich, Y.; Schwantes, R. H.; Shiraiwa, M.; Stutz, J.; Thornton, J. A.; Tilgner, A.; Williams, B. J.; Zaveri, R. A., Nitrate radicals and biogenic volatile organic

650 compounds: oxidation, mechanisms, and organic aerosol. *Atmos. Chem. Phys.* **2017**, *17*
651 (3), 2103-2162.
652 (6) Ehn, M.; Thornton, J. A.; Kleist, E.; Sipilä, M.; Junninen, H.; Pullinen, I.; Springer, M.;
653 Rubach, F.; Tillmann, R.; Lee, B.; Lopez-Hilfiker, F.; Andres, S.; Acir, I. H.; Rissanen, M.;
654 Jokinen, T.; Schobesberger, S.; Kangasluoma, J.; Kontkanen, J.; Nieminen, T.; Kurtén, T.;
655 Nielsen, L. B.; Jørgensen, S.; Kjaergaard, H. G.; Canagaratna, M.; Dal Maso, M.; Berndt,
656 T.; Petäjä, T.; Wahner, A.; Kerminen, V. M.; Kulmala, M.; Worsnop, D. R.; Wildt, J.;
657 Mentel, T. F., A large source of low-volatility secondary organic aerosol. *Nature* **2014**, *506*
658 (7489), 476-479.
659 (7) Tröstl, J.; Chuang, W. K.; Gordon, H.; Heinritzi, M.; Yan, C.; Molteni, U.; Ahlm, L.;
660 Frege, C.; Bianchi, F.; Wagner, R.; Simon, M.; Lehtipalo, K.; Williamson, C.; Craven, J.
661 S.; Duplissy, J.; Adamov, A.; Almeida, J.; Bernhammer, A. K.; Breitenlechner, M.; Brilke,
662 S.; Dias, A.; Ehrhart, S.; Flagan, R. C.; Franchin, A.; Fuchs, C.; Guida, R.; Gysel, M.;
663 Hansel, A.; Hoyle, C. R.; Jokinen, T.; Junninen, H.; Kangasluoma, J.; Keskinen, H.; Kim,
664 J.; Krapf, M.; Kürten, A.; Laaksonen, A.; Lawler, M.; Leiminger, M.; Mathot, S.; Möhler,
665 O.; Nieminen, T.; Onnela, A.; Petäjä, T.; Piel, F. M.; Miettinen, P.; Rissanen, M. P.; Rondo,
666 L.; Sarnela, N.; Schobesberger, S.; Sengupta, K.; Sipilä, M.; Smith, J. N.; Steiner, G.; Tomè,
667 A.; Virtanen, A.; Wagner, A. C.; Weingartner, E.; Wimmer, D.; Winkler, P. M.; Ye, P. L.;
668 Carslaw, K. S.; Curtius, J.; Dommen, J.; Kirkby, J.; Kulmala, M.; Riipinen, I.; Worsnop, D.
669 R.; Donahue, N. M.; Baltensperger, U., The role of low-volatility organic compounds in
670 initial particle growth in the atmosphere. *Nature* **2016**, *533* (7604), 527-531.
671 (8) Hallquist, M.; Wenger, J. C.; Baltensperger, U.; Rudich, Y.; Simpson, D.; Claeys, M.;
672 Dommen, J.; Donahue, N. M.; George, C.; Goldstein, A. H.; Hamilton, J. F.; Herrmann,
673 H.; Hoffmann, T.; Iinuma, Y.; Jang, M.; Jenkin, M. E.; Jimenez, J. L.; Kiendler-Scharr, A.;
674 Maenhaut, W.; McFiggans, G.; Mentel, T. F.; Monod, A.; Prévôt, A. S. H.; Seinfeld, J. H.;
675 Surratt, J. D.; Szmigielski, R.; Wildt, J., The formation, properties and impact of secondary
676 organic aerosol: current and emerging issues. *Atmos. Chem. Phys.* **2009**, *9* (14), 5155-5236.
677 (9) Shrivastava, M.; Cappa, C. D.; Fan, J. W.; Goldstein, A. H.; Guenther, A. B.; Jimenez,
678 J. L.; Kuang, C.; Laskin, A.; Martin, S. T.; Ng, N. L.; Petaja, T.; Pierce, J. R.; Rasch, P. J.;
679 Roldin, P.; Seinfeld, J. H.; Shilling, J.; Smith, J. N.; Thornton, J. A.; Volkamer, R.; Wang,
680 J.; Worsnop, D. R.; Zaveri, R. A.; Zelenyuk, A.; Zhang, Q., Recent advances in
681 understanding secondary organic aerosol: implications for global climate forcing. *Rev.*
682 *Geophys.* **2017**, *55* (2), 509-559.
683 (10) Ng, N. L.; Kwan, A. J.; Surratt, J. D.; Chan, A. W. H.; Chhabra, P. S.; Sorooshian, A.;
684 Pye, H. O. T.; Crounse, J. D.; Wennberg, P. O.; Flagan, R. C.; Seinfeld, J. H., Secondary
685 organic aerosol (SOA) formation from reaction of isoprene with nitrate radicals (NO_3).
686 *Atmos. Chem. Phys.* **2008**, *8* (14), 4117-4140.
687 (11) Rollins, A. W.; Kiendler-Scharr, A.; Fry, J. L.; Brauers, T.; Brown, S. S.; Dorn, H. P.;
688 Dubé, W. P.; Fuchs, H.; Mensah, A.; Mentel, T. F.; Rohrer, F.; Tillmann, R.; Wegener, R.;

Wooldridge, P. J.; Cohen, R. C., Isoprene oxidation by nitrate radical: alkyl nitrate and secondary organic aerosol yields. *Atmos. Chem. Phys.* **2009**, *9* (18), 6685-6703.
(12) Pye, H. O. T.; Chan, A. W. H.; Barkley, M. P.; Seinfeld, J. H., Global modeling of organic aerosol: the importance of reactive nitrogen (NO_x and NO_3). *Atmos. Chem. Phys.* **2010**, *10* (22), 11261-11276.
(13) Ayres, B. R.; Allen, H. M.; Draper, D. C.; Brown, S. S.; Wild, R. J.; Jimenez, J. L.; Day, D. A.; Campuzano-Jost, P.; Hu, W.; de Gouw, J.; Koss, A.; Cohen, R. C.; Duffey, K. C.; Romer, P.; Baumann, K.; Edgerton, E.; Takahama, S.; Thornton, J. A.; Lee, B. H.; Lopez-Hilfiker, F. D.; Mohr, C.; Wennberg, P. O.; Nguyen, T. B.; Teng, A.; Goldstein, A. H.; Olson, K.; Fry, J. L., Organic nitrate aerosol formation via NO_3 + biogenic volatile organic compounds in the southeastern United States. *Atmos. Chem. Phys.* **2015**, *15* (23), 13377-13392.
(14) Fisher, J. A.; Jacob, D. J.; Travis, K. R.; Kim, P. S.; Marais, E. A.; Miller, C. C.; Yu, K. R.; Zhu, L.; Yantosca, R. M.; Sulprizio, M. P.; Mao, J. Q.; Wennberg, P. O.; Crounse, J. D.; Teng, A. P.; Nguyen, T. B.; St Clair, J. M.; Cohen, R. C.; Romer, P.; Nault, B. A.; Wooldridge, P. J.; Jimenez, J. L.; Campuzano-Jost, P.; Day, D. A.; Hu, W. W.; Shepson, P. B.; Xiong, F. L. Z.; Blake, D. R.; Goldstein, A. H.; Misztal, P. K.; Hanisco, T. F.; Wolfe, G. M.; Ryerson, T. B.; Wisthaler, A.; Mikoviny, T., Organic nitrate chemistry and its implications for nitrogen budgets in an isoprene- and monoterpene-rich atmosphere: constraints from aircraft (SEAC(4)RS) and ground-based (SOAS) observations in the Southeast US. *Atmos. Chem. Phys.* **2016**, *16* (9), 5969-5991.
(15) Xu, L.; Guo, H. Y.; Boyd, C. M.; Klein, M.; Bougiatioti, A.; Cerully, K. M.; Hite, J. R.; Isaacman-VanWertz, G.; Kreisberg, N. M.; Knote, C.; Olson, K.; Koss, A.; Goldstein, A. H.; Hering, S. V.; de Gouw, J.; Baumann, K.; Lee, S. H.; Nenes, A.; Weber, R. J.; Ng, N. L., Effects of anthropogenic emissions on aerosol formation from isoprene and monoterpenes in the southeastern United States. *Proc. Natl. Acad. Sci. U.S.A.* **2015**, *112* (1), 37-42.
(16) Guenther, A. B.; Jiang, X.; Heald, C. L.; Sakulyanontvittaya, T.; Duhl, T.; Emmons, L. K.; Wang, X., The model of emissions of gases and aerosols from nature version 2.1 (MEGAN2.1): an extended and updated framework for modeling biogenic emissions. *Geosci. Model. Dev.* **2012**, *5* (6), 1471-1492.
(17) Atkinson, R.; Arey, J., Atmospheric degradation of volatile organic compounds. *Chem. Rev.* **2003**, *103* (12), 4605-4638.
(18) Griffin, R. J.; Cocker, D. R.; Flagan, R. C.; Seinfeld, J. H., Organic aerosol formation from the oxidation of biogenic hydrocarbons. *J. Geophys. Res.: Atmos.* **1999**, *104* (D3), 3555-3567.
(19) Fry, J. L.; Kiendler-Scharr, A.; Rollins, A. W.; Wooldridge, P. J.; Brown, S. S.; Fuchs, H.; Dubé, W.; Mensah, A.; dal Maso, M.; Tillmann, R.; Dorn, H. P.; Brauers, T.; Cohen, R. C., Organic nitrate and secondary organic aerosol yield from NO_3 oxidation of beta-pinene

evaluated using a gas-phase kinetics/aerosol partitioning model. *Atmos. Chem. Phys.* **2009**, *9* (4), 1431-1449.
(20) Boyd, C. M.; Sanchez, J.; Xu, L.; Eugene, A. J.; Nah, T.; Tuet, W. Y.; Guzman, M. I.; Ng, N. L., Secondary organic aerosol formation from the beta-pinene+NO_3 system: effect of humidity and peroxy radical fate. *Atmos. Chem. Phys.* **2015**, *15* (13), 7497-7522.
(21) Claflin, M. S.; Ziemann, P. J., Identification and quantitation of aerosol products of the reaction of beta-pinene with NO_3 radicals and implications for gas- and particle-phase reaction mechanisms. *J. Phys. Chem. A* **2018**, *122* (14), 3640-3652.
(22) Fry, J. L.; Draper, D. C.; Barsanti, K. C.; Smith, J. N.; Ortega, J.; Winkle, P. M.; Lawler, M. J.; Brown, S. S.; Edwards, P. M.; Cohen, R. C.; Lee, L., Secondary organic aerosol formation and organic nitrate yield from NO_3 oxidation of biogenic hydrocarbons. *Environ. Sci. Technol.* **2014**, *48* (20), 11944-11953.
(23) Hallquist, M.; Wängberg, I.; Ljungström, E.; Barnes, I.; Becker, K. H., Aerosol and product yields from NO_3 radical-initiated oxidation of selected monoterpenes. *Environ. Sci. Technol.* **1999**, *33* (4), 553-559.
(24) Perraud, V.; Bruns, E. A.; Ezell, M. J.; Johnson, S. N.; Greaves, J.; Finlayson-Pitts, B. J., Identification of organic nitrates in the NO_3 radical initiated oxidation of alpha-pinene by atmospheric pressure chemical ionization mass spectrometry. *Environ. Sci. Technol.* **2010**, *44* (15), 5887-5893.
(25) Spittler, M.; Barnes, I.; Bejan, I.; Brockmann, K. J.; Benter, T.; Wirtz, K., Reactions of NO_3 radicals with limonene and alpha-pinene: product and SOA formation. *Atmos. Environ.* **2006**, *40* S116-S127.
(26) Lambe, A. T.; Wood, E. C.; Krechmer, J. E.; Majluf, F.; Williams, L. R.; Croteau, P. L.; Cirtog, M.; Féron, A.; Petit, J. E.; Albinet, A.; Jimenez, J. L.; Peng, Z., Nitrate radical generation via continuous generation of dinitrogen pentoxide in a laminar flow reactor coupled to an oxidation flow reactor. *Atmos. Meas. Tech.* **2020**, *13* (5), 2397-2411.
(27) Bianchi, F.; Kurtén, T.; Riva, M.; Mohr, C.; Rissanen, M. P.; Roldin, P.; Berndt, T.; Crounse, J. D.; Wennberg, P. O.; Mentel, T. F.; Wildt, J.; Junninen, H.; Jokinen, T.; Kulmala, M.; Worsnop, D. R.; Thornton, J. A.; Donahue, N.; Kjaergaard, H. G.; Ehn, M., Highly oxygenated organic molecules (HOM) from gas-phase autoxidation involving peroxy radicals: a key contributor to atmospheric aerosol. *Chem. Rev.* **2019**, *119* (6), 3472-3509.
(28) Huang, W.; Saathoff, H.; Shen, X. L.; Ramisetty, R.; Leisner, T.; Mohr, C., Chemical characterization of highly functionalized organonitrates contributing to night-time organic aerosol mass loadings and particle growth. *Environ. Sci. Technol.* **2019**, *53* (3), 1165-1174.
(29) Kirkby, J.; Duplissy, J.; Sengupta, K.; Frege, C.; Gordon, H.; Williamson, C.; Heinritzi, M.; Simon, M.; Yan, C.; Almeida, J.; Tröstl, J.; Nieminen, T.; Ortega, I. K.; Wagner, R.; Adamov, A.; Amorim, A.; Bernhammer, A. K.; Bianchi, F.; Breitenlechner, M.; Brilke, S.; Chen, X. M.; Craven, J.; Dias, A.; Ehrhart, S.; Flagan, R. C.; Franchin, A.; Fuchs, C.; Guida, R.; Hakala, J.; Hoyle, C. R.; Jokinen, T.; Junninen, H.; Kangasluoma, J.; Kim,

767 J.; Krapf, M.; Kürten, A.; Laaksonen, A.; Lehtipalo, K.; Makhmutov, V.; Mathot, S.;
768 Molteni, U.; Onnela, A.; Peräkylä, O.; Piel, F.; Petäjä, T.; Praplan, A. P.; Pringle, K.; Rap,
769 A.; Richards, N. A. D.; Riipinen, I.; Rissanen, M. P.; Rondo, L.; Sarnela, N.; Schobesberger,
770 S.; Scott, C. E.; Seinfeld, J. H.; Sipilä, M.; Steiner, G.; Stozhkov, Y.; Stratmann, F.; Tomé,
771 A.; Virtanen, A.; Vogel, A. L.; Wagner, A. C.; Wagner, P. E.; Weingartner, E.; Wimmer, D.;
772 Winkler, P. M.; Ye, P. L.; Zhang, X.; Hansel, A.; Dommen, J.; Donahue, N. M.; Worsnop,
773 D. R.; Baltensperger, U.; Kulmala, M.; Carslaw, K. S.; Curtius, J., Ion-induced nucleation
774 of pure biogenic particles. *Nature* **2016**, *533* (7604), 521-525.
775 (30) Nah, T.; Sanchez, J.; Boyd, C. M.; Ng, N. L., Photochemical aging of alpha-pinene
776 and beta-pinene secondary organic aerosol formed from nitrate radical oxidation. *Environ.*
777 *Sci. Technol.* **2016**, *50* (1), 222-231.
778 (31) Takeuchi, M.; Ng, N. L., Chemical composition and hydrolysis of organic nitrate
779 aerosol formed from hydroxyl and nitrate radical oxidation of alpha-pinene and beta-
780 pinene. *Atmos. Chem. Phys.* **2019**, *19* (19), 12749-12766.
781 (32) Crounse, J. D.; Nielsen, L. B.; Jørgensen, S.; Kjaergaard, H. G.; Wennberg, P. O.,
782 Autoxidation of organic compounds in the atmosphere. *J. Phys. Chem. Lett.* **2013**, *4* (20),
783 3513-3520.
784 (33) Mentel, T. F.; Springer, M.; Ehn, M.; Kleist, E.; Pullinen, I.; Kurtén, T.; Rissanen, M.;
785 Wahner, A.; Wildt, J., Formation of highly oxidized multifunctional compounds:
786 autoxidation of peroxy radicals formed in the ozonolysis of alkenes - deduced from
787 structure-product relationships. *Atmos. Chem. Phys.* **2015**, *15* (12), 6745-6765.
788 (34) Bohn, B.; Rohrer, F.; Brauers, T.; Wahner, A., Actinometric measurements of NO_2
789 photolysis frequencies in the atmosphere simulation chamber SAPHIR. *Atmos. Chem.*
790 *Phys.* **2005**, *5* 493-503.
791 (35) Rohrer, F.; Bohn, B.; Brauers, T.; Brüning, D.; Johnen, F. J.; Wahner, A.; Kleffmann,
792 J., Characterisation of the photolytic HONO-source in the atmosphere simulation chamber
793 SAPHIR. *Atmos. Chem. Phys.* **2005**, *5* 2189-2201.
794 (36) Sarrafzadeh, M.; Wildt, J.; Pullinen, I.; Springer, M.; Kleist, E.; Tillmann, R.; Schmitt,
795 S. H.; Wu, C.; Mentel, T. F.; Zhao, D. F.; Hastie, D. R.; Kiendler-Scharr, A., Impact of NO_x
796 and OH on secondary organic aerosol formation from beta-pinene photooxidation. *Atmos.*
797 *Chem. Phys.* **2016**, *16* (17), 11237-11248.
798 (37) Zhao, D. F.; Schmitt, S. H.; Wang, M. J.; Acir, I. H.; Tillmann, R.; Tan, Z. F.; Novelli,
799 A.; Fuchs, H.; Pullinen, I.; Wegener, R.; Rohrer, F.; Wildt, J.; Kiendler-Scharr, A.; Wahner,
800 A.; Mentel, T. F., Effects of NO_x and SO_2 on the secondary organic aerosol formation from
801 photooxidation of alpha-pinene and limonene. *Atmos. Chem. Phys.* **2018**, *18* (3), 1611-
802 1628.
803 (38) Wagner, N. L.; Dubé, W. P.; Washenfelder, R. A.; Young, C. J.; Pollack, I. B.; Ryerson,
804 T. B.; Brown, S. S., Diode laser-based cavity ring-down instrument for NO_3, N_2O_5, NO,
805 NO_2 and O_3 from aircraft. *Atmos. Meas. Tech.* **2011**, *4* (6), 1227-1240.

(39) Saunders, S. M.; Jenkin, M. E.; Derwent, R. G.; Pilling, M. J., Protocol for the development of the Master Chemical Mechanism, MCM v3 (Part A): tropospheric degradation of non-aromatic volatile organic compounds. *Atmos. Chem. Phys.* **2003**, *3* 161-180.
(40) Hyttinen, N.; Rissanen, M. P.; Kurtén, T., Computational comparison of acetate and nitrate chemical ionization of highly oxidized cyclohexene ozonolysis intermediates and products. *J. Phys. Chem. A.* **2017**, *121* (10), 2172-2179.
(41) Draper, D. C.; Myllys, N.; Hyttinen, N.; Møller, K. H.; Kjaergaard, H. G.; Fry, J. L.; Smith, J. N.; Kurtén, T., Formation of highly oxidized molecules from NO_3 radical initiated oxidation of delta-3-carene: a mechanistic study. *ACS Earth Space Chem.* **2019**, *3* (8), 1460-1470.
(42) Massoli, P.; Stark, H.; Canagaratna, M. R.; Krechmer, J. E.; Xu, L.; Ng, N. L.; Mauldin, R. L.; Yan, C.; Kimmel, J.; Misztal, P. K.; Jimenez, J. L.; Jayne, J. T.; Worsnop, D. R., Ambient measurements of highly oxidized gas-phase molecules during the Southern Oxidant and Aerosol Study (SOAS) 2013. *ACS Earth Space Chem.* **2018**, *2* (7), 653-672.
(43) Wennberg, P. O.; Bates, K. H.; Crounse, J. D.; Dodson, L. G.; McVay, R. C.; Mertens, L. A.; Nguyen, T. B.; Praske, E.; Schwantes, R. H.; Smarte, M. D.; St Clair, J. M.; Teng, A. P.; Zhang, X.; Seinfeld, J. H., Gas-phase reactions of isoprene and its major oxidation products. *Chem. Rev.* **2018**, *118* (7), 3337-3390.
(44) Zhao, D. F.; Pullinen, I.; Fuchs, H.; Schrade, S.; Wu, R. R.; Acir, I. H.; Tillmann, R.; Rohrer, F.; Wildt, J.; Guo, Y. D.; Kiendler-Scharr, A.; Wahner, A.; Kang, S.; Vereecken, L.; Mentel, T. F., Highly oxygenated organic molecule (HOM) formation in the isoprene oxidation by NO_3 radical. *Atmos. Chem. Phys.* **2021**, *21* (12), 9681-9704.
(45) Pullinen, I.; Schmitt, S.; Kang, S.; Sarrafzadeh, M.; Schlag, P.; Andres, S.; Kleist, E.; Mentel, T. F.; Rohrer, F.; Springer, M.; Tillmann, R.; Wildt, J.; Wu, C.; Zhao, D. F.; Wahner, A.; Kiendler-Scharr, A., Impact of NO_x on secondary organic aerosol (SOA) formation from alpha-pinene and beta-pinene photooxidation: the role of highly oxygenated organic nitrates. *Atmos. Chem. Phys.* **2020**, *20* (17), 10125-10147.
(46) Zhao, D. F.; Kaminski, M.; Schlag, P.; Fuchs, H.; Acir, I. H.; Bohn, B.; Häseler, R.; Kiendler-Scharr, A.; Rohrer, F.; Tillmann, R.; Wang, M. J.; Wegener, R.; Wildt, J.; Wahner, A.; Mentel, T. F., Secondary organic aerosol formation from hydroxyl radical oxidation and ozonolysis of monoterpenes. *Atmos. Chem. Phys.* **2015**, *15* (2), 991-1012.
(47) Huang, Y. L.; Zhao, R.; Charan, S. M.; Kenseth, C. M.; Zhang, X.; Seinfeld, J. H., Unified theory of vapor-wall mass transport in teflon-walled environmental chambers. *Environ. Sci. Technol.* **2018**, *52* (4), 2134-2142.
(48) Riva, M.; Rantala, P.; Krechmer, J. E.; Peräkylä, O.; Zhang, Y. J.; Heikkinen, L.; Garmash, O.; Yan, C.; Kulmala, M.; Worsnop, D.; Ehn, M., Evaluating the performance of five different chemical ionization techniques for detecting gaseous oxygenated organic species. *Atmos. Meas. Tech.* **2019**, *12* (4), 2403-2421.

(49) Lee, B. H.; Lopez-Hilfiker, F. D.; Mohr, C.; Kurtén, T.; Worsnop, D. R.; Thornton, J. A., An iodide-adduct high-resolution time-of-flight chemical-ionization mass spectrometer: application to atmospheric inorganic and organic compounds. *Environ. Sci. Technol.* **2014**, *48* (11), 6309-6317.
(50) Jenkin, M. E.; Valorso, R.; Aumont, B.; Rickard, A. R., Estimation of rate coefficients and branching ratios for reactions of organic peroxy radicals for use in automated mechanism construction. *Atmos. Chem. Phys.* **2019**, *19* (11), 7691-7717.
(51) Wang, S. Y.; Pratt, K. A., Molecular halogens above the arctic snowpack: emissions, diurnal variations, and recycling mechanisms. *J. Geophys. Res.: Atmos.* **2017**, *122* (21), 11991-12007.
(52) Vereecken, L.; Francisco, J. S., Theoretical studies of atmospheric reaction mechanisms in the troposphere. *Chem. Soc. Rev.* **2012**, *41* (19), 6259-6293.
(53) Vereecken, L.; Peeters, J., A structure-activity relationship for the rate coefficient of H-migration in substituted alkoxy radicals. *Phys. Chem. Chem. Phys.* **2010**, *12* (39), 12608-12620.
(54) Praske, E.; Otkjær, R. V.; Crounse, J. D.; Hethcox, J. C.; Stoltz, B. M.; Kjaergaard, H. G.; Wennberg, P. O., Atmospheric autoxidation is increasingly important in urban and suburban North America. *Proc. Natl. Acad. Sci. U.S.A.* **2018**, *115* (1), 64-69.
(55) Rissanen, M. P.; Kurtén, T.; Sipilä, M.; Thornton, J. A.; Kangasluoma, J.; Sarnela, N.; Junninen, H.; Jørgensen, S.; Schallhart, S.; Kajos, M. K.; Taipale, R.; Springer, M.; Mentel, T. F.; Ruuskanen, T.; Petäjä, T.; Worsnop, D. R.; Kjaergaard, H. G.; Ehn, M., The formation of highly oxidized multifunctional products in the ozonolysis of cyclohexene. *J. Am. Chem. Soc.* **2014**, *136* (44), 15596-15606.
(56) Vereecken, L.; Nozière, B., H migration in peroxy radicals under atmospheric conditions. *Atmos. Chem. Phys.* **2020**, *20* (12), 7429-7458.
(57) Atkinson, R.; Arey, J.; Aschmann, S. M., Atmospheric chemistry of alkanes: review and recent developments. *Atmos. Environ.* **2008**, *42* (23), 5859-5871.
(58) Yeh, G. K.; Claflin, M. S.; Ziemann, P. J., Products and mechanism of the reaction of 1-pentadecene with NO_3 radicals and the effect of a -ONO_2 group on alkoxy radical decomposition. *J. Phys. Chem. A* **2015**, *119* (43), 10684-10696.
(59) Kroll, J. H.; Seinfeld, J. H., Chemistry of secondary organic aerosol: formation and evolution of low-volatility organics in the atmosphere. *Atmos. Environ.* **2008**, *42* (16), 3593-3624.
(60) Novelli, A.; Cho, C.; Fuchs, H.; Hofzumahaus, A.; Rohrer, F.; Tillmann, R.; Kiendler-Scharr, A.; Wahner, A.; Vereecken, L., Experimental and theoretical study on the impact of a nitrate group on the chemistry of alkoxy radicals. *Phys. Chem. Chem. Phys.* **2021**, *23* (9), 5474-5495.

(61) Vereecken, L.; Peeters, J., Decomposition of substituted alkoxy radicals-part I: a generalized structure-activity relationship for reaction barrier heights. *Phys. Chem. Chem. Phys.* **2009**, *11* (40), 9062-9074.
(62) Lachowicz, D. R.; Kreuz, K. L., Peroxy nitrates. Unstable products of olefin nitration with dinitrogen tetroxide in the presence of oxygen. New route to .alpha.-nitroketones. *J. Org. Chem.* **1967**, *32* (12), 3885-3888.
(63) Bennett, J. E.; Summers, R., Product studies of the mutual termination reactions of sec-alkylperoxy radicals: evidence for non-cyclic termination. *Can. J. Chem.* **1974**, *52* (8), 1377-1379.
(64) Chim, M. M.; Cheng, C. T.; Davies, J. F.; Berkemeier, T.; Shiraiwa, M.; Zuend, A.; Chan, M. N., Compositional evolution of particle-phase reaction products and water in the heterogeneous OH oxidation of model aqueous organic aerosols. *Atmos. Chem. Phys.* **2017**, *17* (23), 14415-14431.
(65) Jenkin, M. E.; Saunders, S. M.; Pilling, M. J., The tropospheric degradation of volatile organic compounds: a protocol for mechanism development. *Atmos. Environ.* **1997**, *31* (1), 81-104.
(66) Junninen, H.; Ehn, M.; Petäjä, T.; Luosujarvi, L.; Kotiaho, T.; Kostiainen, R.; Rohner, U.; Gonin, M.; Fuhrer, K.; Kulmala, M.; Worsnop, D. R., A high-resolution mass spectrometer to measure atmospheric ion composition. *Atmos. Meas. Tech.* **2010**, *3* (4), 1039-1053.
(67) Paulot, F.; Crounse, J. D.; Kjaergaard, H. G.; Kürten, A.; St Clair, J. M.; Seinfeld, J. H.; Wennberg, P. O., Unexpected epoxide formation in the gas-phase photooxidation of isoprene. *Science* **2009**, *325* (5941), 730-733.
(68) Praske, E.; Otkjær, R. V.; Crounse, J. D.; Hethcox, J. C.; Stoltz, B. M.; Kjaergaard, H. G.; Wennberg, P. O., Intramolecular hydrogen shift chemistry of hydroperoxy-substituted peroxy radicals. *J. Phys. Chem. A* **2019**, *123* (2), 590-600.
(69) Miyoshi, A., Systematic computational study on the unimolecular reactions of alkylperoxy (RO_2), hydroperoxyalkyl (QOOH), and hydroperoxyalkylperoxy (O_2QOOH) radicals. *J. Phys. Chem. A* **2011**, *115* (15), 3301-3325.
(70) Peeters, J.; Müller, J. F.; Stavrakou, T.; Nguyen, V. S., Hydroxyl radical recycling in isoprene oxidation driven by hydrogen bonding and hydrogen tunneling: the upgraded LIM1 mechanism. *J. Phys. Chem. A* **2014**, *118* (38), 8625-8643.
(71) Kerdouci, J.; Picquet-Varrault, B.; Doussin, J. F., Prediction of rate constants for gas-phase reactions of nitrate radical with organic compounds: a new structure-activity relationship. *Chem. Phys. Chem.* **2010**, *11* (18), 3909-3920.
(72) Vereecken, L.; Peeters, J., A theoretical study of the OH-initiated gas-phase oxidation mechanism of β-pinene ($C_{10}H_{16}$): first generation products. *Phys. Chem. Chem. Phys.* **2012**, *14* (11), 3802-3815.

(73) Kaminski, M.; Fuchs, H.; Acir, I. H.; Bohn, B.; Brauers, T.; Dorn, H. P.; Häseler, R.; Hofzumahaus, A.; Li, X.; Lutz, A.; Nehr, S.; Rohrer, F.; Tillmann, R.; Vereecken, L.; Wegener, R.; Wahner, A., Investigation of the beta-pinene photooxidation by OH in the atmosphere simulation chamber SAPHIR. *Atmos. Chem. Phys.* **2017**, *17* (11), 6631-6650.
(74) Xu, L.; Møller, K. H.; Crounse, J. D.; Otkjær, R. V.; Kjaergaard, H. G.; Wennberg, P. O., Unimolecular reactions of peroxy radicals formed in the oxidation of alpha-pinene and beta-pinene by hydroxyl radicals. *J. Phys. Chem. A* **2019**, *123* (8), 1661-1674.
(75) Vereecken, L.; Peeters, J., Theoretical study of the formation of acetone in the OH-initiated atmospheric oxidation of alpha-pinene. *J. Phys. Chem. A.* **2000**, *104* (47), 11140-11146.
(76) Peeters, J.; Vereecken, L.; Fantechi, G., The detailed mechanism of the OH-initiated atmospheric oxidation of alpha-pinene: a theoretical study. *Phys. Chem. Chem. Phys.* **2001**, *3* (24), 5489-5504.
(77) Møller, K. H.; Otkjær, R. V.; Chen, J.; Kjaergaard, H. G., Double bonds are key to fast unimolecular reactivity in first-generation monoterpene hydroxy peroxy radicals. *J. Phys. Chem. A* **2020**, *124* (14), 2885-2896.
(78) Kurtén, T.; Møller, K. H.; Nguyen, T. B.; Schwantes, R. H.; Misztal, P. K.; Su, L. P.; Wennberg, P. O.; Fry, J. L.; Kjaergaard, H. G., Alkoxy radical bond scissions explain the anomalously low secondary organic aerosol and organonitrate yields from alpha-pinene + NO_3. *J. Phys. Chem. Lett.* **2017**, *8* (13), 2826-2834.
(79) Fouqueau, A.; Cirtog, M.; Cazaunau, M.; Pangui, E.; Doussin, J. F.; Picquet-Varrault, B., A comparative and experimental study of the reactivity with nitrate radical of two terpenes: alpha-terpinene and gamma-terpinene. *Atmos. Chem. Phys.* **2020**, *20* (23), 15167-15189.
(80) Berndt, T.; Mender, B.; Scholz, W.; Fischer, L.; Herrmann, H.; Kulmala, M.; Hansel, A., Accretion product formation from ozonolysis and OH radical reaction of alpha-pinene: mechanistic insight and the influence of isoprene and ethylene. *Environ. Sci. Technol.* **2018**, *52* (19), 11069-11077.
(81) Berndt, T.; Scholz, W.; Mentler, B.; Fischer, L.; Herrmann, H.; Kulmala, M.; Hansel, A., Accretion product formation from self- and cross-reactions of RO_2 radicals in the atmosphere. *Angew. Chem., Int. Ed.* **2018**, *57* (14), 3820-3824.
(82) Zhao, Y.; Thornton, J. A.; Pye, H. O. T., Quantitative constraints on autoxidation and dimer formation from direct probing of monoterpene-derived peroxy radical chemistry. *Proc. Natl. Acad. Sci. U.S.A.* **2018**, *115* (48), 12142-12147.
(83) Jokinen, T.; Berndt, T.; Makkonen, R.; Kerminen, V. M.; Junninen, H.; Paasonen, P.; Stratmann, F.; Herrmann, H.; Guenther, A. B.; Worsnop, D. R.; Kulmala, M.; Ehn, M.; Sipilä, M., Production of extremely low volatile organic compounds from biogenic emissions: measured yields and atmospheric implications. *Proc. Natl. Acad. Sci. U.S.A.* **2015**, *112* (23), 7123-7128.

(84) Wang, Y. H.; Riva, M.; Xie, H. B.; Heikkinen, L.; Schallhart, S.; Zha, Q. Z.; Yan, C.; He, X. C.; Peräkylä, O.; Ehn, M., Formation of highly oxygenated organic molecules from chlorine-atom-initiated oxidation of alpha-pinene. *Atmos. Chem. Phys.* **2020**, *20* (8), 5145-5155.
(85) Liu, Y.; Nie, W.; Li, Y.; Ge, D.; Liu, C.; Xu, Z.; Chen, L.; Wang, T.; Wang, L.; Sun, P.; Qi, X.; Wang, J.; Xu, Z.; Yuan, J.; Yan, C.; Zhang, Y.; Huang, D.; Wang, Z.; Donahue, N. M.; Worsnop, D.; Chi, X.; Ehn, M.; Ding, A., Formation of condensable organic vapors from anthropogenic and biogenic VOCs is strongly perturbed by NO_x in eastern China. *Atmos. Chem. Phys.* **2021**, *21*, 14789-14814.
(86) Roldin, P.; Ehn, M.; Kurtén, T.; Olenius, T.; Rissanen, M. P.; Sarnela, N.; Elm, J.; Rantala, P.; Hao, L. Q.; Hyttinen, N.; Heikkinen, L.; Worsnop, D. R.; Pichelstorfer, L.; Xavier, C.; Clusius, P.; Öström, E.; Petäjä, T.; Kulmala, M.; Vehkamäki, H.; Virtanen, A.; Riipinen, I.; Boy, M., The role of highly oxygenated organic molecules in the boreal aerosol-cloud-climate system. *Nat. Commun.* **2019**, *10*, 4370.
(87) Pye, H. O. T.; D'Ambro, E. L.; Lee, B.; Schobesberger, S.; Takeuchi, M.; Zhao, Y.; Lopez-Hilfiker, F.; Liu, J. M.; Shilling, J. E.; Xing, J.; Mathur, R.; Middlebrook, A. M.; Liao, J.; Welti, A.; Graus, M.; Warneke, C.; de Gouw, J. A.; Holloway, J. S.; Ryerson, T. B.; Pollack, I. B.; Thornton, J. A., Anthropogenic enhancements to production of highly oxygenated molecules from autoxidation. *Proc. Natl. Acad. Sci. U.S.A.* **2019**, *116* (14), 6641-6646.
(88) Weber, J.; Archer-Nicholls, S.; Griffiths, P.; Berndt, T.; Jenkin, M.; Gordon, H.; Knote, C.; Archibald, A. T., CRI-HOM: A novel chemical mechanism for simulating highly oxygenated organic molecules (HOMs) in global chemistry-aerosol-climate models. *Atmos. Chem. Phys.* **2020**, *20* (18), 10889-10910.